

AN ABSTRACT OF THE DISSERTATION OF

Adam M. Sibley for the degree of Doctor of Philosophy in Forest Ecosystems and Society presented on June 11, 2021.

Title: Plants and their Environment: Assessing Canopy Microclimate and the Response of Trees to Environmental Stress in a Diversity of Forest Types

Abstract approved:

---

Frederick C. Meinzer,

Christopher J. Still

The topics in this dissertation are centered around the way that trees respond to environmental stress in the climates where they occur. Though forests across the planet are expected to experience change in local climate due to historic and ongoing anthropogenic greenhouse gas emissions, the effects of climate change will not be uniform geographically, nor will change within a forest affect all species equally. Should some species fail to acclimate to new conditions while others do, structural changes may occur that impact forest productivity, soil nutrient cycling, the hydrologic cycle, ecosystem services, and habitat for forest dwelling organisms. Each of the three projects presented in this work addresses a specific change that has been predicted for a forested region and assesses the ability of tree species in the forest to adapt through changes in physiology or opportunistic uptake of dry season dew.

The research projects in the following chapters are built on the biophysical principles which allow us to predict and measure microclimate conditions, the exchange of carbon and water between foliage and atmosphere, tissue water relations, and the concentration of nonstructural carbohydrates (NSC) in living tissues. Chapter 1 is a general overview of the forest ecosystems, study species, expected changes in climate, and techniques used to assess plant response to change in each of the subsequent three chapters. Chapter 2 is an investigation into microclimate conditions from forest floor to canopy top in an old-growth temperate rain forest growing on the western slope of the Cascade mountains in central Oregon. This chapter includes analysis of patterns of wetting and drying in each season of the year by moisture source (rain, dew or frost), with

particular focus on both measuring and predicting dew formation during the dry season and its uptake through the foliage of Douglas-fir (*Pseudotsuga menziesii*). The key findings of this research show that dew formation occurs on one quarter to one third of summer nights, is restricted to the upper 20-30% of the canopy, and may play an important role in canopy hydration in future climates characterized by longer, drier, or hotter dry seasons. Chapter 3 focuses on plastic adjustment to drought stress in the two most abundant canopy trees in native Hawaiian forests, 'ōhi'a (*Metrosideros polymorpha*) and koa (*Acacia koa*). We sampled foliage, stem and trunk tissue from individuals of each species growing across a wide range of moisture availability in order to compare traits related to leaf water relations, leaf level gas exchange, and NSC concentration. The findings from this study show that 'ōhi'a exhibits a broader range of adjustment in traits related to drought resistance across its range than koa. This suggests that individual 'ōhi'a trees will be more capable of making plastic adjustments *in situ* compared to koa, which will have to rely on drought-avoidance strategies to cope with future drought. In chapter 4, we tested the ability of one-seed juniper (*Juniperus monosperma*) and piñon pine (*Pinus edulis*) to acclimate to future warming by exposing their foliage to both long-term, constant warming and short-term, more intense heatwave conditions. Acclimation of processes related to carbon assimilation and gas exchange were measured using temperature and intercellular CO<sub>2</sub> concentration response curves on unheated, long-term heated, and heatwave treated foliage from each species. Key findings of this study showed that one-seed juniper acclimated to long-term warming more than piñon but suffered greater inhibition when exposed to heatwave conditions. Chapter 5 outlines general conclusions from each individual chapter.

©Copyright by Adam M. Sibley

June 11, 2021

All Rights Reserved

Plants and their Environment: Assessing Canopy Microclimate and the Response of Trees to  
Environmental Stress in a Diversity of Forest Types

by  
Adam M. Sibley

A DISSERTATION

Submitted to

Oregon State University

in partial fulfillment of  
the requirements for the  
degree of

Doctor of Philosophy

Presented June 11, 2021  
Commencement June 2022

Doctor of Philosophy dissertation of Adam M. Sibley presented on June 11, 2021

APPROVED:

---

Co-Major Professor, representing Forest Ecosystems and Society

---

Co-Major Professor, representing Forest Ecosystems and Society

---

Head of the Department of Forest Ecosystems and Society

---

Dean of the Graduate School

I understand that my dissertation will become part of the permanent collection of Oregon State University libraries. My signature below authorizes release of my dissertation to any reader upon request.

---

Adam M. Sibley, Author

## ACKNOWLEDGEMENTS

It would be a very tall task to thank all the people who deserve thanks for helping me learn what it took to write this dissertation, or to thank the people who made the last four years in Oregon (or the previous four years in Hawai'i) fun and worthwhile. This list will invariably fall short. To start, I need to thank my committee – Chris Still, Rick Meinzer, Sanna Sevanto, and Mark Schulze – for their patience in teaching me and for all the knowledge bestowed. I'll try to make your investments pay off, I swear! The five of us owe thanks to the teams of people at the Institute of Pacific Islands Forestry, Los Alamos National Lab, and the H.J. Andrews Experimental Forest who keep the instruments running, collect field data, and who do everything else that make studies like the three in this dissertation possible. Special thanks to Adam Collins, Max Ryan, Adam Kennedy and Rob Hamnett for your roles in making the technical aspects of each study go smoo.....well, as smoothly as those things ever go.

No list of acknowledgements would be complete without my parents, Raymond and Susan Sibley, for the many kinds of support they've given me over the years. Pops, thanks for answering some fraction of the millions of questions I asked you as a kid. Karla Jarecke deserves thanks for making sure that I eat real food, sleep enough, exercise, and take time off to have fun. She deserves thanks for being my companion and making me feel loved. Thank you to everyone on the Big Island of Hawai'i for the good times in the amazing ecosystem of that place, and for teaching me about the flora and fauna – Rob Hamnett, Riley DeMattos, Shea Uehana, Susan Cordell and Becky Ostertag, to name but a few. Thank you Mr. W. and Mr. Porier, my high school teachers in digital electronics and physics, for steering me towards a career in science.

## CONTRIBUTION OF AUTHORS

### Chapter 2:

Study design was conceived of by: C. Still, M. Schulze, A. Sibley

Fieldwork was carried out by: A. Sibley, M. Schulze, A. Kennedy

Written by: A. Sibley

Editorial contributions from all authors

### Chapter 3:

Study design was conceived of by: R. Meinzer, S. Cordell

Fieldwork was carried out by: A. Sibley, S. Cordell, R. Hamnett, A. Uowolo

Lab work carried out by: A. Sibley, R. Hamnett

Data analysis carried out by: R. Meinzer, A. Sibley

Written by: A. Sibley

Editorial contributions from all authors

### For Chapter 4:

Study design was conceived of by: S. Sevanto, R. Meinzer, A. Sibley

Fieldwork was carried out by: A. Sibley, A. Collins, S. Sevanto

Lab analysis carried out by: A. Sibley, A. Collins, D. Ulrich

Written by: A. Sibley

Editorial contributions from all authors

## TABLE OF CONTENTS

	<u>Page</u>
CHAPTER 1 .....	1
1.1 GENERAL INTRODUCTION .....	1
1.2 REFERENCES .....	6
CHAPTER 2 WITHIN-CANOPY WETNESS PATTERNS AND THEIR POTENTIAL ROLES IN CANOPY HYDRATION IN A TEMPERATE WET-FOREST .....	9
ABSTRACT .....	10
2.1 INTRODUCTION .....	11
2.2 METHODS.....	13
2.2.1 Site description.....	13
2.2.3 Meteorological Data .....	14
2.2.3 Calculated values.....	16
2.2.4 Canopy wetness classification.....	18
2.2.5 Predicting dry season dewfall at the canopy top .....	20
2.2.6 Seasonal boundary determination .....	22
2.2.7 Dew uptake experiment.....	23
2.3 RESULTS .....	25
2.3.1 Annual wetness patterns.....	25
2.3.2 Cold season wetness patterns .....	27
2.3.3 The shoulder seasons.....	28
2.3.4 The dry season.....	30
2.3.5 Dew uptake experiment.....	35
2.4 CONCLUSIONS .....	38
2.5 REFERENCES .....	38
2.6 ACKNOWLEDGEMENTS.....	42
2.7 FIGURES .....	43
2.8 TABLES .....	52
CHAPTER 3 ADJUSTMENT TO MOISTURE STRESS BY TWO CO-OCCURRING ISLAND ENDEMIC CANOPY TREE SPECIES: IMPLICATIONS FOR THE COMPOSITION OF ACACIA KOA AND METROSIDEROS POLYMORPHA FORESTS UNDER INCREASING DROUGHT STRESS .....	56
ABSTRACT .....	57
3.1 INTRODUCTION .....	58



## TABLE OF CONTENTS (CONTINUED)

	<u>Page</u>
4.4.2 Response to heatwave .....	111
4.5 CONCLUSION.....	113
4.6 ACKNOWLEDGEMENTS.....	114
4.7 REFERENCES .....	115
4.8 FIGURES.....	120
4.9 TABLES .....	128
CHAPTER 5 .....	131
5.1 GENERAL CONCLUSIONS .....	131
5.2 REFERENCES .....	134

## LIST OF FIGURES

<u>Figure</u>	<u>Page</u>
FIGURE 2-1: SITE MAP .....	43
FIGURE 2-2: DEPICTION OF DISCOVERY TREE INSTRUMENTS .....	44
FIGURE 2-3: WATER AVAILABILITY 2006 – 2020 .....	45
FIGURE 2-4: ANNUAL WETTING PATTERNS.....	46
FIGURE 2-5: WETTING PATTERNS BY TYPE.....	47
FIGURE 2-6: DIURNAL PATTERNS OF DEW FORMATION AND DRYING AT TOP OF CANOPY .....	48
FIGURE 2-7: DEW PREDICTOR HISTOGRAMS .....	49
FIGURE 2-8: KERNEL DENSITY PLOTS OF DEW OCCURRENCE.....	50
FIGURE 2-9: RESULTS OF DEW UPTAKE EXPERIMENT .....	51
FIGURE 3-1: SITE LOCATIONS AND STUDY SPECIES FOLIAGE .....	86
FIGURE 3-2: PET : PRECIPITATION RATIO .....	87
FIGURE 3-3: VARIATION IN TRAITS RELATED TO PHOTOSYNTHESIS.....	88
FIGURE 3-4: GAS EXCHANGE TRAITS.....	89
FIGURE 3-5: NSC CONCENTRATIONS .....	90
FIGURE 3-6: TURGOR LOSS POINT VS. TOTAL LEAF SUGARS.....	91
FIGURE 3-7: TURGOR LOSS POINT VS. FULL TURGOR OSMOTIC POTENTIAL .....	92
FIGURE 4-1 STUDY SITE AND WARMING INFRASTRUCTURE. ....	120
FIGURE 4-2. AIR AND LEAF TEMPERATURES THROUGHOUT HEATWAVE PERIOD.....	121
FIGURE 4-3 DIURNAL VARIATION IN FOLIAGE TEMPERATURE .....	122
FIGURE 4-4 TEMPERATURE RESPONSE CURVES. ....	123
FIGURE 4-5 RESPONSE OF STOMATAL CONDUCTANCE TO VPD.....	124
FIGURE 4-6 STOMATAL REGULATION OF GAS EXCHANGE.....	125

FIGURE 4-7: $A_{NET}$ , $V_{C_{MAX}}$ RATIO, AND $R_D : A_{GROSS}$ RATIO FROM A-C <sub>1</sub> DATA. ....	126
FIGURE 4-8 EXAMPLE A-C <sub>1</sub> CURVES AT 25 AND 45 °C MEASUREMENT TEMPERATURE.....	127
FIGURE 4-9 $F_V/F_M$ RATIOS .....	127

## LIST OF TABLES

<u>Table</u>	<u>Page</u>
TABLE 2-1: PERCENT OF TIME SPENT WET EACH SEASON, BY HEIGHT .....	52
TABLE 2-2: ANNUAL MEASURES OF WETTING .....	52
TABLE 2-3 A-D: FREQUENCY AND DURATION OF DEW AND RAIN EVENTS.....	53
TABLE 2-4: SEASONAL BOUNDARIES FOR EACH CALENDAR YEAR.....	55
TABLE 2-5: REGRESSION METRICS .....	55
TABLE 2-6: FALSE POSITIVES AND NEGATIVES FROM DEW PREDICTION .....	55
TABLE 3-1: SITE CLIMATE CHARACTERISTICS .....	93
TABLE 3-2: LEAF WATER RELATION TRAITS.....	93
TABLE 3-3: RELATIVE BASAL AREA INCREMENT .....	93
TABLE 4-1 T-RESPONSE CURVE METRICS .....	128
TABLE 4-2 A-C <sub>1</sub> CURVE METRICS AT 25°C MEASUREMENT TEMPERATURE .....	128
TABLE 4-3 A-C <sub>1</sub> CURVE METRICS AT 35°C MEASUREMENT TEMPERATURE .....	129
TABLE 4-4 A-C <sub>1</sub> CURVE METRICS AT 45°C MEASUREMENT TEMPERATURE .....	130
TABLE 4-5. RESULTS OF V <sub>C<sub>MAX</sub></sub> RATIO T-TEST .....	130

## CHAPTER 1

### 1.1 General Introduction

The reintroduction of prehistoric carbon to our atmosphere via the burning of fossil fuels will be among the primary phenomena of the 20th and 21st century that determine the trajectory of the biosphere and our species. At the time of this writing, the concentration of CO<sub>2</sub> in the atmosphere measured at the Mauna Loa observatory on the Island of Hawai'i was 417 ppm – 137 ppm higher than the pre-industrial era and, to our knowledge, far higher than it has been at any point in the past 800,000 years (Lüthi et al. 2008). Increased CO<sub>2</sub> concentrations increase the radiative forcing of the atmosphere, which modifies the planetary energy balance and creates a cascade of changes through Earth's climate (IPCC 2014). While broad-scale predictions of warmer air temperatures and shifting precipitation regimes can be made from climate models, it is the propagation of these changes through the microclimates of forests that will be experienced by individual tree species and determine the new regimes of environmental stress that trees must adapt to. The effects of climate change will not be uniform geographically, nor will change within a forest affect all species equally. Should some species fail to adapt to new conditions while others do, structural changes may occur that impact forest productivity, soil nutrient cycling, the hydrologic cycle, ecosystem services, and habitat for forest-dwelling organisms. In this dissertation, each chapter will introduce a unique forest ecosystem, outline the changes in climate that are expected in the region of study, explain the experimental methods that were used to assess the ability of our focal species to adapt to coming change, and explain our key findings.

In chapter two we examined patterns of canopy wetting and drying in a temperate rainforest of the Pacific Northwest, where plants experience a prolonged wet season lasting eight months or more, with an intervening dry season (Waring and Franklin 1979). This stark, annual shift in moisture regime means that plants must make use of adaptive strategies to avoid deleterious drought stress effects during the dry season. For Pacific Northwest (PNW) wet forests, the most consequential predicted changes in climate are higher summertime temperatures and vapor pressure deficit and longer dry seasons (Mote and Salathe 2010), making physiological mechanisms for avoiding drought stress damage even more important future determinants of forest health. A common mechanism that can ameliorate foliar water stress among tree species of the PNW region is the direct uptake of water through foliage (Limm et al. 2009). Surface water may be delivered to the canopy in the dry season either by rainfall or dew accumulation. Owing to difficulty in modelling dew occurrence in tall forest canopies, little is known about the frequency or timing of delivery of this water subsidy in these forests.

While rainfall and canopy interception of rainfall are relatively easy to observe and model using rain gauges, dew wetting is a potentially much more frequent, but harder to model, source of canopy wetting (Ritter et al. 2019). Compared to arid climates with small stature vegetation (Agam and Berliner 2006), modelling whether microclimate conditions on a given night will culminate in dew formation in PNW forests is confounded by canopy height and complexity. In forests with tall stature and structurally complex canopies, it is difficult to make simplifying assumptions about rates of radiative cooling from canopy surfaces or the turbulent transport of air around the canopy, both of which are required to accurately model the surface energy balance at any given location in the canopy. Given the uncertainty involved in predicting dew formation

from energy balance models and the scarcity of information about dry season dew formation in this region, we elected to measure surface wetness directly along a vertical gradient in an old-growth *Pseudotsuga menziesii* canopy over the course of four water years (2017-2020) using leaf wetness sensors (LWS). Surface wetting events were classified into wetness caused by dew, frost, or rainfall by applying a simple set of logical rules to each LWS time series. Results of this method were compared to the biophysically based Penman method of predicting dew formation as well as a simple logistic model using dewpoint depression as a predictor. For both predictive models, we tested whether results were significantly improved by using meteorological sensors co-located with the 56 m a.g.l. LWS measurement height when compared to sensors located at a nearby weather station. In addition to quantifying the frequency and location of dew forming events in the dry season and testing predictive models, we conducted an artificial dew wetting experiment of upper canopy foliage and measured shoot response in water potential ( $\Psi_{\text{Leaf}}$ ) and stomatal conductance ( $g_s$ ). Taken together, the results of this chapter illustrate the potential for uptake of dew water to ameliorate dry season drought stress, and provide a baseline understanding of how frequently these events occur.

In chapter three, we compared two canopy dominant tree species which co-occur in the native forests of the Hawaiian Islands. Decreasing precipitation and fog water inputs have been identified as the most likely and potentially most severe climate-driven threat to forests where our study species, *Metrosideros polymorpha* Gaudich. ('ōhi'a) and *Acacia koa* A. Gray (koa), occur (Giambelluca and Luke, 2007). A decreasing trend in the wintertime Hawaiian Rainfall Index has been observed over the past century (Chu, Chen and Schroeder 2010, Frazier and Giambelluca 2017), and model simulations predict substantial shifts toward drier climate in

currently mesic land areas (Fortini, Jacobi and Price 2017). The relative sensitivity of koa and ‘ōhi‘a to future drought is of particular interest given their cultural importance, and that both are keystone species in forests where high rates of endemism give way to unique species interactions (Kier et al. 2009, Ohlemüller et al. 2008, Williams et al. 2003). In this study we sought to compare plasticity in traits which would confer drought resistance in a drier future. As measurement of plasticity in response to drought *in situ* would require opportunistic sampling or costly and logistically challenging rainfall exclusion structures (Binks et al. 2016), we devised a study design where individuals from each species would be compared across a range of moisture availability.

On the Big Island of Hawai‘i we sampled sunlit canopy foliage from our study species at wet, mesic, and dry forest sites. These samples were used to compare traits related to leaf water relations, stomatal control over gas exchange, NSC concentrations, and photosynthetic performance. By sampling this set of traits, we were able to differentiate drought-tolerant behavior from drought-avoidant behavior – specifically, the degree to which each species responded to lower water availability by increasing stomatal restriction of gas exchange, how each species modified turgor loss point ( $\Psi_{TLP}$ ) and osmotic potential at full turgor ( $\Psi_{\pi 100}$ ), made compensatory changes in carbon assimilation to offset stomatal restriction, and maintained NSC concentrations in a way that suggests the NSCs played a role in osmotic adjustment. This study demonstrates a useful set of tools for determining how species will respond to change *in situ* by looking at plastic adjustment to traits across their range.

In the fourth chapter, we focused on the piñon-juniper woodlands of the Southwestern US and the expected increase in temperature and more frequent and/or more severe drought conditions forecasted for the Southwest. Periods of combined drought and high temperature in the early 2000s led to significant mortality where a far greater proportion of piñon trees died than juniper trees (Breshears et al. 2009). While observations of greater insect infestation of drought-weakened piñon compared to juniper (Gaylord et al. 2013, Floyd et al. 2009) could go some way towards explaining differences in mortality, many questions remained about the relative ability of each species to adjust to or tolerate extreme conditions. The Survival Mortality (SUMO) experiment infrastructure at Los Alamos National lab was established in the early 2010's to artificially manipulate water availability and ambient air temperature that each species was exposed to so that we can better understand which traits would acclimate to imposed conditions, or conversely not acclimate, leading to physiological damage (Garcia-Forner et al. 2016, Grossiord et al. 2017a, Grossiord et al. 2017b). While many studies offer insights into the relative vulnerabilities of each species to drought effects, few examine the direct impact of high temperature on photosynthetic capacity.

To test for acclimation of net carbon assimilation ( $A_{\text{net}}$ ) to elevated temperature, we sampled foliage from control trees, trees that had been exposed to  $T_{\text{air}}$  5°C above ambient for six years, and branches exposed to heat-wave like temperatures. Using a portable gas exchange analyzer, we ran temperature response and net assimilation vs. internal CO<sub>2</sub> concentration curves in order to assess the net effect of the two heating treatments. We also used chlorophyll fluorescence measurements to assess the temperature sensitivity of photosystem II. The suite of measurements we made allowed us to examine differences between treatment groups in the biochemical

reactions involved in photosynthesis, mitochondrial respiration rates, stomatal control of gas exchange, and how acclimation or impairment of each component culminated in observed differences in  $A_{\text{net}}$  between treatments.

This dissertation is unique in the diversity of ecosystems that it covers and its focus on mature trees in their natural environment. Taken together, the chapters in this dissertation demonstrate a comprehensive set of tools for assessing the physiological attributes of trees in the context of future change, and present key findings about the relative capacity for adaptation in the focal species.

## 1.2 References

- Agam, N., Berliner, P.R., 2006. Dew formation and water vapor adsorption in semi-arid environments—A review. *Journal of Arid Environments* 65, 572–590.  
<https://doi.org/10.1016/j.jaridenv.2005.09.004>
- Binks, O., Meir, P., Rowland, L., da Costa, A.C.L., Vasconcelos, S.S., de Oliveira, A.A.R., Ferreira, L., Christoffersen, B., Nardini, A., Mencuccini, M., 2016. Plasticity in leaf-level water relations of tropical rainforest trees in response to experimental drought. *New Phytologist* 211, 477–488. <https://doi.org/10.1111/nph.13927>
- Breshears, D.D., Myers, O.B., Meyer, C.W., Barnes, F.J., Zou, C.B., Allen, C.D., McDowell, N.G., Pockman, W.T., 2009. Tree die-off in response to global change-type drought: mortality insights from a decade of plant water potential measurements. *Frontiers in Ecology and the Environment* 7, 185–189. <https://doi.org/10.1890/080016>
- Chu, P.-S., Chen, Y.R., Schroeder, T.A., 2010. Changes in precipitation extremes in the Hawaiian Islands in a warming climate. *J. Climate* 23, 4881–4900.  
<https://doi.org/10.1175/2010JCLI3484.1>
- Floyd, M.L., Clifford, M., Cobb, N.S., Hanna, D., Delph, R., Ford, P., Turner, D., 2009. Relationship of stand characteristics to drought-induced mortality in three Southwestern piñon–juniper woodlands. *Ecological Applications* 19, 1223–1230.  
<https://doi.org/10.1890/08-1265.1>
- Fortini, L.B, Jacobi, J.D., Price, J.P. 2017. Chapter 3. Projecting end-of-century shifts in the pattern of plant available water across Hawai'i to assess implications to vegetation shifts. U.S. Geological Survey Professional Paper 1834.

- Frazier, A.G., Giambelluca, T.W., 2017. Spatial trend analysis of Hawaiian rainfall from 1920 to 2012. *Int. J. Climatol.* 37, 2522–2531. <https://doi.org/10.1002/joc.4862>
- Garcia-Forner, N., Adams, H.D., Sevanto, S., Collins, A.D., Dickman, L.T., Hudson, P.J., Zeppel, M.J.B., Jenkins, M.W., Powers, H., Martínez-Vilalta, J., McDowell, N.G., 2016. Responses of two semiarid conifer tree species to reduced precipitation and warming reveal new perspectives for stomatal regulation: Stomatal regulation in piñon and juniper trees. *Plant, Cell & Environment* 39, 38–49. <https://doi.org/10.1111/pce.12588>
- Gaylord, M.L., Kolb, T.E., Pockman, W.T., Plaut, J.A., Yopez, E.A., Macalady, A.K., Pangle, R.E., McDowell, N.G., 2013. Drought predisposes piñon–juniper woodlands to insect attacks and mortality. *New Phytologist* 198, 567–578. <https://doi.org/10.1111/nph.12174>
- Giambelluca T.W., Luke M.S.A. 2007. Climate change in Hawai'i's mountains. Mountain views: The newsletter of the consortium for integrated climate research in western mountains. Consortium for Integrated Climate Research in Western Mountains 2, 13–17.
- Grossiord, C., Sevanto, S., Adams, H.D., Collins, A.D., Dickman, L.T., McBranch, N., Michaletz, S.T., Stockton, E.A., Vigil, M., McDowell, N.G., 2017a. Precipitation, not air temperature, drives functional responses of trees in semi-arid ecosystems. *Journal of Ecology* 105, 163–175. <https://doi.org/10.1111/1365-2745.12662>
- Grossiord, C., Sevanto, S., Borrego, I., Chan, A.M., Collins, A.D., Dickman, L.T., Hudson, P.J., McBranch, N., Michaletz, S.T., Pockman, W.T., Ryan, M., Vilagrosa, A., McDowell, N.G., 2017b. Tree water dynamics in a drying and warming world: Future tree water dynamics. *Plant, Cell & Environment* 40, 1861–1873. <https://doi.org/10.1111/pce.12991>
- IPCC, 2014: Climate Change 2014: Synthesis Report. Contribution of Working Groups I, II and III to the Fifth Assessment Report of the Intergovernmental Panel on Climate Change [Core Writing Team, R.K. Pachauri and L.A. Meyer (eds.)]. IPCC, Geneva, Switzerland, 151 pp.
- Kier, G., Kreft, H., Lee, T.M., Jetz, W., Ibisch, P.L. et al., 2009. A global assessment of endemism and species richness across island and mainland regions. *Proceedings of the National Academy of Sciences* 106, 9322–9327. <https://doi.org/10.1073/pnas.0810306106>
- Lüthi, D., M. Le Floch, B. Bereiter, T. Blunier, J.-M. Barnola, U. Siegenthaler, D. Raynaud, J. Jouzel, H. Fischer, K. Kawamura, and T.F. Stocker. (2008). High-resolution carbon dioxide concentration record 650,000–800,000 years before present. *Nature*, Vol. 453, pp. 379–382. doi:10.1038/nature06949.
- Mote, P.W., Salathé, E.P., 2010. Future climate in the Pacific Northwest. *Climatic Change* 102, 29–50. <https://doi.org/10.1007/s10584-010-9848-z>

- Ohlemüller, R., Anderson, B.J., Araújo, M.B., Butchart, S.H., Kudrna, O. et al., 2008. The coincidence of climatic and species rarity: high risk to small-range species from climate change. *Biology Letters* 4, 568–572. <https://doi.org/10.1098/rsbl.2008.0097>
- Ritter, F., Berkelhammer, M., Beysens, D., 2019. Dew frequency across the US from a network of in situ radiometers. *Hydrological Earth Systems Science* 20.
- Williams, S.E., Bolitho, E.E., Fox, S., 2003. Climate change in Australian tropical rainforests: an impending environmental catastrophe. *Proceedings of the Royal Society of London. Series B: Biological Sciences* 270, 1887–1892. <https://doi.org/10.1098/rspb.2003.2464>

## **CHAPTER 2**

### **WITHIN-CANOPY WETNESS PATTERNS AND THEIR POTENTIAL ROLES IN CANOPY HYDRATION IN**

#### **A TEMPERATE WET-FOREST**

Adam Sibley, Forest Ecosystems and Society, Oregon State University

Mark Schulze, Forest Ecosystems and Society, Oregon State University

Julia Jones, College of Earth, Ocean and Atmospheric Sciences, Oregon State University

Adam Kennedy, Forest Ecosystems and Society, Oregon State University

Christopher Still, Forest Ecosystems and Society, Oregon State University

**Abstract**

Canopy wetting and drying has a variety of effects on the function of plant foliage, ranging from increased risk of pathogenic infection to reduced diffusion of gases to enhanced leaf water status in plants capable of foliar water uptake. Projected shifts in rainfall regimes and increases in summertime vapor pressure deficit stand to change the timing and duration of canopy wetting, yet current patterns of wetting are poorly understood. In this study, we investigated patterns of wetting by source (rain vs. dew or frost), at different canopy heights, and at annual, seasonal and diurnal time scales using leaf wetness sensor data collected over a 4-year period in an old growth temperate wet forest. We found that at an annual scale canopy layers were wet for roughly half the year with strong seasonal variation, staying wet 83% of the cold winter season and 1.9% of the dry season. Upper canopy layers saw higher frequency, shorter duration wetting in all seasons compared to lower canopy layers. Throughout the year and particularly in the dry season, dewfall was restricted to the upper canopy, occurring on 28.5% of dry season nights. Particular focus was given to understanding dew formation in the dry season, when foliar water uptake of dew would be most beneficial to canopy foliage. Observed dry season dewfall was best predicted using a logistic model trained on observed dewfall and using dewpoint depression as a predictor. This logistic model performed significantly better than the Penman equation, a biophysical model that uses meteorological data to predict when conditions are favorable for condensation. On two nights in late summer of 2020, water was sprayed on selected branches to emulate dewfall on Douglas-fir foliage and effects on foliar water status were observed. While significant changes in foliar water potential were observed, foliar water stress was not large enough at the time of observation for the dew treatment to have a significant effect on morning gas exchange rates compared to control branches.

## 2.1 Introduction

While changes in climate are evident at regional and continental scales, it is the propagation of these changes through the microclimates of terrestrial ecosystems that will determine species responses and changes in ecological interactions (Davis et al. 2019, De Frenne et al. 2013, Pincebourde and Casas 2015, Storlie et al. 2014). The constituent plants of a forest ecosystem occupy niches related in part to their physiological requirements, which at a minimum involve light, temperature and moisture regimes that are suitable for survival. In moist forests, patterns of surface wetting and drying determine niche suitability for poikilohydric epiphytes such as bryophytes and lichens, which can play important roles in forest nutrient cycling (Johnson et al. 1982), increase canopy interception of precipitation (Pypker, Unsworth and Bond 2006), and increase the length of time that water is available for evaporation, thus modifying microclimate energy balances (Pypker et al. 2017). Tree species across a diversity of forest types experience both beneficial and harmful effects related to foliar wetting (Dawson and Goldsmith 2004), ranging from increased pathogen infection rates with increasing duration of wetness to added hydration via foliar water uptake (FWU) in water stressed plant parts. FWU has been observed across a wide variety of plant taxa (Berry et al. 2018) and can be particularly important in times of intense soil water deficit and for the upper foliage of tall trees (Burgess and Dawson 2004, Limm et al. 2009), which perennially face lower foliar water potentials ( $\Psi_L$ ) compared to lower leaves because of increasing gravitational water potential ( $\Psi_g$ ) at a rate  $0.01 \text{ MPa m}^{-1}$  height (Scholander et al. 1965).

Despite the importance of surface wetting for both trees and epiphytic plants, efforts to make general predictions of future change in wetting have not yielded consistent results (Greve et al.

2014). In the case of forests, the complex 3-D structures created by foliage, branches, and trunks of trees confound attempts to capture wetting and drying by applying simple rules to gridded data products or weather station data (Ritter, Berkelhammer and Beysens 2019). Such rules would need to capture the fact that the top of a canopy can be simultaneously hotter, drier, windier and brighter than the forest floor during the day, while the understory experiences more shade, less wind, and dampened diurnal swings in air temperature and relative humidity (von Arx et al. 2013). After precipitation events that wet the entire canopy, it is likely that these differences would lead to faster drying at the canopy top, though upper layers may also receive further wetting from light rains that do not penetrate to lower layers. At night, sky conditions dictate whether net radiation is mildly (cloudy conditions) or strongly (clear conditions) negative for sky-facing surfaces. The radiation balance of these surfaces partly determines whether they cool sufficiently for water vapor to condense and form dew (Monteith and Unsworth 2013). As forests age canopy structural complexity tends to increase, commensurate with increases in overall Leaf Area Index (LAI) (Ehbrecht et al. 2017), increased epiphyte density (McCune 1993) and tree height, while horizontal heterogeneity increases due to tree fall. Gaps formed by standing dead or fallen trees allow more light to penetrate to the forest floor, where understory saplings are recruited, leading eventually to a multi-species, mixed height canopy (Van Pelt and North 1996). With all of these factors at play in tall-stature, old growth forests, greater heterogeneity in wetting and drying within the canopy is expected compared to younger, less complex stands. While forest stands in the Pacific Northwest with the tallest trees and the highest bryophyte densities are likely to be impacted strongly by future changes in wetting, investigations have shown that these same stands buffer against extreme understory temperatures more effectively than neighboring stands of shorter, younger trees (Frey et al. 2016).

In this study, we observed surface wetting throughout the canopy of a tall Douglas-fir (*Pseudotsuga menziesii*) tree in an old growth forest stand. Observations were made at fine temporal resolution (5 minutes) using PHYTOS 31 leaf wetness sensors (section 3.4) and classified by a decision tree into wetness categories resulting from dew, rain and frost. We analyzed patterns of wetting and drying with height at daily, seasonal, and inter-annual time scales, with particular focus on temporal wetting dynamics in the summer dry season. We further examined the effects of dewfall by simulating it on two nights in late August 2020 and observing the physiological response. Before and after spraying foliage with water we measured shoot water potential ( $\Psi_L$ ), relative water content (RWC) and stomatal conductance ( $g_s$ ) to estimate the amount of water taken up by the foliage and to gauge its impact on leaf water status. Patterns of wetting provide informative context for multiple types of canopy dwelling organisms and taken together with measurements of leaf water uptake (LWU) demonstrate the potential physiological impact of surface wetting during the dry season.

## 2.2 Methods

### 2.2.1 Site description

Data for this study were collected at the H.J. Andrews Experimental Forest (henceforth Andrews Forest) in Blue River, OR (Figure 1). The research forest is a 6400-hectare parcel containing deep valleys separated from ridge tops by steep slopes. Elevations range from 430 meters to 1630 meters. Soils are volcanic in origin and range in texture from gravelly clay loam in alluvial areas to gravelly sandy loam and bedrock talus at higher elevations. The forest is composed of a mixture of plantation and old growth conifer stands. Douglas-fir (*Pseudotsuga menziesii* (Mirb.) Franco) is the dominant tree species in these plantations and is a canopy dominant in lower

elevation old growth patches along with western red cedar (*Thuja plicata* Donn ex. D Don) and western hemlock (*Tsuga heterophylla* (Raf.) Sarg.). Mean annual precipitation is 2077 mm (s.d. 477mm) and mean annual temperature is 9.1°C (s.d. 0.86 °C), as measured over the past 30 years at the Primary Meteorological Station (see section 4.2). The synoptic climate regime is Mediterranean – winters are cool and wet while summers are warm and dry, with shoulder seasons that can include a combination of dry and wet spells. Mean rainfall totals for the winter months of December, January and February are 8.5 times greater and potential evapotranspiration is 7 times lower than for June, July and August (868.0 mm vs. 101.7 mm rainfall, 83.9mm vs. 593.4 mm PET) across the years where net radiation data is available (2013 – 2019). While these statistics give some sense of the strength of seasonality in the moisture balance, using seasonal boundaries based on calendar months can mask significant interannual variability in dry season timing. Acknowledging this, we employed a routine for finding seasonal boundaries empirically (see section 3.5).

### ***2.2.3 Meteorological Data***

Meteorological observations were made in two locations – along the vertical axis of an old growth Douglas-fir tree and in a nearby open meadow. The measurement tree, hereafter Discovery Tree, is approximately 450 years old, stands 65 meters tall, and has a diameter of 122 cm at breast height (Figure 2). The tree is in a grove of other old growth Douglas-fir, Western hemlock and Western red-cedar trees, and is bordered to the north by an 60-year old plantation forest. Instrument clusters were installed at 1.5, 10, 20, 30, 40 and 56 meters above ground level (a.g.l.) on the north side of the Discovery Tree. All measurements at all heights were recorded at a five-minute intervals. Measurements for 2017 – 2020 span the full calendar year and are used for calculating annual and seasonal statistics presented in the results.

Observations on/near the measurement tree include air temperature ( $T_{\text{air}}$ ), relative humidity (RH), wind speed and direction, and soil volumetric water content (VWC).  $T_{\text{air}}$  was measured using either CS107 sensors (at 10, 20, 30 and 40 meters a.g.l.), an EE181 sensor (at 1.5 meters a.g.l.) or an HC2S3 sensor (56 meters a.g.l.) (all Campbell Scientific, Logan, UT). All temperature sensors were housed in fan-aspirated shields (Thomas and Smoot 2013, Figure 2b), which reduce bias introduced by radiation loading during direct sun exposure. The top and bottom instrument arrays (1.5 and 56 meters a.g.l.) also returned relative humidity measurements made by the same EE181 and HC2S3 sensors that measured  $T_{\text{air}}$ . Wind speed and direction were measured at the top and bottom arrays by a WS425 WINDCAP ultrasonic wind sensor (Vaisala, Helsinki, Finland). Soil moisture was measured approximately 5 meters from the base of the measurement tree at 10, 20, 50 and 100 centimeters below ground using CS615 water content reflectometers (Campbell Scientific, Logan, UT).

The second measurement location is the Primary Meteorological Station (hereafter “PRIMET”), which was established in 1972 and is situated in a small clearing at the bottom of a steep forested hillslope, ~700 m southwest of the measurement tree. All instruments at the PRIMET station are located between 1 and 6 m a.g.l. on free-standing towers. For this study we used measurements of net radiation ( $R_{\text{net}}$ ; NR01 Hukseflux, Delft, Netherlands),  $T_{\text{air}}$ , RH, incoming solar radiation ( $R_{\text{solar}}$ ), precipitation (TE525 tipping bucket rain gauge, Texas Electronics, Dallas, TX) and VWC at 100 cm depth. The VWC data was examined, and field capacity was approximated at a value of 0.25 and minimum soil moisture was 0.06. Data will be presented as a scaled value between minimum and field capacity (values between 0 and 100).

All PRIMET variables were retrieved from the H.J. Andrews database (Daly and McKee 2019) at a 5-minute time step for the period overlapping the Discovery Tree record, and at a 15-minute time step back to 2005. Data were delivered with QA/QC performed following the principles outlined in Campbell et al., 2013 and using the tools described in Sheldon 2008. All variables at all timestamps where the associated quality flag was “Accepted” were kept, while all data associated with any other flag were discarded. For the measurement tree, provisional data flags were visually inspected. In all cases, values flagged as “Questionable” were discarded.

### 2.2.3 Calculated values

From the meteorological data described in section 3.2 we calculated Potential Evapotranspiration (PET) using the Priestley-Taylor equation (Priestley and Taylor 1972) for determination of seasonal boundaries (section 2.5). We also calculated Latent heat flux using the Penman equation (Monteith and Unsworth 2013) and dewpoint depression for two methods of predicting dewfall.

For PET:

$$PET = \alpha \frac{\Delta}{\Delta + \gamma} R_{net} \quad (1)$$

Where  $\alpha$  is 1.26 (empirical constant),  $\gamma$  is the psychrometric constant ( $0.066 \text{ kPa } ^\circ\text{C}^{-1}$ ), and  $\Delta$  is the slope of the saturation vapor pressure curve at a given  $T_{air}$  ( $\text{kPa } ^\circ\text{C}^{-1}$ ) and is defined as:

$$\Delta = \frac{17.502 \times 240.97 \text{es}(T_{air})}{(T_{air} + 240.97)^2} \quad (2)$$

In the above,  $\text{es}(T_{air})$  is the saturation vapor pressure and is given by the following, with  $T_{air}$  in Celsius:

$$es(T_{air}) = 0.61121 \exp\left(\frac{17.502 \times T_{air}}{T_{air} + 240.97}\right) \quad (3)$$

From  $es(T_{air})$  and relative humidity (RH), actual vapor pressure is given as:

$$e = es(T_{air}) * RH \quad (4)$$

From these same quantities, one can calculate both specific humidity (SH) and predict the rate of latent heat flux during periods of minimal transpiration using the Penman equation. For specific humidity:

$$SH = \frac{0.622 * e}{101.3 - (0.378 * e)} \quad (5)$$

For the Penman equation:

$$LE = \frac{\Delta R_n + \rho c_p (es(T_{air}) - e) r_H^{-1}}{\Delta + \gamma \left(\frac{r_v}{r_H}\right)} \quad (6)$$

Where  $R_n$  is net radiation ( $W m^{-2}$ ),  $\rho$  is the density of air ( $1.15 kg m^{-3}$ ),  $c_p$  is the specific heat capacity of air ( $1005 J kg^{-1} C^{-1}$ ), the ratio of  $r_v$  to  $r_H$  is assumed to be constant at 0.926, and  $r_H$  – aerodynamic resistance to heat transfer – is given by Nobel 1990:

$$r_H = \frac{\sqrt{\frac{d}{u}}}{.255} \quad (6)$$

Where  $d$  is the average of foliage length and width in meters (here 0.03 m and 0.003 m respectively) and  $u$  is wind speed in  $m s^{-1}$ . This formulation results in a resistance in units of  $s mol^{-1} m^{-2}$ . It is necessary to convert to units of  $s m^{-1}$  for equation 5, which we did by multiplying  $r_H$  by the ideal gas constant ( $R$ ,  $8.3145 J mol^{-1} K^{-1}$ ),  $T_{air}$  in Kelvin, and one over atmospheric pressure (101,300 Pascals). Equation 5 predicts latent heat flux in  $W m^{-2}$ , which can be expressed in a rate of water loss or dew accumulation in  $mm hr^{-1}$ :

$$LE_{mm\ hr^{-1}} = \frac{3600 * LE_W\ m^{-2}}{\lambda} \quad (7)$$

Where 3600 is the number of seconds in an hour and  $\lambda$  is the latent heat of vaporization ( $J\ kg^{-1}$ ).

The above set of equations can all be supplied with data from the years 2014-2020. Prior to 2014, net radiation data was not available, and daytime  $R_{net}$  was supplied using the following equation, adapted from (McMahon et al. 2013):

$$R_{net\ approx} = R_{solar}(1 - \alpha) - \sigma T_{air}^4 (0.34 - 0.24\sqrt{e}) \left( \frac{1.35R_{solar}}{R_{clearsky} - 0.35} \right) \quad (8)$$

Where  $R_{solar}$  is incoming shortwave radiation ( $W\ m^{-2}$ ),  $\alpha$  is albedo (0.28 in this case),  $\sigma$  is the Stefan-Boltzmann constant,  $T_{air}$  is in Kelvin, and  $R_{clearsky}$  is estimated clear sky incoming shortwave.  $R_{clearsky}$  that accounts for topographic shading was modeled as described in Daly et al. (2007) but with climatological effective clear-sky optical depth and surface albedo varying by day of year.

#### **2.2.4 Canopy wetness classification**

Canopy wetness was measured alongside every instrument cluster on the Discovery Tree (Figure 2) using Phytos 31 Leaf wetness sensors (METER group, Pullman, WA). These sensors are fiberglass, leaf shaped devices 12 cm long and 8.5 cm wide, with a specific heat capacity of  $1480\ J\ m^{-2}\ K^{-1}$ . Measurements are made by applying an excitation voltage to electrodes embedded in the fiberglass sensor body and measuring the return voltage, which can be used to infer the dielectric constant of a zone approximately 1cm from the upper surface of the sensor (Phytos 31 manual). The dielectric constant of both water and ice (80 and 5, respectively) are much higher than that of air (1), meaning the return voltage will be significantly higher in the presence of surface wetness, and noticeably higher in the presence of frost.

The range of observable return voltages depends in part on the applied excitation voltage, which in this study was 2500 mV. Based on the data collected from all sensors during our four-year study period, 99.9% of return voltages fell between 255 mV and 1000 mV. Using this range and recommendations from the sensor manual, we chose a dry sensor threshold of 275 mV, below which all values were considered dry. By inspecting the data on known frost days and comparing with values published in the manual we chose 290mV as an upper threshold, meaning that only observations between 275 and 290 mV are candidates for being classified as frost in the rules that follow.

Using the leaf wetness observations in millivolts, the thresholds mentioned above, precipitation data from PRIMET, and  $T_{\text{air}}$  observations at each instrument cluster on the measurement tree, we applied a decision tree (supplemental Figure 1) to each leaf wetness data stream to classify every 5-minute time period as dry, wet by rain, wet by dew, frosted, or wet by ambiguous source. The decision tree uses the following seven rules:

- i) If the sensor value is below 275 mV, it is dry.
- ii) If the sensor value is above 275 mV and any depth of rainfall is registered within the preceding 2 hours, it is wet by rain.
- iii) If it has not rained in the preceding 2 hours but the sensor has never been dry since the last rain wetting and values have been trending towards dry (slope is less than zero) the sensor is wet by rain.
- iv) If, after a dry period, the sensor becomes wet in the absence of rain, it is wet by dew.

v) If during a wet period caused by rain the sensor becomes wetter (slope of wetness sensor values  $> 30$  mV per hour) but no rain has fallen in the past two hours, the classification becomes wet by dew.

vi) If a decrease in wetness is observed in conjunction with  $T_{\text{air}}$  dropping below  $0^{\circ}$  Celsius followed by an increase in wetness when  $T_{\text{air}}$  goes above  $0^{\circ}$  C, this interval is classified as “frost”. The same wetness class that was determined before the frost event is assigned to the period after the event (note: simplified description of this rule is given in supplemental figure).

vii) Any case that does not satisfy any of the above six rules is wet by ambiguous source.

In addition to classifying observations into the five wetness categories, we converted millivolt signals into approximate depths of water ( $\text{mm m}^{-2}$ ) using an empirically derived relationship provided by the manufacturer:

$$Depth = \frac{1.95 e^{0.00864 \times mV}}{1000} \quad (8)$$

This exponential relationship is most robust in the range between 255 and 500 mV, beyond which the predictive ability diminishes because the sensor will read higher mV values when the same mass of water is present as one large pool versus several smaller droplets. For this reason and based on the distribution of readings in our data, we chose to present events as those which result in  $< 0.1$ mm of water accumulation, and those which result in 0.1mm accumulation and above.

### ***2.2.5 Predicting dry season dewfall at the canopy top***

To explore how meteorological conditions come together to determine when dew forms during the dry season at our site, we employed two methods which use met data to classify each five-minute interval as being either a period of dew accumulation or a period of drying/surface

dryness. In the first method, we simply solve the Penman equation (Equation 5) using wind speed, relative humidity, and air temperature data from the 56m instrument cluster on the Discovery Tree and  $R_{\text{net}}$  data from PRIMET to create a binary prediction. When the calculation yields a negative latent heat flux estimate we classify that time period as an interval of dew accumulation, and all LE predictions of zero or higher are classified as non-dew forming periods. To test the efficacy of this approach, we compared predicted values to observations of dew formation in the dry season ( $n = 1811$ ) and created a confusion matrix to examine the rate of true, false positive and false negative predictions. This approach does not show the importance of individual met variables directly, but rather tests whether basic theory is able to capture how various conditions must come together to culminate in dewfall. To test this same approach at the daily scale, we asked the question: on days when dew accumulation is observed for greater than one hour, does Penman predict over one hour of dewfall? Throughout the manuscript, this method of predicting dewfall will be referred to as the Penman approach.

In our second approach we examined dew-relevant predictor variables by fitting a logistic regression to each predictor individually and to a linear combination of all predictors, using observations from the 56m LWS as a binary response variable (0 = no dew accumulation, 1 = dew accumulation). This method has the benefit of allowing us to scrutinize individual predictors on their own to see which segregate non-dew from dew nights most effectively. In total we fitted seven models; one each for wind speed,  $R_{\text{net}}$ , Dewpoint depression (DPD), Vapor pressure deficit (VPD), RH and  $T_{\text{air}}$ , in addition to a three-variable model of  $\text{DPD} + \text{Wind speed} + R_{\text{net}}$ . To make the dataset for these regressions, we pooled all five-minute data points which occurred during the dry seasons of 2017-2020 when dew accumulation was observed, resulting in 1811 individual observations. Non-dew data were collected from every observation interval between midnight

and 6 a.m. on every completely dry day (no wetting registered of any type) in the dry season, resulting in 29,672 observations.

All regression fitting and validation were done in R, using the rms package (version 6.0-1). For each logistic model, the portion of variance in observed dewfall that the model could explain was evaluated using index corrected  $R^2$ . The fit of each model was assessed using the Area Under the Receiver Operator Curve (AUROC), a metric that ranges between 0.5 and 1 and characterizes the diagnostic ability of the model across the full range of possible probability thresholds.

### ***2.2.6 Seasonal boundary determination***

In this study, we sought to determine seasonal boundaries in each calendar year that maximally separate the relatively rain-free dry season from the relatively rainy shoulder seasons before and after it. We also sought to define a winter cold period that is relevant to the vegetation of the region. Winter, spring, summer and fall will be referred to interchangeably as the cold season, spring shoulder season, dry season, and fall shoulder season.

The winters in this region are characterized by temperatures at which the evergreen tree species within the forest are considered largely dormant. In summer the limiting factor on productivity in vegetation is moisture limitation. The spring and fall shoulder seasons are a time of transition, both in temperature and precipitation (Waring and Franklin 1979). Beginning with the dry season, a three-week moving average of daily precipitation – PET was calculated moving both forward and backwards from July 15<sup>th</sup> (the midpoint of the historically driest month). The start and end of the season were marked when the moving average crossed from below to above -5 mm per day. Defining the start of the dry season this way always places the start date within a

period of continuous dry-down in volumetric water content (VWC) at 100cm depth below the soil surface. Among the years 2005 – 2020, VWC at the start of the dry season ranged between 0.21 and 0.15, where field capacity at this depth is 0.25, and the observed minimum in the record 0.06.

The start and end of the dormant cold season were then determined using a three-week moving average of  $T_{\text{air}}$ , and a threshold of 5°C. The start date of the cold season was marked as the last day in the first 3-week window where average daily  $T_{\text{air}}$  went below 5°C. The end of the cold season was then marked as the last day in the 3-week window after the start of the following calendar year that the average crossed above the 5°C threshold. The spring and fall shoulder seasons were then defined as the periods between the cold and dry seasons for each year.

### ***2.2.7 Dew uptake experiment***

To investigate dew uptake in the foliage of the measurement tree, we chose two nights (predicted and confirmed to be dew-free) in the summer of 2020 (August 26<sup>th</sup> and 28<sup>th</sup>) to spray foliage at 56 meters above ground level with deionized water from a small spray bottle. The spray bottle emits a fine mist of approximately 0.11 g of water each spray. On each night we approximated the amount of water we were adding to the foliage by weighing the spray bottles before and after treatment. To estimate the area of foliage sprayed, we chose a main branch that had a symmetric distribution of side branches and foliage, resulting in an approximately triangular arrangement of foliage. We measured the height and width of the triangle of foliage selected for spraying, calculated the area, and made a visual estimate that the average area of foliage within each triangle was 50%. Using this estimate of foliage area and the weight of water sprayed each night, we calculated the quantity of water applied in depth per square meter of foliage as 0.041 and

0.028 mm on nights one and two (equivalent to 40.5 and 27.9 g m<sup>-2</sup> foliage). A review of dewfall quantities across different ecosystem types (Tomaszkiewicz et al. 2015) measured using dew condensers gives an average of 0.13 mm per night (0.1mm SD) (Ritter, Berkelhammer and Beysens 2019). Sprayed amounts were near the lower end of the range, while also being at or close to the limit for what the foliage could hold – additional sprayed water would have largely dripped off the target needles. This suggests that on nights with higher dewfall totals, surface water on foliage would need to be absorbed at the same time that additional water vapor is condensing in order for foliage to take full advantage of deposited dew. Otherwise, water beyond a ~0.041mm depth would likely result in more and more drip from the needles. To check for agreement between the quantities of water applied to the foliage and what the corresponding leaf wetness sensor values would be, we solved equation 8 for sensor millivolts and found that the sprayed amounts on the two experiment nights should result in 353 and 308 mV responses from the leaf wetness sensors. However, on the nights of the dew spray experiments, we tested the leaf wetness sensor response to 2 sprays (0.22g on 0.008 m<sup>2</sup> area, or 0.028 mm depth) and 3 sprays (0.044 mm depth) of water, which resulted in much higher mV readings than would be expected – 374 and 468 mV. These results are in line with the notion that water that coalesces into larger droplets on the sensor will make the LWS give erroneously high water depth predictions (see section 3.4). In all further discussion of leaf water uptake, depths of water will refer to known amounts applied via weighing the spray bottle before and after application.

Spraying was done at 4:10am and 4:40am on the two nights – roughly two hours before daybreak and three and a half hours before the sun emerged over the local ridgeline and exposed the foliage to direct sun. On the first day all visible traces of sprayed water were gone (either

absorbed, evaporated, or shed) by the time the tree was climbed for the first post-spray measurements at 7:10am. On the second day dew drying was observed continuously in the tree, and all visible water traces were gone by 6:45am.

Before and at several timepoints after each spray we measured shoot water potential ( $\Psi_L$ ), relative water content (RWC) and stomatal conductance ( $g_s$ ) on sprayed branches (treatment group) and adjacent unsprayed branches (control group). Shoot water potential was measured using a pressure chamber (PMS Instrument Company, Albany, OR, USA) on three excised shoots per group and at each time point on the first day (4:10, 7:50, 11:05 and 14:05), and four shoots per group and timepoint on the second day (4:18, 6:48, 8:00, 9:08 and 10:49). These samples were also used to determine RWC – each sample was weighed before measurement in the pressure chamber, then allowed to rehydrate with cut ends in water filled florist tubes for two hours in a cool, dark container and reweighed. Dry weights were determined after the samples were air dried for 30h at 70°C in a drying oven. Stomatal conductance was measured *in situ* using an AP4 porometer (Delta-T Devices, Burwell, Cambridge, UK) immediately before shoot sampling and at each subsequent sampling timepoint. The number of measurements at each time point ranged from four per group for pre-dawn measurements to 10 per group post-dawn. Illumination conditions for the post-dawn measurements ranged from 131 to 704 W m<sup>-2</sup> on the first day and from 374 to 856 W m<sup>-2</sup> on the second day.

## **2.3 Results**

### ***2.3.1 Annual wetness patterns***

In the climate region where our study took place, the seasonality of rainfall (dry summers) makes it instructive to look at annual patterns in terms of a water year, which runs from the start of fall

to the start of the subsequent fall, thus grouping the three wettest seasons together and ending the year with the dry season. At the annual scale and looking only at wet vs dry periods, patterns of wetness from forest floor to canopy top were very similar – at each height, roughly half of each year was spent wet (Table 1). Averaging all heights together, in the water years 2018 – 2020 the forest spent 50.2, 44.0, and 48.6% of the time wet, respectively (Table 2). Viewed another way, at least one layer of the forest was experiencing surface wetness for an average of 59.7% of each year (Table 2). The water years examined in this study were all below the fifteen-year mean in annual rainfall, ranging from 0.56 to 1.4 standard deviations below the mean (Figure 3), suggesting that past years in the record experienced higher proportions of time spent wet.

Rainfall duration, measured by counting the five-minute intervals where the rain gauge recorded a value above zero, ranged from 20.6 to 22.9 days' equivalent a year. While this definition of rain duration is likely to underestimate the true duration during periods of light drizzle where water accumulates across multiple 5-minute intervals before one tip of the rain gauge is registered, it does give a general sense of the amount of time it rains in a year vs. the amount of time the canopy spends wet. Across 2018-2020 the ratio of average time spent rain wet to time spent raining ranges from 5.9 to 6.8, with water lingering on at least one canopy layer for up to 9.0 times the rainfall duration. Dew wetting on average accounted for an additional 22.8 days of wetness, resulting in 16.4% more time spent wet than if we considered rainfall alone. Dew water lingered on at least one canopy layer for up to 76.3 days a year, though this figure is likely exaggerated by phenomena happening in the lower canopy during the cold season (see section 2.3.2).

Though these annual numbers are useful for giving a rough idea of how much wetting one would expect for a given amount of annual rainfall, they mask significant seasonal variation (Figure 4). Averaged across all layers, the forest spent an average of 87.9% of the time wet in the winter, 4.7% of the time wet in the dry season, and 43.7 and 51.3% during the spring and fall, respectively. Within each season, significant patterns can be seen with height as well.

### ***2.3.2 Cold season wetness patterns***

Even at the basic wet vs. dry distinction, differences among canopy heights can be seen during the cold season. The upper canopy spent less time wet than the forest floor (Table 1) but saw far more distinguishable individual events and intervening dry periods. Dew formed on 61% of days and rain wetting was present on 68% of days at canopy top. The relatively shorter duration wetting events in the top two canopy layers are attributable to a combination of factors related to drip and evaporation – namely wind speed, air temperature, relative humidity and incident solar radiation. Average daily wind speeds were 0.58 (SD 0.19) m s<sup>-1</sup> at canopy top compared to 0.21 (SD 0.07) m s<sup>-1</sup> at the forest floor during the cold season, which increased the likelihood of drip from upper canopy foliage and enhanced evaporation (equations 5 and 6), as did higher average daytime air temperatures (5.2 °C (SD 3.6) vs 2.9 °C (SD 2.7), top to bottom), lower average daytime RH (90.5% (SD 12.9) vs 99.4% (SD 2.4)), and more incident radiation given that shortwave radiation transmittance to the forest floor is on the order of 0.081 in forest stands of this species composition and age (Parker, Davis and Chapotin 2002). Frost events also contributed to the pattern of high frequency, short duration wetting events in the upper canopy and fewer, longer events lower down (Table 3a). Indeed, frost events were less frequent but longer in the lower canopy, and surface drying took an order of magnitude longer. Rain wetting events averaged 6.3, 7.4 and 5.9 days long in the bottom three canopy layers (Table 4a), with one

rain wetting at the 1.5m height that took 89 days to dry out. The concept of a distinct “event” breaks down below the canopy during the winter, with water likely coming from a combination of rainfall, dew deposition, and drip while taking many days to evaporate or drip dry entirely (Figure 4). Attribution of wetness to different sources becomes an opaque concept in lower canopy layers in a season with such a high percentage of time spent wet.

### ***2.3.3 The shoulder seasons***

Compared to the cold season, the shoulder seasons were relatively frost free and characterized by a less extreme version of the same pattern of higher frequency, shorter duration wetting events at the top of the canopy and longer events lower down. In both the spring and fall clear patterns emerged after rainy spells where drying was ranked fastest to slowest from canopy top to bottom (Figure 4, supplemental figures 2 and 3, Table 4 b & d). At the top layer of the canopy, 13.2% of dewfall events in spring and 46.3% in fall occurred while some part of the vertical profile was still wet from rain - the rest occurred when all other sensors had dried out. This suggests that water vapor coming from evaporating rain could be ventilated out of the stand more slowly after rainfall in the fall compared to spring, which is corroborated by findings of more frequent temperature inversion formation in this valley in fall compared to spring (Rupp et al. 2020). Eddy-covariance data and/or isotopic tracers would be needed to fully evaluate the extent to which local recycling differs between seasons (Berkelhammer et al. 2013).

Unlike the winter, each shoulder season contained dry spells, some of which lasted several weeks at heights 30m and below. In the upper canopy, dew events recur 1 – 7 consecutive nights after rainfall and occur as well on nights where antecedent rainfall does not appear to be a factor (Figure 4). More dewfall was observed in the fall than the spring at the top of the canopy, both as

a percentage of total time spent wet at 49.6% (SD 10.8) vs 25.5% (SD 6.1) (Figure 5) and in number of hours spent wet by dew at 261.6 hr (SD 124.0) and 236.0 hr (SD 83.4) (Table 3 b & d). The appearance that the fall had a higher proportion of dew wetting is supported by a t-test and a p value threshold of  $< 0.05$  ( $p = 0.02$ ), though the difference in duration of dew wetting between seasons did not pass this test ( $p = 0.5$ ). It is difficult to speculate whether this pattern is a perennial feature or an artefact of interannual variability in the years sampled in our study. The fifteen year record at the PRIMET station does not show a significant difference between spring and fall in rainfall (612 mm in spring, 584 mm in fall,  $p$  value = 0.96) nor in dewpoint depression in the two hours pre-dawn ( $0.17^\circ$  in spring,  $0.13^\circ$  in fall,  $p = 0.12$ ), though shortwave radiation was significantly higher in the six hours after sunrise in the spring ( $361 \text{ W m}^{-2}$  in spring,  $271 \text{ W m}^{-2}$  in fall,  $p < 0.01$ ) and dew events were substantially shorter in the spring than in the fall (table 3 b., c.), suggesting enhanced evaporation in the spring compared to the fall.

Vertical patterns in the shoulder seasons showed interesting patterns with respect to the biology of poikilohydric organisms like bryophytes and lichens. In general terms, the lower heights in the canopy were the most stably wet and stably dry and exhibited the longest completely dry periods. If we define moisture stability as the number of transitions from dry to wet to dry, the average number of transitions from bottom to top were 27, 29, 28, 32, 64 and 109 in the spring and 11, 11, 12, 16, 36 and 62 in the fall. These patterns of wetness stability would suggest that desiccation tolerant organisms living below 40m in the canopy would go through fewer cycles of desiccation and resurrection than those living above that line. While bryophytes and lichens are capable of enduring long periods of dormancy, entering dormancy requires the assembly of intracellular structures that prevent damage to organelles as cells desiccate and shrink, and the building of these structures is energy costly (Proctor et al. 2007). The patterns of moisture

stability shown in this study are in good agreement with well-established patterns of epiphytic bryophyte and lichen biomass densities with height in old growth canopies of the Pacific Northwest (McCune et al. 2000). That is, the regions of the canopy with the fewest transitions in our study are also the regions where bryophyte densities are generally highest, while the upper canopy has more transitions and tends to have lower densities of bryophytes and cyanobacterial lichens (but higher densities of green algal lichens). Measurements of bryophyte biomass density measured on the Discovery tree (Heffernan 2017) also follow this pattern. There are multiple factors which may be involved in determining patterns of epiphyte density, including dispersal limitations, frost tolerances, and light exposure - further study would be needed to establish the carbon penalty of dormancy and resurrection as well as diurnal patterns of carbon assimilation while wet to determine when wetting “pays off” and when it results in a net negative carbon balance for a given species of epiphyte. We expect that relatively short wetting periods that occur mostly at night (dew, top of canopy; Csintalan et al. 2000) are likely to be less advantageous than longer wetting that persists through the day (rain, lower canopy). However, desert lichens which subsist primarily on fog and dew water as opposed to rain take advantage of the narrow window in the early morning when tissue hydration and photon flux density are conducive to photosynthesis (Lange et al. 2006), demonstrating that net positive carbon balance can be maintained in this way by some organisms.

#### ***2.3.4 The dry season***

In the dry season, dewfall takes over as the predominant source of canopy wetting both in frequency of events (Table 3d) and proportion of wetting (Figure 5). According to our season boundary finding criteria the dry seasons of 2017 - 2020 lasted 80, 101, 98 and 76 days (Table

4). For comparison, the dry seasons of 2017 and 2020 were within one standard deviation of the long-term mean season length (78 days), while 2018 and 2019 were  $> 1.3$  standard deviations above the mean. Through the four dry seasons of our study, dewfall occurred on at least one canopy level on 32.5%, 26.7%, 29.6% and 25% of nights. Across years, the average duration of a dew event at the top of the canopy was 3.3 hr (SD 3.3). Dewfall was restricted primarily to the 56 m and 40 m sensor heights, which resulted in more time spent wet at the top of the canopy (3.8%, SD 2.1) than at the forest floor (1.2%, SD 2.3), a reversal of the pattern seen in all other seasons (Table 1). Following on the discussion of wetness stability from section 4.3, the middle and lower canopy layers continue to be more stable than the top of the canopy – from bottom to top 5, 8, 8, 8, 12 and 32 average transitions per season.

Dew events in the dry season were shorter and had more separation from adjacent wetting than in other seasons, making it possible to look more in-depth at the timing of individual events and the meteorological conditions on dewy and dry nights. Dew formed universally at night and ranged in starting hour from shortly after sundown to briefly before sunrise (Figure 6a). For the 70% of dew events that lasted past sunrise, some dried immediately, one event took 6 hours to dry, and average time to dry was 1.4 hours (SD 1.0). Examination of meteorological conditions during dew forming periods in the dry season and on non-dew nights (see section 2.5) revealed that observed net radiation and wind speed values were relatively similar in their distributions across dew and non-dew nights, while the distributions of observed dewpoint depression were distinctly different (Figure 7). The distribution of  $R_{\text{net}}$  values on dry nights was bimodal, with peaks at  $\sim -50 \text{ W m}^{-2}$  and  $-10 \text{ W m}^{-2}$ , the later likely corresponding to cloudy conditions. Cloudy skies at night enhance the local greenhouse effect which results in slower surface cooling and mildly negative  $R_{\text{net}}$  values, which at our site resulted in insufficient surface cooling for dew formation

to occur in almost all cases. Outside of relatively rare cloudy dry season nights are the much more frequent clear nights, where there is little distinction in the distributions of  $R_{\text{net}}$  values between dry and dewy nights (Figure 7). Most dew formation happened when DPD was  $< 1^{\circ}\text{C}$ , while DPD ranged above  $12^{\circ}\text{C}$  on dry nights and was rarely  $< 1^{\circ}\text{C}$ . Wind speed distributions are indistinguishable between dew and non-dew nights and largely represent still conditions ( $< 1 \text{ m s}^{-1}$ ). Put simply, the majority of dry season nights appear to be sufficiently still and have sufficiently negative net radiation to promote dewfall, with DPD acting as the determining factor.

This general observation is supported by the results of the logistic models applied to summer night data (Table 5).  $R^2$  values for  $R_{\text{net}}$  and Wind Speed indicate the relative inability of these variables to explain the variance in dewfall observations, while DPD alone can explain 87% of the variance and had an AUC value of 0.994, indicating strong separation between Dew and Non-dew observations using DPD. The model based on RH performed similarly well, which is expected given that both DPD and RH capture the degree of saturation of the air in slightly different ways. Compared to the one-term, DPD model, a three variable model involving all the examined predictors ( $\text{Dew} \sim \text{DPD} + R_{\text{net}} + \text{Windspeed}$ ) had only a marginally better  $R^2$  of 0.9 and an AUC of 0.997. As the one-term DPD based model was more parsimonious we chose to show the results of applying the DPD model with a probability threshold of 0.5 to the summer of 2017 in Figure 5c (summers of 2018-2020 in Supplemental Figures 4-6) to illustrate the efficacy of this method in capturing the timing and duration of dew events compared to the Penman method (fig 5b), which produced a high rate of false positive classifications. The logistic DPD model produced far fewer false positives when using a probability threshold of 0.5, which corresponds with a threshold of  $\sim 1^{\circ}$  dewpoint depression. On the five-minute scale, across all

years Penman predicted 1.39 times as many dew forming intervals as actually occurred and missed 29% of true dew accumulating intervals, while Logistic DPD yielded a 23% false positive rate and missed 11% of true dew intervals (Table 6). On the daily scale and asking whether each method correctly predicts greater than or less than one hour of dew formation in a day, Penman improved to 0.93 times overprediction and 5% missed mornings, while Logistic DPD accuracies remain virtually unchanged (Table 6). Of the mornings where dew formation is correctly predicted as being > 1hr, the logistic model does a better job of capturing the true event length, with a root-mean square error of 0.8 hr vs. 1.2 hr with Penman. One notable advantage to the Penman model is that it returns a predicted rate of dew accumulation, however, in this study predicted rates were roughly ten times greater than observed rates calculated from depth estimates from the 56 m LWS. While more in line with the expected 0 - 0.07 mm hr<sup>-1</sup> range (Monteith and Unsworth 2013), accumulation rates from the LWS are also subject to a fair degree of uncertainty owing to complications in the conversion of sensor mV to dew depth (section 2.4), making it unfruitful to compare Penman predictions to LWS measured rates of accumulation. In the realm of binary prediction of dew / no dew, the logistic model outperformed Penman at both the five minute and daily timescales and has the added benefit of being tunable; by adjusting the probability threshold used to create a dew / no dew classification, one can increase or decrease the ratio of false positives to false negatives to suit a given application. Also of note, applying the Penman and the logistic DPD models to data collected at the nearby PRIMET weather station resulted in far worse prediction accuracies compared to the in-tree data (Table 6), highlighting the importance of closely co-located microclimate measurements in the prediction of dew accumulation.

The results of our classification exercise drive home the importance of dewpoint depression in determining whether dewfall occurs on a given clear-sky night in the dry season at our site. Intuitively one would expect higher relative humidity and lower nighttime DPD after rain events and early in the season, when residual moisture from spring rains has not left the stand. While this phenomenon can be seen (Figure 8), it is hardly the rule - dewfall that happened more than five days since the last registered rainfall made up 61.6 % of all dew events (Figure 8a), and 63.6 % of events happened when seasonal cumulative Precip-PET was at least  $-300\text{mm}$  (Figure 7b). These numbers suggest that a large proportion of summer dewfall is driven by meteorological conditions not related to recent delivery of aboveground moisture, which is corroborated by the specific humidity (SH) and  $T_{\text{air}}$  histograms in Figure 7 and regression results in Table 5. Specific humidity and  $T_{\text{air}}$  are the two determinants of dewpoint depression and viewing them independently provides a clue as to which influence, air cooling or an increase in specific water vapor content, is responsible for  $\text{DPD} < 1^\circ\text{C}$  and the occurrence of dewfall. The histograms for these two variables show greater overlap in SH between dew and non-dew periods than in  $T_{\text{air}}$ , while the  $T_{\text{air}}$  logistic model yields a much higher  $R^2$  and AUC than the SH model. As far as  $T_{\text{air}}$  and SH can be viewed independently, it appears that air cooling determines when dew occurs more than an increase in SH – in fact, there is no clear evidence that SH is higher on dew nights than on non-dew nights.

The driver of enhanced air cooling in our study area is an open question and merits further investigation. Two possible drivers are cold air pooling in the valley in which the Discovery tree stands and synoptic scale changes in wind patterns. Cold air pooling events occur much more frequently than the formation of dewfall in the summer months in the Andrews forest (Rupp et al. 2020), meaning that the strength of the pooling, the depth of the cold air pool, and the drivers

of particularly cold events would merit investigation. In the case of synoptic scale influences, determining the drivers of dewfall would require a more complete understanding of how weather is “delivered” to the Andrews forest, which could be gained by analyzing regional scale reanalysis data. One potential determinant of dewfall may be the strength of the westerly winds, which bring relatively cooler, more humidified air to the Western cascades from above the Pacific Ocean, in contrast to Easterly winds, which bring drier, warmer, continental air masses to the forest. Pinning down the larger scale mechanisms responsible for dry season dewfall will be important for assessing how observed and predicted changes at the regional scale will impact canopy hydration in the future. In the following section, we evaluate the potential for leaf water uptake by Douglas-fir late in the dry season to further interrogate the role of dew in canopy hydration.

### ***2.3.5 Dew uptake experiment***

The influence of leaf water uptake (LWU) of simulated dewfall on leaf water status was observed directly on the Discovery Tree. After dewfall was simulated at 4:10 am on August 26<sup>th</sup> (morning of first experiment), a significant difference in shoot water potential was observed between sprayed and control branches in the first period after spraying (Figure 9a,  $p = 0.02$ ), but not in any subsequent periods. On August 28<sup>th</sup> (second experiment morning), no significant differences were observed at any timepoints. An independent set of branches was chosen on the second morning roughly one meter above the first day branches, and pre-spray  $\Psi_{\text{Leaf}}$  were less negative on the second night than on the first. One possible explanation for why uptake appears to have happened the first morning and not the second is that day-to-day variation in pre-dawn water potential ( $\Psi_{\text{PD}}$ ) may have had an impact on the uptake mechanism. More work is needed to assess the importance of the  $\Psi$  gradient between intercellular and surface water (Berry et al.

2018), and whether it plays a role in moving water through the uptake pathway. The nature of the uptake pathway in different plant species is an area of open exploration (Berry et al. 2018).

Whether the primary mode of uptake is via abraded areas of the waxy cuticle, direct diffusion through partially open stoma, or wicking of water through stoma by the hyphae of endophytic fungi will determine how important  $\Psi_{\text{Leaf}}$  at the time of dew accumulation is.

On the first morning, relative water content of foliage increased by 1.52% on sprayed foliage and declined by 1.25% in control foliage between 4:10 and 7:50 am (for a net difference of 2.77%). A rough estimate of the percent of sprayed water that was taken up to explain these changes in RWC can be made using the ratio of turgid-to-dry weights across our samples (2.26), leaf mass per area of Douglas-fir foliage ( $84.03 \text{ g m}^{-2}$ , Berner and Law 2016), and our estimate of  $40.5 \text{ g m}^{-2}$  of water sprayed on the foliage. If we assume that only the 1.52% change in RWC in treatment foliage was caused by LWU, the foliage took up 3.98% of the sprayed water. If on the other hand we assume that treatment RWC would have declined as much as the control and that uptake was offsetting that difference as well, then the uptake percentage is 7.25%. The data from the second morning showed a 0.5% increase in RWC in the treatment branches and a 1.0% decrease in control branches, yielding an estimate of 1.9 – 5.7 % uptake of sprayed water. In the case of the first night, a relatively small amount of sprayed water was taken up, with the majority dripping off or evaporating. It should be noted that in spraying we added water to foliage all at once, while most observed dew formation in this study happened gradually over the course of an hour or longer. Depending on the underlying mechanism, a more realistic conception of uptake may be that as dew is gradually and continuously deposited on a leaf surface, the water is gradually and continuously taken up.

It is of interest that despite testing for foliar water uptake late in the 2020 dry season, evidence suggests that  $\Psi_{\text{soil}}$  was not so negative that upper canopy foliage was experiencing significant stress from soil water deficits.  $\Psi_{\text{PD}}$  for the sampled groups ranged between -1.04 and -1.51 MPa. Taking out gravitational  $\Psi$  of 0.56 MPa for foliage sampled 56 m a.g.l. indicates that minimum integrated  $\Psi_{\text{soil}}$  was between -0.48 and -0.95 MPa at the time of sampling, generally above what would be expected to result in low early morning stomatal conductance ( $g_s$ ).  $g_s$  values through the morning on both days corroborate the supposition that foliage had adequate access to soil water to support relatively unimpaired  $g_s$  (Fig 9c-d). It is possible that the dry season of 2020 was relatively less dry than usual, as it started later than in the other years of our record due to rainfall in late June (Table 3). It is also possible that this tree has access to deep soil moisture that minimizes water stress despite drying in the upper soil column. At one meter depth at the PRIMET station it is clear that minimum VWC is  $\sim 0.06$ , and that by the end of most dry seasons VWC reaches or is within 5% of this minimum (Figure 3). However, it is not clear whether VWC declines to a minimum by the end of the dry season at the 1 m deep sensor that is located adjacent to the Discovery Tree, and the roots of the tree may well extend 2 m or more below ground (Brooks et al. 2002). While this tree sits on an alluvial terrace with potential deep soil moisture and is in a valley bottom where water vapor may return at night after it has been advected upslope in the day (Rupp 2020), trees in different topographic positions, such as on ridge tops, may experience very different water stress from lack of adequate soil moisture late in the dry season or enhanced drying throughout the dry season. Future work should investigate late dry season  $\Psi_{\text{leaf}}$  and LWU across contrasting topographic positions to assess whether observed quantities of LWU have an inverse relationship with  $\Psi_{\text{leaf}}$  (greater LWU at lower  $\Psi_{\text{leaf}}$ ).

## 2.4 Conclusions

In this study we observed patterns of canopy wetting in an old-growth temperate wet forest across four annual cycles and put observed patterns in the context of the long-term record. We found that dewfall was a frequent source of canopy wetting across the dry season, even in dry seasons that lasted 23 days longer than the long-term mean. Our results suggest that dew formation in this system will be most sensitive to future changes in nighttime cooling of the air, with a tipping point of  $\sim 1^\circ\text{C}$  dewpoint depression required for dew to form. Uptake of summer dew by canopy foliage was demonstrated, though further investigation will be needed to establish the relationship between  $\Psi_{\text{Leaf}}$  and amount of LWU at the time of dewfall. More investigation is also needed to understand how patterns of soil moisture availability and canopy microclimate across the landscape may interact to determine the importance of LWU for individual trees in the forest.

## 2.5 References

- Agam, N., Berliner, P.R., 2006. Dew formation and water vapor adsorption in semi-arid environments—A review. *Journal of Arid Environments* 65, 572–590.  
<https://doi.org/10.1016/j.jaridenv.2005.09.004>
- Berkelhammer, M., Hu, J., Bailey, A., Noone, D.C., Still, C.J., Barnard, H., Gochis, D., Hsiao, G.S., Rahn, T., Turnipseed, A., 2013. The nocturnal water cycle in an open-canopy forest: NOCTURNAL FOREST WATER. *J. Geophys. Res. Atmos.* 118, 10,225–10,242.  
<https://doi.org/10.1002/jgrd.50701>
- Berner, L.T., Law, B.E., 2016. Plant traits, productivity, biomass and soil properties from forest sites in the Pacific Northwest, 1999–2014. *Scientific Data* 3, 160002.  
<https://doi.org/10.1038/sdata.2016.2>
- Berry, Z.C., Emery, N.C., Gotsch, S.G., Goldsmith, G.R., 2018. Foliar water uptake: Processes, pathways, and integration into plant water budgets: Foliar Water Uptake. *Plant Cell Environ* 42, 410–423. <https://doi.org/10.1111/pce.13439>

- Burgess, S.S.O., Dawson, T.E., 2004. The contribution of fog to the water relations of *Sequoia sempervirens* (D. Don): foliar uptake and prevention of dehydration. *Plant Cell Environ* 27, 1023–1034. <https://doi.org/10.1111/j.1365-3040.2004.01207.x>
- Brooks, J.R., Meinzer, F.C., Coulombe, R., Gregg, J., 2002. Hydraulic redistribution of soil water during summer drought in two contrasting Pacific Northwest coniferous forests. *Tree Physiology* 22, 1107–1117. <https://doi.org/10.1093/treephys/22.15-16.1107>
- Campbell, J.L., Rustad, L.E., Porter, J.H., Taylor, J.R., Dereszynski, E.W., Shanley, J.B., Gries, C., Henshaw, D.L., Martin, M.E., Sheldon, W.M., Boose, E.R., 2013. Quantity is Nothing without Quality: Automated QA/QC for Streaming Environmental Sensor Data. *BioScience* 63, 574–585. <https://doi.org/10.1525/bio.2013.63.7.10>
- Csintalan, Z., Takacs, Z., Proctor, M.C.F., Nagy, Z., Tuba, Z., 2000. Early morning photosynthesis of the moss *Tortula ruralis* following summer dew fall in a Hungarian temperate dry sandy grassland. *Plant Ecology* 151: 51 – 54.
- Daly, C.; McKee, W. 2019. Meteorological data from benchmark stations at the Andrews Experimental Forest, 1957 to present. Long-Term Ecological Research. Forest Science Data Bank, Corvallis, OR. [Database]. Available: <http://andlter.forestry.oregonstate.edu/data/abstract.aspx?dbcode=MS001> (5 November 2019) DOI:<http://dx.doi.org/10.6073/pasta/c96875918bb9c86d330a457bf4295cd9>.
- Daly C, Smith JW, Smith JI, McKane RB. 2007. High-resolution spatial modeling of daily weather elements for a catchment in the Oregon Cascade Mountains, United States. *Journal of Applied Meteorology and Climatology*, 46(10): 1565–1586. <https://doi.org/10.1175/JAM2548.1>
- Davis, K.T., Dobrowski, S.Z., Holden, Z.A., Higuera, P.E., Abatzoglou, J.T., 2019. Microclimatic buffering in forests of the future: the role of local water balance. *Ecography* 42, 1–11. <https://doi.org/10.1111/ecog.03836>
- Dawson, T.E., Goldsmith, G.R., 2018. The value of wet leaves. *New Phytol* 219, 1156–1169. <https://doi.org/10.1111/nph.15307>
- De Frenne, P., Rodriguez-Sanchez, F., Coomes, D.A., Baeten, L., Verstraeten, G., et al. 2013. Microclimate moderates plant responses to macroclimate warming. *Proceedings of the National Academy of Sciences* 110, 18561–18565. <https://doi.org/10.1073/pnas.1311190110>
- Ehbrecht, M., Schall, P., Ammer, C., Seidel, D., 2017. Quantifying stand structural complexity and its relationship with forest management, tree species diversity and microclimate. *Agricultural and Forest Meteorology* 242, 1–9. <https://doi.org/10.1016/j.agrformet.2017.04.012>
- Frey, S.J.K., Hadley, A.S., Johnson, S.L., Schulze, M., Jones, J.A., Betts, M.G., 2016. Spatial models reveal the microclimatic buffering capacity of old-growth forests. *Sci. Adv.* 2, e1501392. <https://doi.org/10.1126/sciadv.1501392>

- Greve, P., Orlowsky, B., Mueller, B., Sheffield, J., Reichstein, M., Seneviratne, S.I., 2014. Global assessment of trends in wetting and drying over land. *Nature Geosci* 7, 716–721. <https://doi.org/10.1038/ngeo2247>
- Heffernan, E. 2017. Canopy microclimates and epiphytes: Examining dynamic patterns and influences. Oregon State University, Masters thesis. [https://ir.library.oregonstate.edu/concern/graduate\\_thesis\\_or\\_dissertations/t722hf886?locale=en](https://ir.library.oregonstate.edu/concern/graduate_thesis_or_dissertations/t722hf886?locale=en)
- Johnson, D. W.; Cole, D. W.; Bledsoe, C. S. et al. 1982. Nutrient cycling in forests in the Pacific Northwest. In: Edmonds, R. L., ed. *Analysis of coniferous forest ecosystems in the Western United States*. US/IBP Synthesis Ser 14. Stroudsburg, PA: Hutchinson Ross Publishing Co.: Chapter 7.
- Lakatos, M., Obregón, A., Büdel, B., Bendix, J., 2012. Midday dew - an overlooked factor enhancing photosynthetic activity of corticolous epiphytes in a wet tropical rain forest. *New Phytologist* 194, 245–253. <https://doi.org/10.1111/j.1469-8137.2011.04034.x>
- Lange, O.L., Allan Green, T.G., Melzer, B., Meyer, A., Zellner, H., 2006. Water relations and CO<sub>2</sub> exchange of the terrestrial lichen *Teloschistes capensis* in the Namib fog desert: Measurements during two seasons in the field and under controlled conditions. *Flora - Morphology, Distribution, Functional Ecology of Plants* 201, 268–280. <https://doi.org/10.1016/j.flora.2005.08.003>
- Limm, E.B., Simonin, K.A., Bothman, A.G., Dawson, T.E., 2009. Foliar water uptake: a common water acquisition strategy for plants of the redwood forest 11.
- Liu, M., Cen, Y., Wang, C., Gu, X., Bowler, P., Wu, D., Zhang, L., Jiang, G., Beysens, D., 2020. Foliar uptake of dew in the sandy ecosystem of the Mongolia Plateau: A life-sustaining and carbon accumulation strategy shared differently by C3 and C4 grasses. *Agricultural and Forest Meteorology* 287, 107941. <https://doi.org/10.1016/j.agrformet.2020.107941>
- McCune, B., 1993. Gradients in Epiphyte Biomass in Three *Pseudotsuga-Tsuga* Forests of Different Ages in Western Oregon and Washington. *The Bryologist* 96, 405. <https://doi.org/10.2307/3243870>
- McCune, B., Rosentreter, R., Ponzetti, J.M., Shaw, D.C., 2000. Epiphyte Habitats in an Old Conifer Forest in Western Washington, U.S.A. *The Bryologist* 103, 417–427. [https://doi.org/10.1639/0007-2745\(2000\)103\[0417:EHIAOC\]2.0.CO;2](https://doi.org/10.1639/0007-2745(2000)103[0417:EHIAOC]2.0.CO;2)
- McMahon, T.A., Peel, M.C., Lowe, L., Srikanthan, R., McVicar, T.R., 2013. Estimating actual, potential, reference crop and pan evaporation using standard meteorological data: a pragmatic synthesis. *Hydrology and Earth System Sciences* 17, 1331–1363. <https://doi.org/10.5194/hess-17-1331-2013>

- Miralles, D.G., Gash, J.H., Holmes, T.R.H., de Jeu, R.A.M., Dolman, A.J., 2010. Global canopy interception from satellite observations. *J. Geophys. Res.* 115, D16122. <https://doi.org/10.1029/2009JD013530>
- Monteith, J.L., Unsworth, M.H., 2013. *Principles of environmental physics: plants, animals, and the atmosphere*, 4th ed. ed. Elsevier/Academic Press, Boston, MA.
- Nobel P.S. 1991. *Physicochemical and Environmental Physiology*. Academic Press, San Diego, CA.
- Parker, G.G., Davis, M.M., Chapotin, S.M., 2002. Canopy light transmittance in Douglas-fir-western hemlock stands. *Tree Physiology* 22, 147–157. <https://doi.org/10.1093/treephys/22.2-3.147>
- Pincebourde, S., Casas, J., 2015. Warming tolerance across insect ontogeny: influence of joint shifts in microclimates and thermal limits. *Ecology* 96, 986–997. <https://doi.org/10.1890/14-0744.1>
- Priestley, C.H.B. and Taylor, R.J. On the Assessment of Surface Heat Flux and Evaporation Using Large-Scale Parameters. *Monthly Weather Review* 100, 81-92.
- Proctor, M.C.F., Oliver, M.J., Wood, A.J., Alpert, P., Stark, L.R., Cleavitt, N.L., Mishler, B.D., 2007. Desiccation-tolerance in bryophytes: a review. *The Bryologist* 110, 595–621. [https://doi.org/10.1639/0007-2745\(2007\)110\[595:DIBAR\]2.0.CO;2](https://doi.org/10.1639/0007-2745(2007)110[595:DIBAR]2.0.CO;2)
- Pypker, T.G., Unsworth, M.H., Bond, B.J., 2006. The role of epiphytes in rainfall interception by forests in the Pacific Northwest. II. Field measurements at the branch and canopy scale. *Canadian Journal of Forest Research* 36, 819–832. <https://doi.org/10.1139/x05-286>
- Pypker, T.G., Unsworth, M.H., Van Stan, J.T., Bond, B.J., 2017. The absorption and evaporation of water vapor by epiphytes in an old-growth Douglas-fir forest during the seasonal summer dry season: Implications for the canopy energy budget: Impact of epiphytes on the canopy hydrology of Douglas-fir forests. *Ecohydrology* 10, e1801. <https://doi.org/10.1002/eco.1801>
- Ritter, F., Berkelhammer, M., Beysens, D., 2019. Dew frequency across the US from a network of in situ radiometers. *Hydrol. Earth Syst. Sci.* 20.
- Rupp, D.E., Shafer, S.L., Daly, C., Jones, J.A., Frey, S.J.K., 2020. Temperature Gradients and Inversions in a Forested Cascade Range Basin: Synoptic- to Local-Scale Controls. *J. Geophys. Res. Atmos.* 125. <https://doi.org/10.1029/2020JD032686>
- Rutter, A.J., Morton, A.J., Robins, P.C., 1975. A Predictive Model of Rainfall Interception in Forests. II. Generalization of the Model and Comparison with Observations in Some Coniferous and Hardwood Stands. *The Journal of Applied Ecology* 12, 367. <https://doi.org/10.2307/2401739>

- Scholander, P.F., Bradstreet, E.D., Hemmingsen, E.A., Hammel, H.T., 1965. Sap Pressure in Vascular Plants: Negative hydrostatic pressure can be measured in plants. *Science* 148, 339–346. <https://doi.org/10.1126/science.148.3668.339>
- Sheldon, W.M., 2008. Dynamic, Rule-based Quality Control Framework for Real-time Sensor Data ([http://gcelter.marsci.uga.edu/public/im/tools/data\\_toolbox.htm](http://gcelter.marsci.uga.edu/public/im/tools/data_toolbox.htm)).
- Storlie, C., Merino-Viteri, A., Phillips, B., VanDerWal, J., Welbergen, J., Williams, S., 2014. Stepping inside the niche: microclimate data are critical for accurate assessment of species' vulnerability to climate change. *Biol. Lett.* 10, 20140576. <https://doi.org/10.1098/rsbl.2014.0576>
- Thomas, C.K., Smoot, A.R., 2013. An Effective, Economic, Aspirated Radiation Shield for Air Temperature Observations and Its Spatial Gradients. *Journal of Atmospheric and Oceanic Technology* 30, 526–537. <https://doi.org/10.1175/JTECH-D-12-00044.1>
- Tomaszkiewicz, M., Abou Najm, M., Beysens, D., Alameddine, I., El-Fadel, M., 2015. Dew as a sustainable non-conventional water resource: a critical review. *Environ. Rev.* 23, 425–442. <https://doi.org/10.1139/er-2015-0035>
- Van Pelt, R., and North, M.P., 1996. Analyzing Canopy Structure in Pacific Northwest Old-Growth Forests with a Stand-Scale Crown Model. *Northwest Science* 70, 15 – 30.
- von Arx, G., Graf Pannatier, E., Thimonier, A., Rebetez, M., 2013. Microclimate in forests with varying leaf area index and soil moisture: potential implications for seedling establishment in a changing climate. *J Ecol* 101, 1201–1213. <https://doi.org/10.1111/1365-2745.12121>
- Waring, R. H. and Franklin, J. F. 1979. Evergreen Coniferous Forests of the Pacific Northwest. *Science* 204, 1380–1386

## 2.6 Acknowledgements

Data and facilities were provided by the HJ Andrews Experimental Forest and the Long Term Ecological Research (LTER) program, administered cooperatively by the USDA Forest Service Pacific Northwest Research Station, Oregon State University, and the Willamette National Forest. This material is based upon work supported by the National Science Foundation under the following Grants: LTER8 DEB-2025755 (2020-2026) and LTER7 DEB-1440409 (2012-2020)."

## 2.7 Figures

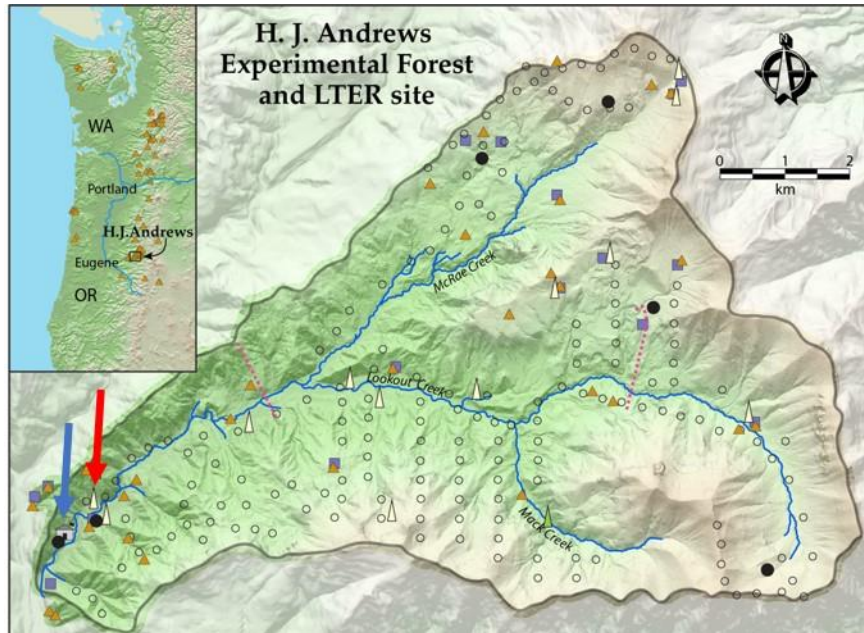


**Figure 2-1: Site map**

Map of the H.J. Andrews Experimental Forest, with the position of the instrumented tree marked with a red arrow. The blue arrow indicates the location of the meteorological station where net radiation and precipitation were measured.

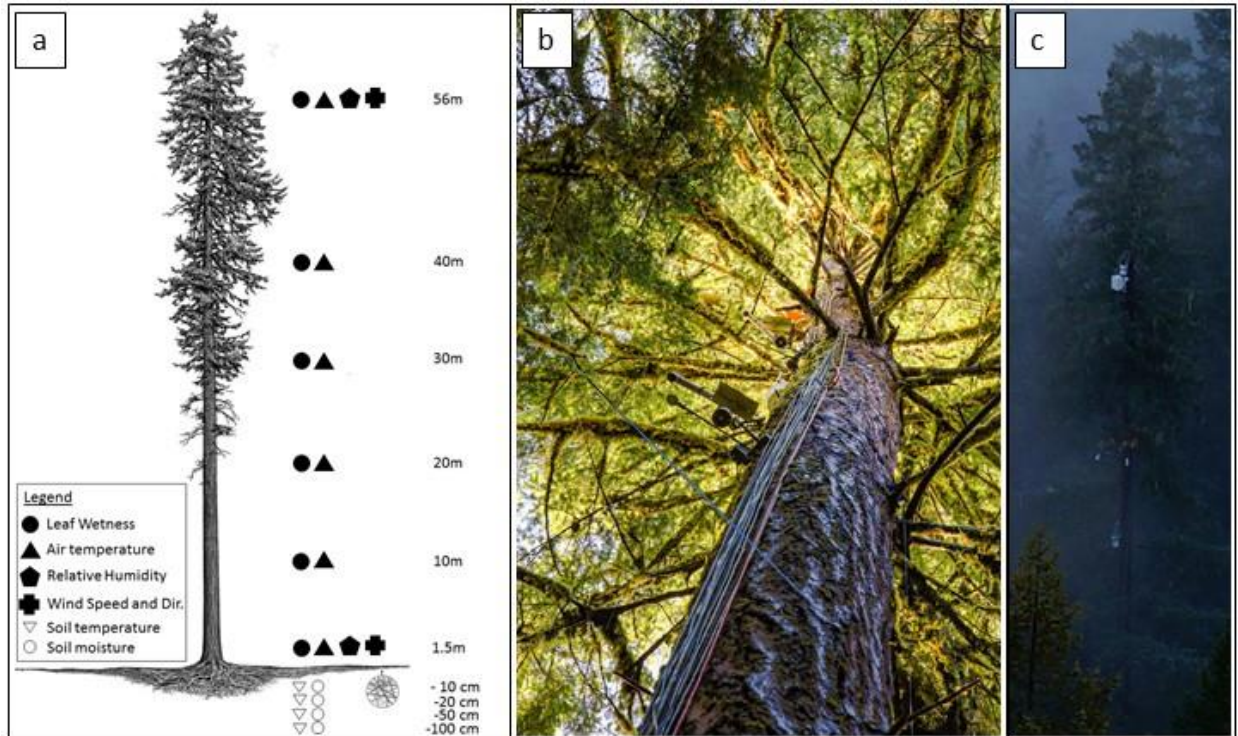


**Figure 2-2: Depiction of Discovery Tree Instruments**

a) Illustration of the measurement tree, measurement heights within the tree, and the variables recorded at each height (illustration by Robert Van Pelt). b) View of the instrument clusters at 20 and 30 meters above ground (photo credit Leah Wilson). c) View of the upper 30 meters of the tree. The white instrument enclosure in the photo is at 56 meters a.g.l. (photo credit Adam Sibley).

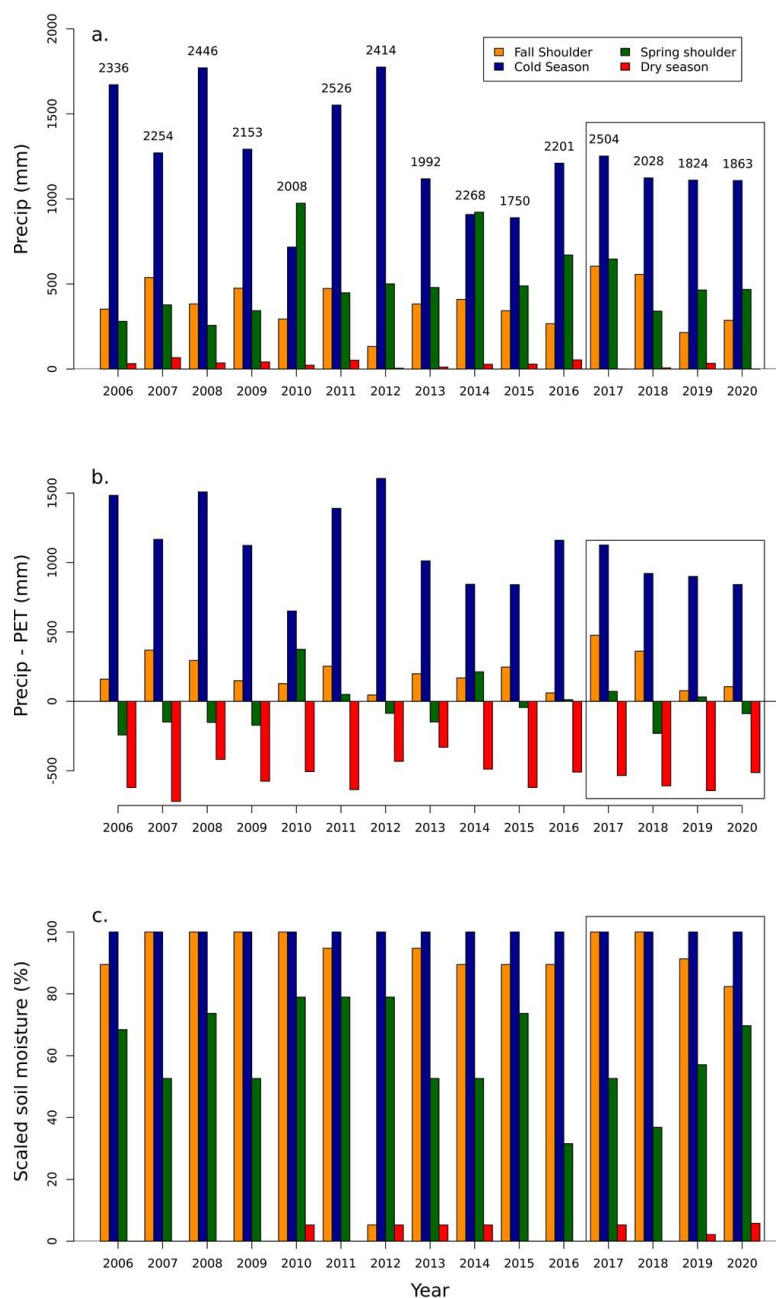


**Figure 2-3: Water Availability 2006 – 2020**

Water availability in the water years 2006 to 2020, which have been divided into seasons using the methods described in section 2.6. a. Total rainfall values within season. Numbers above each group of bars indicate total annual rainfall in mm. b. Total precipitation minus PET within each season. c. remaining soil moisture at the end of each season, scaled between field capacity (0.25) and the observed minimum over the extant record (0.06).

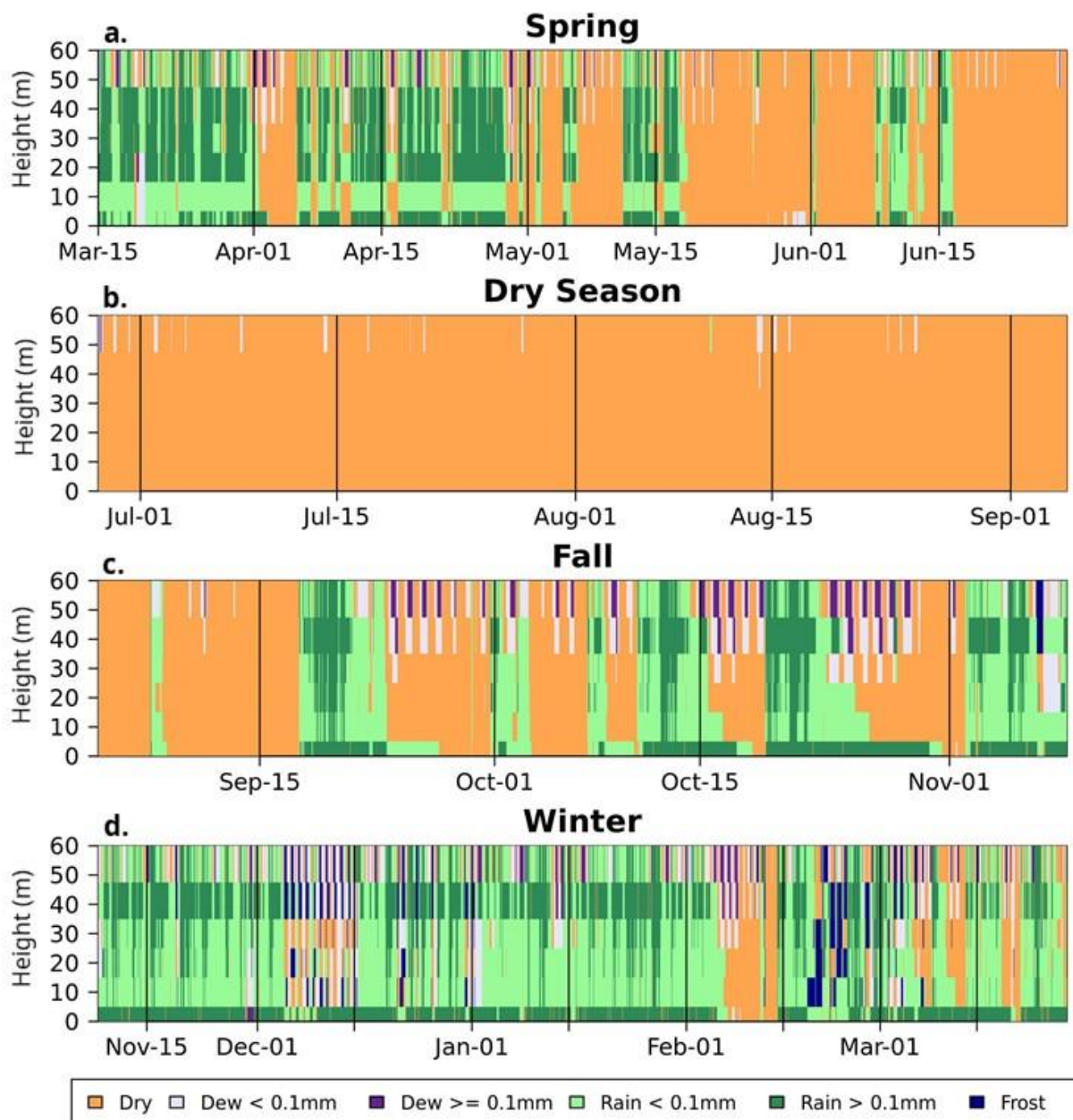


**Figure 2-4: Annual wetting patterns**

Wetting by height for the (a) spring, (b) dry season, (c) fall and (d) winter seasons of 2017. Wetness sensors were located at 1.5, 10, 20, 30, 40 and 56m in the canopy. Data from these sensors were converted to color bars representing intervals from 0-5 m, 5 – 15 m, 15 – 25 m, 25 – 35m, 35 – 45m, and 45 – 60 m.

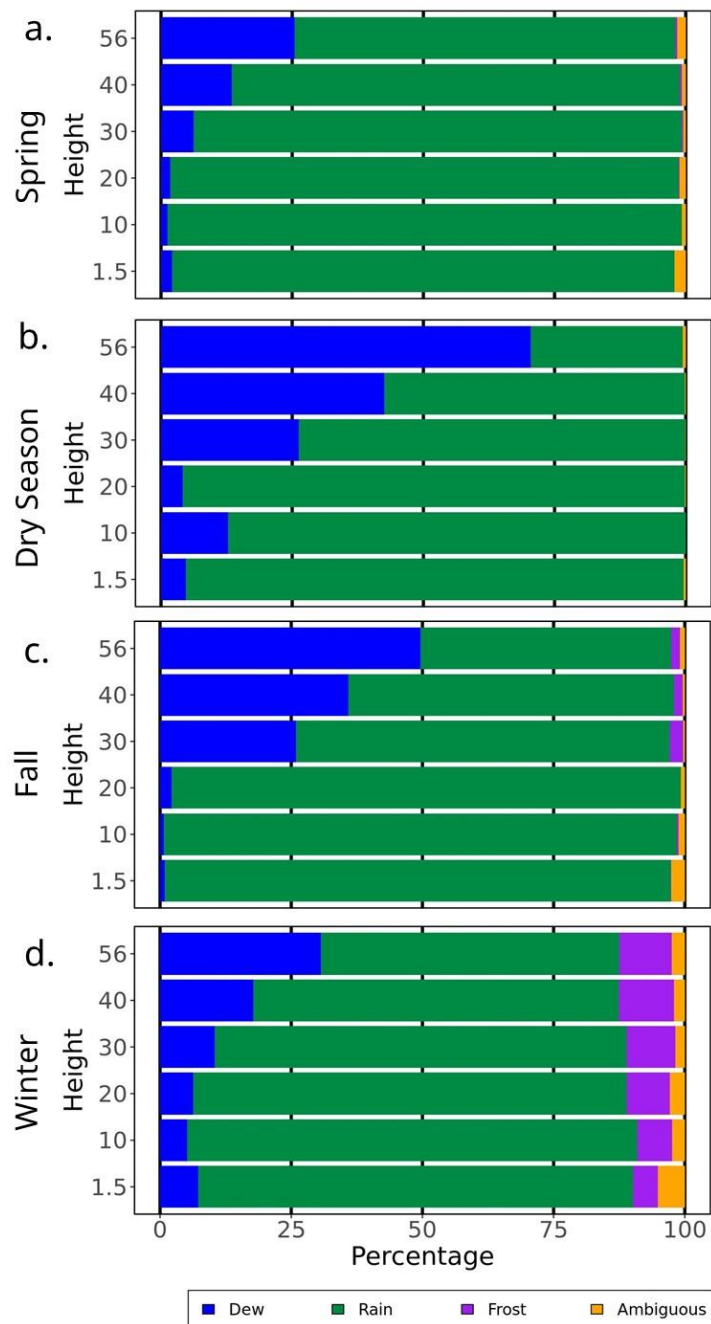


**Figure 2-5: Wetting patterns by type**

Contributions to canopy wetness by type for each season across the years 2017 - 2020. Percentages are based on time spent wet (i.e., not the percent of time that sensors were wetted by each phenomenon, as that varied dramatically across seasons).

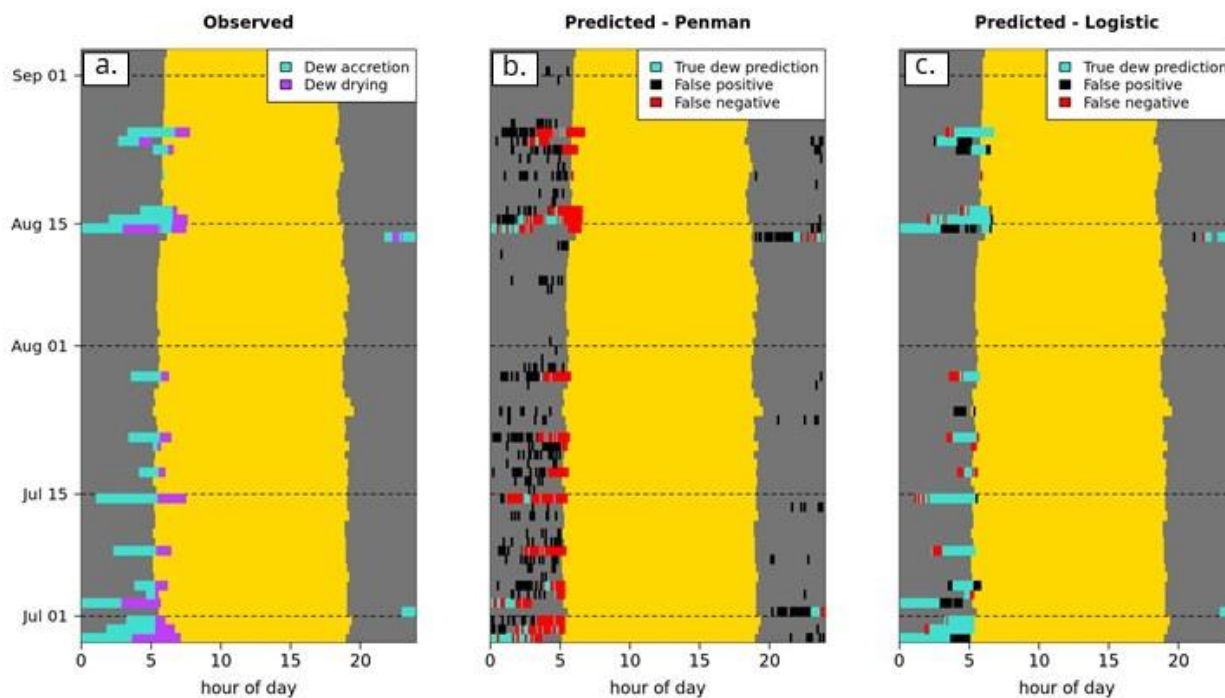


**Figure 2-6: Diurnal patterns of dew formation and drying at top of canopy**

Observed and predicted dew accretion and drying during the dry season of 2017 (see supplemental figures for 2018, 2019 and 2020). Transition between night and day denoted in all panels using gray and yellow background colors (day defined as  $> 10 \text{ W m}^{-2}$  incident solar radiation). Panel a shows observed intervals of dew accretion and dew drying through the season. Panel b shows dew accretion as predicted by the Penman equation, where  $LE < 0 \text{ mm}$  is classified as a dew forming period. Panel b shows dew accretion as predicted using a logistic function with dewpoint depression as a predictor and a probability threshold of 0.5. False positives indicate where dewfall was predicted but not observed. False negatives indicate where dewfall was not predicted, but it was observed.

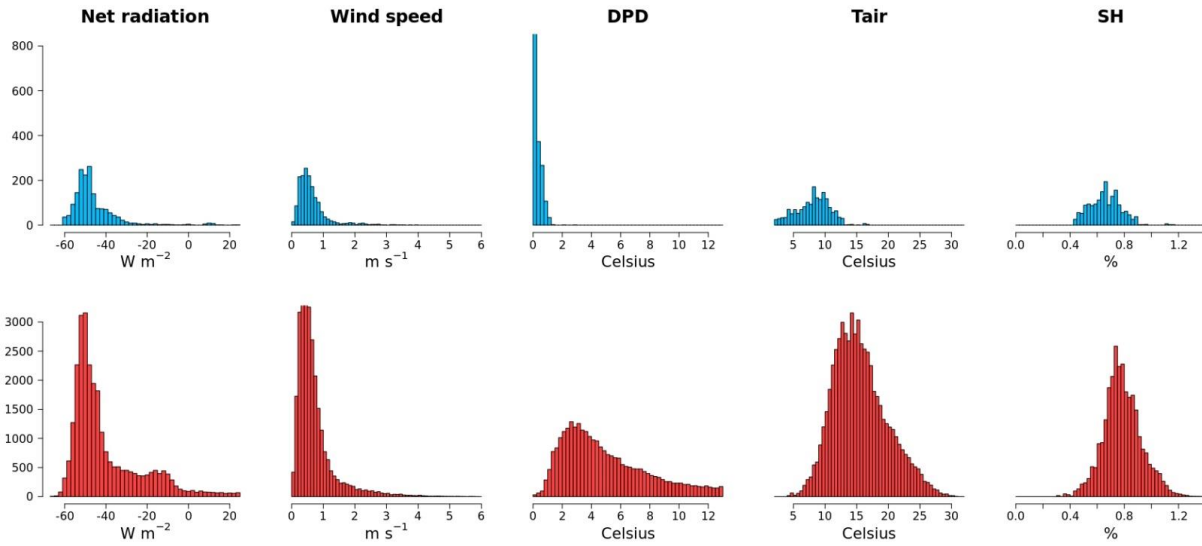


**Figure 2-7: Dew predictor histograms**

Histograms of observed net radiation, wind speed, dewpoint depression (DPD), air temperature ( $T_{\text{air}}$ ) and Specific Humidity (SH) during periods of dew formation (top row) and from mornings (midnight to 6am) where no dew formed (bottom row) during the dry seasons of 2017-2020.

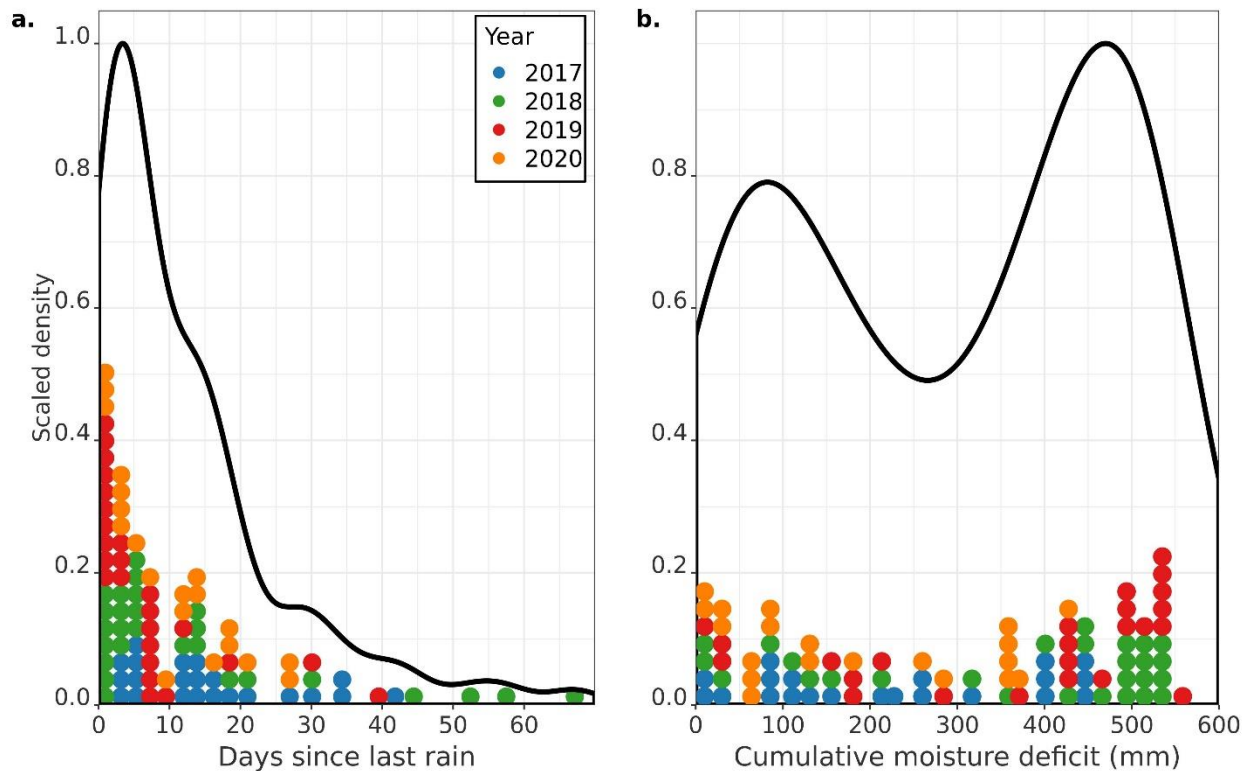


**Figure 2-8: Kernel density plots of dew occurrence**

Frequency of dew events relative to the number of days since the most recent rain event (a), and the cumulative moisture deficit since the beginning of the dry season (b). Filled circles along the x-axis each represent one event within a given bin, where bin sizes are 2 and 20 for panel a and b respectively. Continuous density functions (black line) were determined by pooling all points across years and applying a gaussian kernel density estimate.

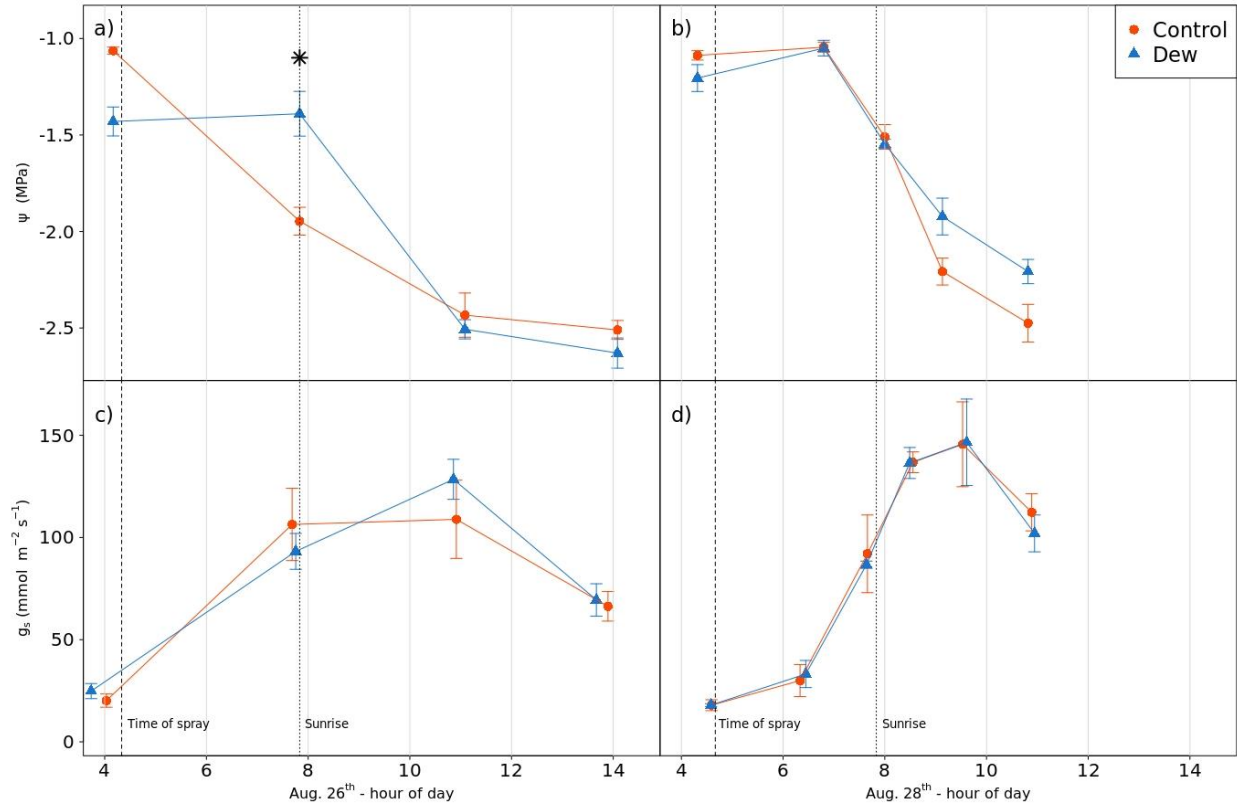


**Figure 2-9: Results of dew uptake experiment**

Panels a and b show average shoot water potentials (MPa) sampled at different timepoints on sprayed (“Dew”) and unsprayed (“Control”) branches on the two sampling days. Panels c and d show average stomatal conductance values ( $\text{mmol m}^{-2} \text{s}^{-1}$ ). All error bars represent one standard error. The star symbol denotes a timepoint where the Dew and Control groups are significantly different at the  $p < 0.05$  level.

## 2.8 Tables

**Table 2-1: Percent of time spent wet each season, by height**

Percent of time that each canopy layer spends wet or dry on an annual basis and within the four seasons of the year. Statistics were calculated using all data from 2017 – 2020. Values represent the mean percentage across years, and values in parenthesis are one standard deviation.

Canopy Layer	Annual		Cold Season		Spring Shoulder Season		Dry season		Fall Shoulder Season	
	Dry	Wet	Dry	Wet	Dry	Wet	Dry	Wet	Dry	Wet
1.5m	48.0 (6.9)	48.9 (8.3)	12.4 (11.2)	84.7 (12.7)	60.6 (9.7)	39.0 (9.4)	96.2 (4.6)	1.2 (2.3)	51.6 (15.9)	47.7 (16.4)
10 m	48.3 (3.8)	48.6 (3.5)	12.9 (7.0)	84.2 (8.4)	58.8 (7.7)	40.8 (7.7)	95.7 (4.6)	1.6 (2.8)	55.2 (4.9)	44.1 (5.2)
20 m	49.2 (3.8)	47.7 (5.5)	12.8 (9.8)	84.4 (10.1)	58.8 (9.2)	40.9 (8.9)	96.0 (4.6)	1.4 (2.6)	56.6 (6.1)	42.8 (6.3)
30 m	43.7 (3.6)	51.1 (2.6)	12.3 (8.3)	87.4 (8.2)	53.5 (3.3)	45.4 (4.0)	97.8 (2.9)	2.0 (3.1)	48.8 (11.1)	51.2 (11.1)
40 m	46.7 (5.6)	48.9 (6.9)	12.7 (7.4)	82.0 (12.5)	59.0 (9.8)	40.2 (9.9)	97.7 (2.3)	1.7 (2.6)	50.4 (12.1)	49.6 (12.1)
56 m	47.6 (3.4)	48.0 (5.2)	15.5 (7.1)	79.1 (8.7)	56.9 (6.2)	42.3 (6.3)	95.6 (1.5)	3.8 (2.1)	49.7 (8.1)	50.3 (8.1)
All layers	47.7 (4.2)	48.6 (5.2)	13.1 (7.6)	83.1 (9.8)	58.5 (7.8)	40.8 (7.7)	96.5 (2.6)	1.9 (2.4)	52.8 (8.3)	46.8 (8.6)

**Table 2-2: Annual measures of wetting**

Annual measures of wetting and PET derived from the summation of five-minute observations over the course of the water years 2018, 2019 and 2020. Time spent wet presented both as an average across all height, and the length of time when any layer of the canopy was wet by a given source. Mean rainfall rate is the total depth of rainfall measured in a year, divided by the total duration of rainfall.

Year	Time spent wet (days)		Dew duration (days)		Rain wetting duration (days)		Rainfall duration (days)	Mean Rainfall rate (mm hr-1)	PET (m)
	Average	Any layer	Average	Any layer	Average	Any layer			
<b>2018</b>	183.3	224.3	22.2	76.3	150.6	207.1	22.9	3.68	1.30
<b>2019</b>	160.6	205.5	23.0	73.1	121.6	176.3	20.6	3.70	1.22
<b>2020</b>	177.5	224.4	23.1	74.5	144.4	189.3	21.1	3.60	1.30
<b>Mean</b>	173.8	218.1	22.8	74.6	138.9	190.9	21.5	3.66	1.27

**Table 2-3 a-d: Frequency and duration of dew and rain events**

Average and standard deviation of the frequency (n) and length of dew and rain wetting events across the 2017-2020 calendar years. Tables a – d present statistics for the cold season, spring shoulder season, dry season and fall shoulder season respectively.

Cold season												
a.	Dew Events				Rain Events				Frost Events			
Height	n		length (hrs)		n		length (hrs)		n		length (hrs)	
	mean	s.d.	mean	s.d.	mean	st. dev.	mean	s.d.	mean	st. dev.	mean	s.d.
1.5m	12	11.7	18.2	26.4	11.5	11.1	152.7	290.7	15.2	18.9	5.3	9
10 m	11.5	9.5	7.9	10.3	10.5	8.3	178.2	351.9	18	16.1	5.9	6.1
20 m	14.8	10.6	8.1	8.9	13.2	10.3	143.6	232.7	16.8	12.3	6.2	6.7
30 m	29	22.1	9.2	10.9	14.2	11.1	119	171.7	19.8	14.2	5.8	5.3
40 m	49.5	39.8	9.3	8.6	17	11.9	88.4	158.3	27.5	18.5	6	4.9
56 m	82.8	58.3	9.1	9.8	38	28.6	30.3	39.3	26.2	18.1	5.4	4.1

Spring shoulder season												
b.	Dew Events				Rain Events							
Height	n		length (hrs)		n		length (hrs)					
	mean	s.d.	mean	s.d.	mean	st. dev.	mean	s.d.				
1.5m	6.2	5.1	3.6	6.2	26	10.9	28.7	61.9				
10 m	9.8	1.7	1.1	3.7	24.8	7.8	30.9	62.3				
20 m	12.8	6.1	1.2	3.6	25.8	8.8	31	61.9				
30 m	24.2	14.4	2.2	3.2	25.8	8.5	27	41.3				
40 m	36.8	1.5	3	3.9	39	7	17.7	24.2				
56 m	64.2	12	3.6	4.2	66	28.7	9.9	16				

c.		Dry Season							
		Dew Events				Rain Events			
		n		length (hrs)		n		length (hrs)	
		mean	s.d.	mean	s.d.	mean	s.d.	mean	s.d.
Height									
1.5m	0.5	1	11.2	14.2	4.2	4.3	22.2	44	
10 m	2.2	2.6	2	3.2	5.5	6.2	22.2	41	
20 m	1.8	1.3	3.4	7.9	6.8	6.2	13.2	26.3	
30 m	2.8	3.4	4.5	8.6	6	5.5	10.6	15.1	
40 m	4.5	3.1	3.8	5.8	5.8	5.9	11.9	12.7	
56 m	23.5	3.1	3.3	3.3	7.5	9.3	7.3	6.9	

d.		Fall shoulder season							
		Dew Events				Rain Events			
		n		length (hrs)		n		length (hrs)	
		mean	s.d.	mean	s.d.	mean	st. dev.	mean	s.d.
Height									
1.5m	1	0.8	5.6	8.8	8	5.8	79.2	125.1	
10 m	4.2	4	0.6	0.7	7.5	4.8	81.6	128	
20 m	4.5	1.7	3	7.3	8.5	4.7	54.4	60.8	
30 m	11.5	6.8	7.3	7.2	8.5	3.4	49.4	56.5	
40 m	26	7.2	6.9	5.9	9.8	4	39.4	47	
56 m	40	14.4	6.6	6.3	20.5	16.1	13.7	17.6	

**Table 2-4: Seasonal boundaries for each calendar year**

Year	Spring	Dry season	Fall	Winter
2017	Mar. 15th	June 28th	Sept. 4th	Nov. 8th
2018	Mar. 27th	June 29th	Sept. 11th	Nov. 8th
2019	Mar.26th	June 9th	Sept. 8th	Nov. 2nd
2020	Mar.29th	July 4th	Sept. 15th	Nov. 1st

**Table 2-5: Regression metrics**

Index corrected  $R^2$ , AUC, intercept and slope coefficients for one-variable logistic models using data from 56m height in the Discovery Tree. Response variable is the binary classification of dew forming (1) or non-dew-forming (0) periods, determined using the 56m leaf wetness sensor and the routine described in section 2.4.

Model	$R^2$	AUC	Coefficients	
			Intercept	Var
Wind Speed	0.001	0.505	-1.94	-0.11
$R_{net}$	0.052	0.631	-4.26	-0.05
$T_{air}$	0.50	0.916	5.54	-0.72
Specific Humidity	0.13	0.74	2.84	-6.84
Relative Humidity	0.87	0.994	-87.93	0.92
DPD	0.87	0.994	4.33	-5.90

**Table 2-6: False positives and negatives from dew prediction**

Rates of false positive and false negative predictions, relative to the number of true dew accumulation events as determined by leaf wetness sensor, for each of the tested models. “In tree” models used data from the 56m sensor height in the Discovery Tree, while “PRIMET” models used data from the nearby PRIMET weather station.

	In tree				PRIMET			
	Penman		Logistic		Penman		Logistic	
	5-minute	> 1hr						
False positive rate	1.39	0.932	0.233	0.203	24.6	2.25	4.62	2.64
False negative rate	0.292	0.051	0.3	0.322	0.00842	0.644	0.0068	0

### CHAPTER 3

#### ADJUSTMENT TO MOISTURE STRESS BY TWO CO-OCCURRING ISLAND ENDEMIC CANOPY TREE

#### SPECIES: IMPLICATIONS FOR THE COMPOSITION OF *ACACIA KOA* AND *METROSIDEROS*

#### *POLYMORPHA* FORESTS UNDER INCREASING DROUGHT STRESS

Adam M. Sibley, Forest Ecosystems and Society, Oregon State University

Frederick C. Meinzer, Pacific Northwest Research Station, USDA Forest Service

Rebecca Ostertag, Department of Biology, University of Hawai'i at Hilo

Susan Cordell, Institute of Pacific Islands Forestry, USDA Forest Service

Robert Hamnett, National Ecological Observation Network - Pu'u Maka'ala NAR office

Amanda Uowolo, Institute of Pacific Islands Forestry, USDA Forest Service

## Abstract

Increasing drought frequency and severity is projected for forested ecosystems across the planet. Changing drought regimes are likely to impact individual tree species differently, which may lead to changes in forest form and function. Changes in form and function are expected to particularly impact ecosystems where high rates of endemism produce unique and rare species interactions. In this study, we focused on functional traits related to drought resistance that can range from relatively fixed in some species to relatively plastic in others. We compared functional traits related to drought resistance in two co-occurring, canopy dominant tree species, *M. polymorpha* and *A. koa*, which occur over a broad range of water availability on the Hawaiian Islands. While they co-occur across large parts of their native ranges, they differ substantially in ancestry, life history strategies, and phenotypic plasticity. We found that traits related to leaf water balance, carbon acquisition, and the regulation of nonstructural carbohydrates (NSCs) varied significantly across a range of moisture availability in *M. polymorpha* in ways that suggest adjustment to drought, while site-to-site differences in *A. koa* suggested less adaptive, more drought-avoidant behavior. We conclude that of the two species, *M. polymorpha* is more likely to be able to adjust to new drought regimes *in situ* compared to *A. koa*.

### 3.1 Introduction

Forest ecosystems around the world have evolved in concert with natural disturbances, which cause tree mortality from the individual to landscape scale (Trumbore, Brando and Hartmann 2015). Periodic drought is an important factor shaping species composition in some biogeographic systems and is a regular part of decadal scale fluctuations in the tropics and subtropics (Lyon 2004). However, anthropogenic climate change may significantly increase the intensity and frequency of drought events in the tropics (Williams et al. 2007), bringing into question the stability of future ecosystem dynamics. One global analysis of post-drought recovery in 127 tropical forest plots found elevated mortality compared to pre-drought levels for an average of two years and found larger trees and species with low wood density to be at greater risk of drought-induced mortality at most sites (Phillips et al. 2010). Johnson et al. (2018) also show that drought impacts in tropical forests have been unequal among tree size classes, with larger trees at greater risk of mortality. Both studies anticipate structural changes in tropical forests in the future, which would be particularly consequential for systems where high rates of endemism give way to unique and rare species interactions (Kier et al. 2009, Ohlemüller et al. 2008, Williams et al. 2003). However, such a broad scale synthesis is not able to pinpoint the aspects of plant physiology that determine the ultimate fate of a tree species - for any given forest stand, the response of each individual will depend upon a species-specific set of coordinated functional traits that can range from relatively static to relatively dynamic in response to environmental conditions. The cumulative effect of the adaptive responses of each trait related to drought resistance will, in aggregate, determine the degree to which trees will adapt to new drought regimes.

While understanding the plasticity of functional traits is crucial to understanding how species will be affected by future drought, direct comparison of trait plasticity among mature, canopy-dominant trees in a given stand is challenging. Measurements would need to occur opportunistically pre- and post-drought event, which requires luck; alternatively, rainfall exclusion structures would need to be built around a subset of trees (Binks et al. 2016). These structures are expensive, labor intensive, and logistically challenging to implement and monitor. A good substitute for serendipitous sampling or cost-prohibitive rain exclusion structures – and arguably a better assessment of drought-trait interactions and adaptations - is to measure individuals from the same species growing in locations with different rainfall amounts. Comparing the same traits in populations experiencing different water availability is a good surrogate for examining plasticity *in situ*; that is, if a trait remains fixed across sites, it is less likely to be adjustable *in situ*, whereas if trait expression and coordination differs significantly from site to site, it is more likely that the trait is plastic within individuals of that species.

The island of Hawai'i and the two species studied here provide relevant context and ideal comparators for investigating adjustment to future drought in contrasting, co-occurring species in an ecosystem with high rates of endemism. Decreasing precipitation and fog water inputs have been identified as the most likely and potentially most severe climate-driven threat to forests where these study species, *Metrosideros polymorpha* Gaudich. ('ōhi'a) and *Acacia koa* A. Gray (koa), occur (Giambelluca and Luke, 2007) and have outsized importance for the preservation of endangered native bird and plant species displaced from lower elevations by disease, land use change and invasive species (Benning et al. 2002, Vitousek et al. 1987). A decreasing trend in the wintertime Hawaiian Rainfall Index has been observed over the past century (Chu, Chen and

Schroeder 2010, Frazier and Giambelluca 2017), and model simulations predict substantial shifts toward drier climates in currently mesic land areas (Fortini, Jacobi and Price 2017). Observed changes in the altitude and frequency of formation of the Trade Wind Inversion layer (Cao 2007) would disproportionately impact montane *M. polymorpha* and *A. koa* forests, which have demonstrated sensitivity to short-term drought events (Crausbay et al. 2014, Michaud et al. 2015). While *Metrosideros polymorpha* and *Acacia koa* co-occur as canopy dominant species in montane wet and mesic forests, they differ substantially in their phylogenies, life history strategies and geographic ranges, making them ideal candidates for comparison.

*Metrosideros* is among the most widespread tree genera in the Pacific, containing ~ 50 species (Wright et al. 2000). *M. polymorpha* is a slow growing pioneer species originating from an ancestor in New Zealand (Wright et al. 2000). It is found across a climatic range of < 400 to > 10,000 mm mean annual rainfall and at altitudes from 0 – 2500 m above sea level (Cordell et al. 1998). The species name *polymorpha* reflects the drastic change in form the species exhibits; it can colonize bare lava rock, taking on a small shrub-like form, or emerge as a late successional canopy species and attain diameters at breast height (DBH) over one meter in forests on older substrate. In contrast to *M. polymorpha*, *Acacia koa* is a faster-growing leguminous nitrogen fixer. It shares the *Acacia* genus with 1044 other species, most of which are confined to Australia with the remainder distributed across South-East Asia, Africa, Oceania and the Neotropics (Brown et al. 2012). *A. koa* is limited to areas with mean annual rainfall > 700mm (Ares and Fownes 1999) and occupies a smaller altitudinal range than *M. polymorpha*, with its distribution limited at low elevations by fungal pathogens (Dudley et al. 2016, Nelson 2009) and above 2100 m elevation by frost (Whitsell et al. 1990). *A. koa* shares several disturbance-adapted attributes with its Australian kin, including regeneration via root suckers (Baker, Scowcroft and Ewel

2009), modified mature leaves or phyllodes, and the ability to quickly refoliate after near complete defoliation by Koa looper moth (*Scotorythra paludicola*) outbreaks (Haines et al. 2009) or hurricane winds.

In this study, we measured traits related to water use and carbon gain in *M. polymorpha* and *A. koa* at sites with different annual rainfall totals. While both species have been studied extensively, few studies have done so in a comparative context at sites where they co-occur. Specifically, we investigated site-to-site differences in leaf tissue water relations, stomatal regulation of water loss, the degree to which foliar nutrients and higher photosynthetic rates could offset stomatal restriction of carbon gain, the role of stored carbohydrates in osmotic adjustment, and the relative sensitivity of growth vs. photosynthesis to water stress. Because *M. polymorpha* is found across a broader range of mean annual rainfall totals in Hawai'i, we predicted that site-to-site differences in the areas of resistance to drought stress that we measured would show that this species has greater potential for plastic adjustment to future drought conditions. Past studies of these species individually compared traits among trees planted in common gardens (Fisher et al. 2007), across altitude gradients (Corn and Hiesey 1973, Joel et al. 1994, Cordell et al. 1999), or in potted greenhouse plants (Ares and Fownes 1999). Based on these prior studies, we expected to find plasticity in traits that could compensate for increased stomatal restriction of gas exchange in response to drier conditions in *M. polymorpha* and less compensatory change in *A. koa*. However, it was not clear if results derived from seedlings or relatively young trees would represent the true potential for adjustment in mature trees in extant forests. In this study, we examined plasticity in mature trees in dominant canopy positions by climbing high in the crown and sampling sunlit, canopy leaves from both species in a wet and

mesic forest stand and from a third, dry location where only *M. polymorpha* was present, allowing us to assess the vulnerability of these rare and unique forests to drought-driven changes in form and function.

## 3.2 Methods

### 3.2.1 Study sites

Data for this study were collected at three sites on the Island of Hawai'i and at four sampling intervals over the course of a year. Sampling campaigns took place in October 2015 and January, April, and August of 2016 – timed to correspond with the four seasons and to cover the full annual reproductive cycle of both species.

Study sites were selected where our target species are dominant components of the tree canopy and where data on detailed climate and tree species demographics are available (Hawai'i Island Permanent Plot Network or HIPNET sites, Ostertag et al. 2014. Figure 1). Site names are Laupāhoehoe, Pu'u Wa'awa'a and Māmalahoa and will be referred to as wet, mesic, and dry sites. The three sites were also chosen to represent a broad range of precipitation and likely plant-available soil water. Site climate conditions are summarized in Table 1, using data collected at ten-minute intervals by climate stations at each site and aggregated to yearly averages. At all sites, four component net radiation was measured using net radiometers (NR01, Hukseflux, Delft, Netherlands). Air temperature ( $T_{\text{air}}$ ) and relative humidity (RH) were measured using temperature/RH sensors (HMP45C, Campbell Scientific, Logan, UT), and precipitation was measured using tipping bucket rain gauges (TR-525, Texas Electronics, Dallas, TX). At the wet and mesic sites, all measurements were made at the top of towers that protrude above the

canopy (by ~ 5 m at wet site and ~3 m at mesic site). At the dry site, measurements were made approximately 2 m above ground level from a tower in an open clearing.

Mean annual rainfall measured at the wet site is nearly an order of magnitude greater than at the mesic site (6773 vs 886 mm) while both sites experience comparable mean annual atmospheric vapor pressure deficit (VPD) values (~0.25 kPa). Taking VPD as a proxy for evaporative demand experienced at the leaf surface if leaves are at air temperature, this translates to the same evaporative demand but a much smaller supply of precipitation at the mesic site. Water supply is likely to be further limited by the lower soil water holding capacity of the younger, coarser substrate at the mesic site (3,000 – 5,000 years old) compared to the wet site (4,000 – 14,000 years old) (Wolfe and Morris 1996, Figure 1). The dry site, 8.9 km to the North and 509 m downslope of the mesic site, is situated on 1,500 – 3,000-year-old substrate and experiences substantially higher VPD and less rainfall than the other two sites, making it the most water limited. Viewed another way, Figure 2 shows the ratio of monthly mean potential evapotranspiration (PET) to precipitation (P). The PET:P ratio is similar in the mesic and wet sites, but substantially greater in the dry site. PET was calculated on a daily timestep using site specific data from the climate stations and a version of the Priestley-Taylor method which takes daily minimum and maximum air temperature and relative humidity, daily net radiation, elevation, and uses an alpha modifier value of 1.26 (McMahon et al. 2013).

To characterize physiological traits influenced by water availability, we chose five canopy dominant individuals of each species at each site for repeated sampling. On each sampling campaign, we clipped three representative branches with multiple terminal branchlets holding

sunlit, canopy leaves from each tree. Both species have unique leaf properties (Figure 1), which we accounted for in sampling. *A. koa* has compound juvenile leaves that are replaced by phyllodes in the sapling stage (Pasquet-Kok et al. 2010); we chose to sample branches with mature phyllodes and no bean pods. *M. polymorpha* grows annual cohorts of leaves on a given branch (Cordell et al. 2001); we selected samples with at least four leaf cohorts, representing four periods of growth. One branch sample from each tree was used to determine nonstructural carbohydrate (NSC) concentrations on a subset of leaves (section 4.2), shoot water relations (section 4.3), and gas exchange rates (section 4.4). A subset of the NSC samples was used to run carbon isotope discrimination analyses (section 4.5). In addition to the branch samples, a 1-cm-long contiguous section of trunk sapwood was extracted at 1.3m height with an increment borer on each campaign for NSC analysis.

### ***3.2.2 Nonstructural carbohydrate extraction***

Glucose, fructose, sucrose and starch concentrations were analyzed in foliage (*M. polymorpha* leaves, *A. koa* phyllodes), terminal branch (leaf bearing twigs), and trunk tissues from each tree. *M. polymorpha* leaf samples were taken from two- and three-year-old cohorts and analyzed separately. Tissue samples were put on dry ice immediately after collection to halt metabolism. In the lab, samples were taken off dry ice and microwaved on a high power setting for ninety seconds to further ensure all living tissues were dead, then dried in a 60° C oven. Eight to ten dried leaves from each sample were homogenized in a coarse grinder, then a 50 mg subsample was ground to a fine powder, from which a 14-15 mg final sample was taken. Several terminal branch segments from each sample tree were stripped of bark and processed the same way, while one 1-cm-long contiguous section of trunk sapwood was used for trunk NSC analyses.

NSC extraction was done following the protocols in Woodruff and Meinzer (2011). The 14-15 mg powdered samples were mixed with 1.6 mL of water in sample tubes and heated in a steam bath for 90 min to extract carbohydrates. Each sample was split into four subsamples to which different enzymatic treatments were added to convert glucose, glucose + fructose, glucose + fructose + sucrose, and all NSCs to gluconate-6-phosphate. Each of the four treated subsamples were read using a 96-well microplate photometer (Multiskan FC, Thermo Scientific, Waltham, MA). Gluconate-6-phosphate concentrations were determined by comparing readings in the 340 nm absorbance band to a glucose reference standard which was transformed to Gluconate-6-phosphate during the enzymatic treatments. Concentrations of glucose + fructose, sucrose and starch were then calculated by simple subtraction of the concentrations reported for each of the four enzymatic treatments. Results are reported on a mass per leaf area basis for foliage, and on a percent dry weight basis for foliage, stem, and trunk wood.

### ***3.2.3 Tissue water relations***

Pressure-volume (P-V) curves (Tyree and Hammel 1972) were constructed for foliage of each sample tree for each sampling campaign. Branches 30 – 50 cm long were cut from portions of the canopy with high sun exposure. Each sample was enclosed in a sealed plastic bag with the cut end of the branch inserted in a water-filled florist tube. Samples were placed in a dark, cool environment overnight to ensure they stayed fully hydrated. The following day, a 10-15 cm lateral branch with healthy foliage was cut from the larger sample and used to conduct pressure-volume analyses. Samples were allowed to slowly dehydrate in the laboratory and paired measurements were periodically made of sample fresh weight (to 1 mg precision using a Mettler Toledo ME103TE balance) and shoot water potential ( $\Psi_L$ , MPa) with a pressure chamber (PMS Instrument Company, Albany, OR, USA). The procedure was repeated until at least five

consecutive sets of measurements showed a linear positive relationship between decreasing fresh mass and decreasing  $1/\Psi_L$ .

From these data, saturated osmotic potential ( $\Psi_{\pi 100}$ , MPa) was determined by fitting a regression to the points on the linear portion of the  $1/\Psi_L$  vs. relative water deficit (RWD) curve and taking the inverse of the y-intercept, where RWD is the ratio of turgid weight minus shoot weight to turgid weight minus dry weight. Osmotic potential at turgor loss point ( $\Psi_{TLP}$ ), which is related to the minimum  $\Psi_L$  that leaves can experience without wilting, was determined by finding the intersection of this same linear regression with a negative exponential function fit to the points in the non-linear portion of the curve. Pre-turgor loss shoot capacitance ( $C$ , in  $\text{g g}^{-1} \text{dw MPa}^{-1}$ ) was estimated from the slope of a plot of RWD against  $\Psi_L$ , and is a measure of the buffering capacity of the shoot against rapid changes in  $\Psi_L$ . Shoot bulk modulus of elasticity (MOE) was calculated as the ratio of the change in  $\Psi_L$  to the change in RWD over the nonlinear portion of the curve, multiplied by total relative water content (Turner 1988). MOE is an indication of how much cell walls deform in response to changes in turgor pressure, where higher MOE would indicate less deformation as  $\Psi_L$  is lowered.

### ***3.2.4 Gas exchange***

Gas exchange measurements were done in the field at the time of sampling using two portable systems (LiCor 6400, LiCor Biosciences, Lincoln, NE, USA). During all four sampling campaigns, measurements were made between 0900 and 1300h on a randomly selected subset of four of the five sample trees for each species. Cut shoots were kept hydrated using florist tubes and one healthy leaf per shoot was selected to entirely cover the  $6 \text{ cm}^2$  cuvette aperture. Inside the cuvette, leaves were exposed to a constant  $1200 \mu\text{mol m}^{-2} \text{ s}^{-1}$  photon flux density, and air

temperature and relative humidity were set to match ambient conditions. Photosynthetic CO<sub>2</sub>-response (A-C<sub>i</sub>) curves were obtained by repeatedly varying chamber CO<sub>2</sub> concentrations and allowing CO<sub>2</sub> exchange rates to come to an equilibrium before recording an assimilation (*A*) value at a given CO<sub>2</sub> concentrations. Carbon dioxide concentrations started at 400 ppm and were dropped to 300, 200, 100 and 50 ppm before returning to 400 ppm and increasing by 200 ppm each time step to a maximum of 2000 ppm or until a clear asymptote in *A* was reached (minimum of nine points per curve). *A*<sub>max</sub> was estimated as the upper asymptote of the *A* vs. C<sub>i</sub> curve.

### ***3.2.5 Carbon isotope and Nitrogen concentration analysis***

Carbon isotope analysis was done on leaf tissue samples from each tree from the first (October 2015) sampling campaign. Approximately 1 mg of sample material was obtained from leftover dried and powdered leaf tissue prepared for NSC extraction (described in section 2.1). Sample combustion, carbon isotope analysis and nitrogen concentration determination were carried out by the University of Hawaii at Hilo Analytical Laboratory (Hilo, HI). Each sample was combusted and analyzed using a Costech 4010 Elemental Analyzer and a Thermo Delta V Isotope Ratio Mass Spectrometer. Ratios of <sup>13</sup>C to <sup>12</sup>C are expressed in delta notation (δ) on a per mil basis (‰, parts per thousand) in relation to Vienna Peedee Belemnite standard:

$$\delta = \left( \frac{R_{sample}}{R_{standard}} - 1 \right) \quad (1)$$

International standards USGS 40 and 41 L-glutamic acid were used to calibrate sample runs and checked against NIST 1547 Peach Leaf check standard. By measuring two sample duplicates and

repeated measurements of the check standard, carbon isotope ratio data were calculated to be accurate to  $\pm 0.2\%$  and Nitrogen concentration data were shown to be accurate to 0.01%.  $\delta^{13}\text{C}$  signatures in leaf tissue ( $\delta^{13}\text{C}_{\text{leaf}}$ ) come from the fractionation of ambient  $\text{CO}_2$ , owing to two leaf-level processes which discriminate against the heavier  $^{13}\text{C}$  isotope.

$$\delta^{13}\text{C}_{\text{leaf}} = \delta^{13}\text{C}_{\text{air}} - a - (b - a) \frac{C_i}{C_a} \quad (2)$$

Where  $a$  is the 4.4‰ diffusional fractionation of  $\text{CO}_2$  across stomata, and  $b$  is the 27‰ fractionation associated with several intercellular processes, including photorespiratory fractionation and ribulose biphosphate carboxylase-oxygenase (RuBisCO) discrimination against  $^{13}\text{C}$  during  $\text{CO}_2$  fixation (Farquhar et al. 1989). Assuming a constant  $\delta^{13}\text{C}_{\text{air}} = -8.4\%$  (Long et al. 2005, Kerr et al. 2015) across sites and ambient air  $\text{CO}_2$  concentrations ( $C_a$ ) of 400 ppm, equation 2 can be solved for  $C_i$ , or the average concentration of intercellular  $\text{CO}_2$  of the sampled foliage over its growth history. For each individual tree in the study we used  $C_i$  values estimated in this way with the A- $C_i$  curve fits for that tree (described in section 4.4) to estimate time-integrated assimilation rates ( $A$ ). Integrated  $A$  estimates were averaged across all sampling campaigns for each individual and then across individuals of the same species at each site. Finally, by again assuming  $C_a = 400$  ppm and using the estimates of  $C_i$  and time-integrated  $A$  described above, we calculated integrated  $g_s$  via equation 3:

$$g_s = \frac{1.6A}{C_a - C_i} \quad (3)$$

### 3.2.6 *Relative basal area increment*

Rates of growth were calculated from repeated measurements of diameter at breast height (DBH) within the HIPNET plots associated with each study site (Ostertag et al. 2014). The field methodology was developed by the Center for Tropical Forest Science ForestGEO network (Anderson-Teixeira et al. 2015). All live, native woody plants  $\geq 1$  cm diameter at breast height (DBH, at 130 cm) were mapped, tagged, identified to species and measured for DBH. The wet site plot is 4 ha, while the mesic and dry site plots are 1 ha. Growth was quantified using Relative Basal Area Increment (RBAI) for all stems between 10 and 60 cm DBH that had been measured at least twice.

$$RBAI = \frac{(r_{t_2}^2 - r_{t_1}^2) * 365}{r_{t_1}^2 * (t_2 - t_1)} \quad (4)$$

Where  $r_{t_2}$  and  $r_{t_1}$  are the measured radii at breast height at survey dates one and two and  $t_1$  and  $t_2$  are expressed in Julian days. The result is a percentage increase in basal area per year.

### 3.2.7 *Statistics*

Simple outlier analysis was performed on NSC data to exclude negative values of carbohydrate concentrations and those samples with an unrealistic change in concentration between sampling campaigns. P-V and A-C<sub>i</sub> curves were also quality checked, and curves where a good fit could not be made were excluded from analysis. Repeated measurements of the same individual trees across the four sampling campaigns were not treated as fully independent measurements – rather, estimated metrics were pooled across campaigns first by averaging the results for individual trees, and then those means were used to compute the mean of species and site combinations, resulting in between three and five true independent samples per species + site combination. In

all cases where the means of species + site combinations were compared, the comparisons were done using one-way ANOVA in R (R core team 2020). The significance of differences between means was assessed in a pair-wise fashion using Tukey's honestly significant difference (HSD) test with a p-value threshold of 0.05.

### 3.3 Results

We found evidence of greater physiological adjustment across sites in *M. polymorpha* than in *A. koa*. A one-way analysis of variance to compare between sites within species revealed that  $\Psi_{\text{TLP}}$ ,  $C$ , and MOE were all significantly different across sites only for *M. polymorpha* (Table 2) - more specifically,  $\Psi_{\text{TLP}}$  became increasingly negative from wetter to drier sites (though the mesic and dry sites were nearly identical, Table 2).  $C$  declined monotonically and MOE increased monotonically from wet to dry sites. One-way ANOVA and Tukey's HSD test showed significant differences in LMA at the  $p < 0.05$  level between wet site *M. polymorpha* and *M. polymorpha* at the two drier sites (Figure 3a). Both  $N_{\text{area}}$  ( $\text{mmol m}^{-2}$ ) and  $A_{\text{max}}$  ( $\mu\text{mol m}^{-2} \text{s}^{-1}$ ) were significantly higher at the dry site compared to the wet site (Figure 3b-c). Non-pairwise comparison of *M. polymorpha* at the three sites showed significant differences in LMA ( $p < 0.0001$ ),  $N_{\text{area}}$  ( $p = 0.0001$ ),  $A_{\text{max}}$  ( $p = 0.022$ ) and PNUE ( $p < 0.0001$ ), demonstrating that this species displayed thicker leaves with less surface area, greater nitrogen concentration per unit area, and monotonically increasing  $A_{\text{max}}$  across the wet-dry range of sites, with generally greater similarity between mesic and dry site trees in some traits ( $\Psi_{\text{TLP}}$ , LMA, PNUE) and greater similarity between wet and mesic site trees in other traits (MOE,  $N_{\text{area}}$ ). In terms of basal area growth, *M. polymorpha* grew significantly faster at the wet site than it did at the mesic or dry site, which were not significantly different from each other (Table 3).

In contrast to *M. polymorpha*, no significant differences were found across sites in *A. koa* in any of the aforementioned foliar properties related to water relations, LMA,  $A_{\max}$ ,  $N_{\text{area}}$  or PNUE (Table 2, Figure 3). *A. koa* showed a significant increase in  $\delta^{13}\text{C}$  ( $p = 0.005$ ) and significant decreases in integrated  $A$  ( $p = 0.021$ ) and especially in  $g_s$  ( $p = 0.002$ ) from wet to mesic (Figure 4), indicating an increasing relative stomatal limitation on photosynthesis. The substantial increase in  $\delta^{13}\text{C}$  values between wet and mesic sites indicates a higher intrinsic water use efficiency (iWUE) change when compared to *M. polymorpha*. Between the wet and mesic site there were no significant differences in  $\delta^{13}\text{C}$ , integrated  $A$ , or  $g_s$  in *M. polymorpha*, though a highly significant increase in  $\delta^{13}\text{C}$  and a decrease in  $g_s$  was seen between the mesic and dry environment (Figure 4).

No significant seasonal variation in concentrations of total NSC or any of its components was detected in ANOVA analyses by species and site. For all further results, concentrations from seasonal sampling campaigns were pooled, and site-to-site and interspecies comparisons were made. In *M. polymorpha*, there were significant differences in total NSC concentrations across sites in foliage ( $p = 0.0006$ ) and stems ( $p = 0.022$ ), with monotonic increases from the wettest to driest site in foliage and trunk tissues (Figure 5). In contrast, NSC concentrations in *A. koa* decreased from the wet to mesic site – significantly so in the case of stem ( $p = 0.022$ ) and trunk ( $p = 0.05$ ) tissues. The largest fraction of simple sugars was found in *M. polymorpha* leaves, while the stem wood of *A. koa* at the wet site was notable for its high NSC concentration and high proportion of starch.

To examine how foliar sugar concentrations might play a role in leaf osmotic properties and water use efficiency, we plotted total foliar sugar concentration against turgor loss point for both species across sites and found a strong linear relationship ( $R^2 = 0.916$ ) wherein  $\Psi_{\text{TLP}}$  decreased by  $\sim 0.35$  MPa per  $\text{mg g}^{-1}$  dw increase in sugar content (Figure 6). When  $\Psi_{\text{TLP}}$  and  $\Psi_{\pi 100}$  data were pooled across sites and plotted, a consistently larger offset from the 1:1 line was seen in *M. polymorpha* compared to *A. koa*, signifying a greater difference between  $\Psi_{\pi 100}$  and  $\Psi_{\text{TLP}}$  in *M. polymorpha* and potentially a greater range of foliar osmotic adjustment (Figure 7). Leaf total NSC concentrations in *M. polymorpha* were significantly correlated with  $\delta^{13}\text{C}_{\text{Leaf}}$  (Figure 8), with less negative  $\delta^{13}\text{C}_{\text{Leaf}}$  values (higher iWUE) corresponding to higher foliar sugar concentrations.

### 3.4 Discussion

Although these two canopy species are co-dominants in Hawaiian forests, this study demonstrates that they have very different water-use strategies: *M. polymorpha* is more drought tolerant in relation to *A. koa*, which showed more drought avoidant characteristics. Drought tolerators are generally defined as plants which make greater physiological adjustments to maintain stomatal conductance during dry periods (more anisohydric), while drought avoiders are more apt to respond to dry periods with less physiological adjustment and greater stomatal resistance (more isohydric, Touchette et al. 2007). Our findings from mature trees in intact native forests corroborate earlier findings from greenhouse and common garden experiments. Cordell et al. (1998) suggested that variation in anatomical traits related to gas exchange in *M. polymorpha* were more heavily determined by plastic adjustment to environmental conditions than by source genetics in a common garden, while Ares and Fownes (1999) found in a paired greenhouse and wet-to-dry gradient study that *A. koa* water use efficiency increased with increasing water deficit, a phenomenon that was best explaining by increasing stomatal resistance.

Several pieces of evidence in our study demonstrate that *M. polymorpha* trees have greater plasticity, and thus a greater potential range of adjustment to drier conditions, as compared to *A. koa*. First, of the 14 different ecophysiological variables measured for the two species, *M. polymorpha* had significant differences among sites in 10 of them, while *A. koa* only significantly differed in five variables across sites, though it should be acknowledged that *A. koa* was only found at two of our study sites. Second, plant distributions at each site also suggest that *M. polymorpha* has greater adaptive potential. *M. polymorpha* is found across a broader set of rainfall conditions than *A. koa* and in this study, it was found at the dry site (n = 57 trees), while *A. koa* was not. *M. polymorpha* and *A. koa* are the most common trees at the wet site (n = 2688 and n = 153 respectively), but the mesic site has a higher ratio of *A. koa* (n = 133) to *M. polymorpha* (n = 292). Third, across all sites, *M. polymorpha* had consistently larger difference between  $\Psi_{\pi 100}$  and  $\Psi_{TLP}$  (Figure 7) and showed greater adjustment of  $\Psi_{TLP}$  across the wet-to-dry range (Table 2). A review of plasticity in  $\Psi_{TLP}$  between pre and post drought periods for plant species around the planet found an average adjustment of 16% from pre-drought levels (Bartlett et al. 2015), while extremely drought tolerant tree species dynamically adjust  $\Psi_{TLP}$  by >1.5-2.5 MPa (Bowman and Roberts 1985, Davis and Mooney 1986, Meinzer et al. 1988, 2014). From the wet to dry site in our study,  $\Psi_{TLP}$  adjustment was on average -0.27 MPa (12.7%) in *M. polymorpha*. While the method for evaluating plasticity in Bartlett et al. (2015) and our study are different, their work provides helpful context for evaluating the relative level of plasticity in our study - *M. polymorpha* being moderately plastic in this context and *A. koa* not significantly plastic (5.6%, Table 2) compared to plants globally.

These relative differences in plasticity in *M. polymorpha* and *A. koa* were also seen in shoot capacitance and modulus of elasticity (Table 2). Decreasing capacitance from wet to dry in *M. polymorpha* may be related to increasing LMA (Figure 3i), if greater LMA was caused by higher leaf density ( $\text{g mL}^{-1}$ ) and thus lower symplast volume per gram of dry weight at a given  $\Psi_{\text{leaf}}$  (de la Riva et al. 2016). Increasing MOE from wet to dry sites may suggest an adjustment to maintain cell volume at the drier sites where  $\Psi_{\text{leaf}}$  drops to more negative values (Clifford et al. 1998) – that is, in order to maintain a given symplast volume, MOE must be higher (making cell walls more rigid) when osmotic potential becomes more negative, which would be the case if *M. polymorpha* makes osmotic adjustments in response to water limitation at the drier end of its range. In *A. koa*, LMA, Capacitance and MOE were virtually unchanged between sites.

The limited capacity of *A. koa* and the greater capacity of *M. polymorpha* to osmotically adjust may be related to differences in soluble carbohydrate concentrations maintained in foliar tissues (Figure 6). Though it is difficult to determine the amount of stored NSC necessary for functions like osmotic adjustment and what amount is held as a carbon safety margin (Hartmann and Trumbore 2016), the stability of total NSC concentrations across seasons and within different tissues at each site suggests some degree of active regulation of stored NSC in both species. The marked increase in foliar free sugars from wetter to drier conditions (Figure 5a) and the corresponding drop in  $\Psi_{\text{TLP}}$  (Figure 6) further suggests that foliar sugar content is regulated to aid turgor maintenance in *M. polymorpha*. This finding supports a growing body of evidence suggesting that NSC's play both direct and indirect roles in determining plant osmoregulation in response to water stress (Clifford et al. 1998, Martínez-Vilalta et al. 2016, O'Brien et al. 2014, Sapes et al. 2020).

*M. polymorpha* was able to allocate more resources to growth at the wet end of its range, while *A. koa* grew more rapidly at the mesic site (Table 3). NSC concentrations increased from wetter to drier conditions in *M. polymorpha* foliage, stem and trunk tissues and there was a strong positive correlation between  $\delta^{13}\text{C}_{\text{Leaf}}$  and foliar NSC concentration in this species (Figure 7) consistent with findings that as water stress increases, the of carbohydrates to growth diminishes more than does carbohydrate production (Hsiao et. al. 1976, Muller et al. 2011, Piper et. al. 2017, Granda and Camarero 2017). If this buildup of carbohydrates with drier conditions was a consequence of turgor-related limits on growth (Sala and Hoch 2009) one would expect that from the wetter to drier sites, less turgor-driven cell expansion would result in greater leaf mass per area (LMA) values, which was the case for *M. polymorpha*, but not for *A. koa* (Fig 3a). It would follow that in a future climate regime with more intense and/or longer droughts, the growth vs. storage tradeoff would shift towards diminished growth and enhanced NSC storage for *M. polymorpha*.

In contrast to *M. polymorpha*, *A. koa* grew significantly faster at the mesic site compared to its growth at the wet site (Table 4) and had lower concentrations of stored carbohydrates and lower integrated *A* at the mesic site compared to the wet. The growth estimates presented here should be interpreted with caution, as they represent growth over a 5-year time period for most measured trees, and interannual variability may play a large role in determining observed site-to-site differences. It should also be noted that bole growth at DBH may not be an appropriate measure of overall biomass accumulation for *A. koa*, given the relatively large diversity of crown growth forms observable in the field, varying from trees with tall, straight boles with high

crowns to those that bifurcate close to ground level and support sprawling crowns with multiple major sub-boles. Given these caveats, faster growth at the mesic site may suggest that a set of factors other than water stress governed differences in growth. The fact that *A. koa* is relatively more abundant at the mesic site also suggests that water limitations are not the primary determinant of *A. koa* success across the studied range. Despite *A. koa*'s higher growth rates and abundance at the mesic site, our observations of relatively limited adjustment in drought-related traits across a wet to mesic range imply that drying out of wetter sites would not be advantageous for *A. koa* unless growth inhibition is caused by factors directly related to rainfall, such as nutrient leaching of phosphorus (Jordan 1982), light limitation due to cloud cover (Letts and Mulligan 2005), or the growth of fungal pathogens (Belisário et al. 2020). Also of note is that the 886 mm mean annual precipitation at our mesic study site is not far from the lowest mean annual totals observed in the literature for *A. koa* stands (700 mm, Ares and Fownes 1999; 850 mm, Harrington et al. 1995). Both Ares and Fownes (1999) and Harrington et al. (1995) found a decline in productivity at the dry end of the climate gradients in their studies, suggesting either a sharp decline in productivity at sites drier than our mesic site, or that fog water inputs observed (but not quantified) at our mesic study site enhanced water availability in a way that was not captured in this study. Predicted shifts from mesic to dry climates in some regions of the Hawaiian Islands (Fortini, Jacobi and Price 2017) along with predicted changes in montane fog water input (Giambelluca and Luke 2007) have the potential to subject mesic *A. koa* forests to drier regimes. Our study suggests that in these scenarios, *A. koa* may have limited ability to adjust at the foliar level.

One of the more intriguing aspects of this study is that when *M. polymorpha* varies among sites, some variables are more similar between the wet and mesic sites and for other variables the mesic and dry site trees are more alike. The similarity in  $\Psi_{TLP}$  of *M. polymorpha* sampled at the dry and mesic sites (Table 2) may indicate that it is near its limit for osmotic adjustment at the mesic site, and that at sites with lower water availability longer periods of greater stomatal restriction of gas exchange may be required to prevent the risk of turgor loss at dangerously negative  $\Psi_{Leaf}$ . Indeed,  $\delta^{13}C$  increased sharply and  $g_s$  decreased sharply, in *M. polymorpha* at the dry site compared with the wet and mesic sites (Figure 4), another sign of a change in leaf physiological behavior at the dry end of the range.

The simultaneous increase in  $A_{max}$  and decrease in  $g_s$  in dry site *M. polymorpha* compared to the mesic site is likely responsible for the observed increase in  $\delta^{13}C$  (increased iWUE, Cordell et al. 1999); the inferred decrease in  $g_s$  in dry site *M. polymorpha* may be evidence of a movement towards drought-avoiding behavior. Despite the increase in iWUE and stomatal restriction of gas exchange, bole growth was comparable between mesic and dry sites in *M. polymorpha* (Table 4); however, as was noted for *A. koa<sub>2</sub>*, this metric of growth may not be the best indicator of overall growth in a species which displays radical changes in morphology over its native range (dry site trees were notably shorter than mesic or wet site trees). Nevertheless, carbon gain in dry site *M. polymorpha* did not appear impaired relative to trees at wetter sites; the highest NSC concentrations were found in dry site *M. polymorpha* (Figure 5) and increasing relative stomatal limitation of photosynthesis did not result in a significant reduction of integrated  $A$  (Figure 4b), likely owing to increases in  $N_{area}$  and subsequently  $A_{max}$  (Figure 3b - c) from wet to dry conditions. Higher  $N_{area}$  is a good indicator of both higher chlorophyll concentration and Rubisco

concentrations, which should lead to higher  $A_{\max}$  (Reich et al 1994). The pattern of increasing  $N_{\text{area}}$  and  $A_{\max}$  from wet to dry sites means that greater stomatal restriction of gas exchange at the dry site may be compensated for by higher  $A$  during times when conditions for gas exchange are favorable, as was also observed across a gradient from low to high elevation by Cordell et al. (1999). In contrast, *A. koa* did not show significant differences in  $N_{\text{area}}$  or  $A_{\max}$  between sites (Figure 3); by contrast, because leaf carbon isotope composition was more enriched at the drier site in this species, a significant decrease in time-integrated  $A$  and lower  $g_s$  was inferred for the drier site (Figure 4b - c). The implication is that future droughts may negatively impact the carbon balance of *A. koa* by limiting gas exchange, without compensatory changes in photosynthetic rates when gas exchange is possible (see also Ares and Fownes 1999).

### 3.5 Conclusions

We measured physiological traits of *A. koa* and *M. polymorpha* across a broad gradient of moisture availability to understand how populations of each species might respond to changes in climate regimes. Our findings lead us to conclude that *M. polymorpha* has a greater potential range of adjustment of leaf-level properties than *A. koa*. This work demonstrates how co-occurring, canopy-dominant species in forests with endemic species assemblages may have different capacities to adjust to drought conditions. *M. polymorpha*, a slow growing pioneer species, is more likely to see diminished growth and increased NSC accumulation under more frequent or severe drought regimes throughout its range, while adjustments to  $A_{\max}$  would be important to the long-term carbon balance of *M. polymorpha* at dry sites where stomatal limitation of gas exchange may increase. *A. koa*, a faster growing legume, is more likely to avoid drought and experience detrimental effects on the driest end of its range, with limited ability to change foliar properties in response to changing drought regimes. *A. koa* may be able to rely on

defoliation and regrowth of juvenile leaves (Pasquet-Kok et al. 2010) to avoid fatal drought stress, though the resource penalty associated with this transition is not known. This study serves as a framework for evaluating plasticity in drought resistance traits in mature trees by sampling across a range of water availabilities, which should be useful to other researchers who seek to understand how future drought may change the form and function of forests by differentially impacting the tree species that make up the canopy.

### 3.6 Acknowledgments

The Authors would like to thank Anna Hee for her help in the field. Support to establish the HIPNET plot network came from NSF EPSCoR grants 0554657 and 0903833. AS and RO were supported by funding to UH Hilo from the Pacific Island Climate Center entitled “Stand level water-use in forests of contrasting rainfall regimes: assessing the impacts of future drying on native Hawaiian ecosystems. Financial support was also provided by the USDA Forest Service Pacific Southwest Research Station Institute of Pacific Islands Forestry (USFS-IPIF). We thank the USFS-IPIF and the Hawaii Division of Forestry and Wildlife/Department of Land and Natural Resources for access to the Hawaii Experimental Tropical Forest.

### 3.7 References

- Ares, A., Fownes, J.H., 1999. Water supply regulates structure, productivity, and water use efficiency of *Acacia koa* forest in Hawaii. *Oecologia* 121, 458–466.  
<https://doi.org/10.1007/s004420050952>
- Baker, P.J., Scowcroft, P.G., Ewel, J.J., 2009. Koa (*Acacia koa*) ecology and silviculture (No. PSW-GTR-211). U.S. Department of Agriculture, Forest Service, Pacific Southwest Research Station, Albany, CA. <https://doi.org/10.2737/PSW-GTR-211>
- Belisário, R., Aucique-Pérez, C.E., Abreu, L.M., Salcedo, S.S., Oliveira, W.M. de, Furtado, G.Q., 2020. Infection by *Neopestalotiopsis* spp. occurs on unwounded eucalyptus leaves and is favoured by long periods of leaf wetness. *Plant Pathology* 69, 194–204.  
<https://doi.org/10.1111/ppa.13132>

- Benning, T.L., LaPointe, D., Atkinson, C.T., Vitousek, P.M., 2002. Interactions of climate change with biological invasions and land use in the Hawaiian Islands: Modeling the fate of endemic birds using a geographic information system. *Proceedings of the National Academy of Sciences* 99, 14246–14249. <https://doi.org/10.1073/pnas.162372399>
- Binks, O., Meir, P., Rowland, L., da Costa, A.C.L., Vasconcelos, S.S., de Oliveira, A.A.R., Ferreira, L., Christoffersen, B., Nardini, A., Mencuccini, M., 2016. Plasticity in leaf-level water relations of tropical rainforest trees in response to experimental drought. *New Phytologist* 211, 477–488. <https://doi.org/10.1111/nph.13927>
- Brown, G.K., Murphy, D.J., Kidman, J., Ladiges, P.Y., 2012. Phylogenetic connections of phyllodinous species of *Acacia* outside Australia are explained by geological history and human-mediated dispersal. *Australian Systematic Botany* 25, 390. <https://doi.org/10.1071/SB12027>
- Bowman, W.D. and Roberts, S.W. 1985. Seasonal and diurnal water relations adjustments in three evergreen chaparral shrubs. *Ecology* 66: 738 – 742. <https://doi.org/10.2307/1940534>
- Chu, P.-S., Chen, Y.R., Schroeder, T.A., 2010. Changes in precipitation extremes in the Hawaiian Islands in a warming climate. *J. Climate* 23, 4881–4900. <https://doi.org/10.1175/2010JCLI3484.1>
- Clifford, S.C., Arndt, S.K., Corlett, J.E., Joshi, S., Sankhla et al., 1998. The role of solute accumulation, osmotic adjustment and changes in cell wall elasticity in drought tolerance in *Ziziphus mauritiana* (Lamk.) *Journal of Experimental Botany* 49, 967-977.
- Cordell, S., Goldstein, G., Mueller-Dombois, D., Webb, D., Vitousek, P.M., 1998. Physiological and morphological variation in *Metrosideros polymorpha*, a dominant Hawaiian tree species, along an altitudinal gradient: the role of phenotypic plasticity. *Oecologia* 113, 188–196.
- Cordell, S., Goldstein, G., Meinzer, F.C., Handley, L.L., 1999. Allocation of nitrogen and carbon in leaves of *Metrosideros polymorpha* regulates carboxylation capacity and  $\delta^{13}\text{C}$  along an altitudinal gradient: Photosynthesis along an altitudinal gradient. *Functional Ecology* 13, 811–818. <https://doi.org/10.1046/j.1365-2435.1999.00381.x>
- Cordell, S., Goldstein, G., Meinzer, F.C., Vitousek, P.M., 2001. Regulation of leaf life-span and nutrient-use efficiency of *Metrosideros polymorpha* trees at two extremes of a long chronosequence in Hawai'i. *Oecologia* 127, 198–206. <https://doi.org/10.1007/s004420000588>
- Corn, C.A., Hiesey, W.M., 1973. Altitudinal variation in Hawaiian *Metrosideros*. *American Journal of Botany* 60, 991-1002.
- Crausbay, S.D., Frazier, A.G., Giambelluca, T.W., Longman, R.J., Hotchkiss, S.C., 2014. Moisture status during a strong El Niño explains a tropical montane cloud forest's upper limit. *Oecologia* 175, 273–284. <https://doi.org/10.1007/s00442-014-2888-8>

- Davis, S.D., Mooney, H.A., 1986. Water use patterns of four co-occurring chaparral shrubs. *Oecologia* 70, 172–177. <https://doi.org/10.1007/BF00379236>
- Dudley, N., Jones, T., James, R., Sniezko, R., Wright, J., et al. 2016. Applied genetic conservation of Hawaiian *Acacia koa*: an eco-regional approach. Banking on the Future: General Technical Report PNW-GTR-963.
- Farquhar, G.D., Ehleringer J.R., Hubick K.T., 1989. Carbon isotope discrimination and photosynthesis. *Annual Review of Plant Physiology and Plant Molecular Biology* 40,503-537.
- Frazier, A.G., Giambelluca, T.W., 2017. Spatial trend analysis of Hawaiian rainfall from 1920 to 2012. *Int. J. Climatol.* 37, 2522–2531. <https://doi.org/10.1002/joc.4862>
- Fortini, L.B, Jacobi, J.D., Price, J.P. 2017. Chapter 3. Projecting end-of-century shifts in the pattern of plant available water across Hawai'i to assess implications to vegetation shifts. U.S. Geological Survey Professional Paper 1834.
- Giambelluca T.W., Luke M.S.A. 2007. Climate change in Hawai'i's mountains. Mountain views: The newsletter of the consortium for integrated climate research in western mountains. Consortium for Integrated Climate Research in Western Mountains 2, 13–17.
- Granda, E., Camarero, J.J., 2017. Drought reduces growth and stimulates sugar accumulation: new evidence of environmentally driven non-structural carbohydrate use. *Tree Physiology* 37, 997–1000.
- Haines, W.P., Heddle, M.L., Welton, P., Rubinoff, D., 2009. A recent outbreak of the Hawaiian Koa Moth, *Scotorythra paludicola* (Lepidoptera: Geometridae), and a review of outbreaks between 1892 and 2003. *Pacific Science* 63, 349–369. <https://doi.org/10.2984/049.063.0305>
- Harrington, R.A., Fownes, J.H., Meinzer, F.C., Scowcroft, P.G., 1995. Forest growth along a rainfall gradient in Hawaii: *Acacia koa* stand structure, productivity, foliar nutrients, and water- and nutrient-use efficiencies. *Oecologia* 102, 277–284.
- Hartmann, H., Trumbore, S., 2016. Understanding the roles of nonstructural carbohydrates in forest trees - from what we can measure to what we want to know. *New Phytologist* 211, 386–403.
- Hsiao, T.C., Acevedo, E., Fereres, E., Henderson, D.W., 1976. Water stress, Growth, and Osmotic Adjustment. *Philosophical Transactions of the Royal Society B: Biological Sciences* 273, 479–500.
- Johnson, D.J., Needham, J., Xu, C., Massoud, E.C., Davies, S.J., et al. 2018. Climate sensitive size-dependent survival in tropical trees. *Nature Ecology and Evolution* 2, 1436–1442. <https://doi.org/10.1038/s41559-018-0626-z>

- Joel, G., Aplet, G., Vitousek, P.M., 1994. Leaf morphology along environmental gradients in Hawaiian *Metrosideros polymorpha*. *Biotropica* 26, 17 - 22.
- Jordan, C.F., 1982. The nutrient balance of an Amazonian rain forest. *Ecology* 63, 647–654. <https://doi.org/10.2307/1936784>
- Kier, G., Kreft, H., Lee, T.M., Jetz, W., Ibisch, P.L. et al., 2009. A global assessment of endemism and species richness across island and mainland regions. *Proceedings of the National Academy of Sciences* 106, 9322–9327. <https://doi.org/10.1073/pnas.0810306106>
- Letts, M.G., Mulligan, M., 2005. The impact of light quality and leaf wetness on photosynthesis in north-west Andean tropical montane cloud forest. *J. Trop. Ecol.* 21, 549–557. <https://doi.org/10.1017/S0266467405002488>
- Long, E.S., Sweitzer, R.A., Diefenbach, D.R., Ben-David, M., 2005. Controlling for anthropogenically induced atmospheric variation in stable carbon isotope studies. *Oecologia* 146, 148–156. <https://doi.org/10.1007/s00442-005-0181-6>
- Ludlow, M. M. 1989. Strategies of response to water stress. In ‘Structural and functional responses to environmental stresses’, (Eds K.H. Kreeb, H. Richter and T.M. Hinckley). Pp. 269-281. (SPB Academic: The Hague)
- Lyon, B., 2004. The strength of El Niño and the spatial extent of tropical drought. *Geophysical Research Letters* 31, L21204. <https://doi.org/10.1029/2004GL020901>
- Martínez-Vilalta, J., Sala, A., Asensio, D., Galiano, L., Hoch, G., Palacio, S., Piper, F.I., Lloret, F., 2016. Dynamics of non-structural carbohydrates in terrestrial plants: a global synthesis. *Ecol Monogr* 86, 495–516. <https://doi.org/10.1002/ecm.1231>
- Meinzer, F.C., Sharifi, M.R., Nilsen, E.T., Rundel, P.W., 1988. Effects of manipulation of water and nitrogen regime on the water relations of the desert shrub *Larrea tridentata*. *Oecologia* 77, 480–486. <https://doi.org/10.1007/BF00377263>
- Meinzer, F.C., Woodruff, D.R., Marias, D.E., McCulloh, K.A., Sevanto, S., 2014. Dynamics of leaf water relations components in co-occurring iso- and anisohydric conifer species. *Plant, Cell & Environment* 37, 2577–2586. <https://doi.org/10.1111/pce.12327>
- Michaud, J., Cordell, S., Cole, T.C., Ostertag, R., 2015. Drought in an invaded Hawaiian lowland wet forest. *Pacific Science* 69, 367–383. <https://doi.org/10.2984/69.3.6>
- McCulloh, K.A., Johnson, D.M., Meinzer, F.C., Woodruff, D.R., 2014. The dynamic pipeline: hydraulic capacitance and xylem hydraulic safety in four tall conifer species: The dynamic pipeline. *Plant, Cell & Environment* 37, 1171–1183. <https://doi.org/10.1111/pce.12225>

- McMahon, T.A., Peel, M.C., Lowe, L., Srikanthan, R., McVicar, T.R., 2013. Estimating actual, potential, reference crop and pan evaporation using standard meteorological data: a pragmatic synthesis. *Hydrology and Earth System Sciences* 17, 1331–1363.
- Muller, B., Pantin, F., Génard, M., Turc, O., Freixes, et al. 2011. Water deficits uncouple growth from photosynthesis, increase C content, and modify the relationships between C and growth in sink organs. *Journal of Experimental Botany* 62, 1715–1729.  
<https://doi.org/10.1093/jxb/erq438>
- Nelson, S., 2009. Rusts of *Acacia koa*: *Atelocauda digitata* (Gall Rust). UH-CTAHR Technical Document PD – 63.
- O'Brien, M.J., Leuzinger, S., Philipson, C.D., Tay, J., Hector, A., 2014. Drought survival of tropical tree seedlings enhanced by non-structural carbohydrate levels. *Nature Clim Change* 4, 710–714. <https://doi.org/10.1038/nclimate2281>
- Ohlemüller, R., Anderson, B.J., Araújo, M.B., Butchart, S.H., Kudrna, O. et al., 2008. The coincidence of climatic and species rarity: high risk to small-range species from climate change. *Biology Letters* 4, 568–572. <https://doi.org/10.1098/rsbl.2008.0097>
- Ostertag, R., Inman-Narahari, F., Cordell, S., Giardina, C.P., Sack, L., 2014. Forest structure in low-diversity tropical forests: A study of Hawaiian wet and dry Forests. *PLoS ONE* 9, e103268.
- Pasquet-Kok, J., Creese, C., Sack, L., 2010. Turning over a new 'leaf': multiple functional significances of leaves versus phyllodes in Hawaiian *Acacia koa*: Leaves versus phyllodes of *Acacia koa*. *Plant, Cell & Environment* 33, 2084–2100. <https://doi.org/10.1111/j.1365-3040.2010.02207.x>
- Phillips, O.L., van der Heijden, G., Lewis, S.L., López-González, G., Aragão, L.E.O.C., et. al. 2010. Drought-mortality relationships for tropical forests. *New Phytologist* 187, 631–646. <https://doi.org/10.1111/j.1469-8137.2010.03359.x>
- Piper, F.I., Fajardo, A., Hoch, G., 2017. Single-provenance mature conifers show higher non-structural carbohydrate storage and reduced growth in a drier location. *Tree Physiology* 37, 1001–1010.
- Reich, P.B, Walters, M.B., Ellsworth, D.S., Uhl, C. 1994. Photosynthesis-nitrogen relations in Amazonian tree species. I. Patterns among species and communities. *Oecologia* 97, 62-72.
- de la Riva, E.G., Olmo, M., Poorter, H., Ubera, J.L., Villar, R., 2016. Leaf mass per Area (LMA) and its relationship with leaf structure and anatomy in 34 Mediterranean woody species along a water availability gradient. *PLoS ONE* 11, e0148788.  
<https://doi.org/10.1371/journal.pone.0148788>

- R Core Team (2020). R: A language and environment for statistical computing. R Foundation for Statistical Computing, Vienna, Austria. URL <https://www.R-project.org/>.
- Sala, A., Hoch, G., 2009. Height-related growth declines in ponderosa pine are not due to carbon limitation. *Plant, Cell & Environment* 32, 22–30.
- Sapes, G., Demaree, P., Lekberg, Y., Sala, A., 2020. Plant carbohydrate depletion impairs water relations and spreads via ectomycorrhizal networks. *New Phytol* *nph.17134*.  
<https://doi.org/10.1111/nph.17134>
- Touchette, B.W., Iannacone, L.R., Turner, G.E., Frank, A.R., 2007. Drought tolerance versus drought avoidance: A comparison of plant-water relations in herbaceous wetland plants subjected to water withdrawal and repletion. *Wetlands* 27, 656–667.
- Trumbore, S., P. Brando, and H. Hartmann. 2015. Forest health and global change. *Science* 349, no. 6250: 814–18.
- Turner, N.C., 1988. Measurement of plant water status by the pressure chamber technique. *Irrigation Science* 9, 289–308.
- Tyree, M.T., Hammel, H.T., 1972. The measurement of the turgor pressure and the water relations of plants by the pressure-bomb technique. *Journal of Experimental Botany* 23, 267–282.
- Vitousek, P.M., Walker, L.R., Whiteaker, L.D., Mueller-Dombois, D., Matson, P.A., 1987. Biological invasion by *Myrica faya* alters ecosystem development in Hawaii. *Science* 238, 802–804. <https://doi.org/10.1126/science.238.4828.802>
- Williams, J.W., Jackson, S.T., Kutzbach, J.E., 2007. Projected distributions of novel and disappearing climates by 2100 AD. *Proceedings of the National Academy of Sciences* 104, 5738–5742. <https://doi.org/10.1073/pnas.0606292104>
- Williams, S.E., Bolitho, E.E., Fox, S., 2003. Climate change in Australian tropical rainforests: an impending environmental catastrophe. *Proceedings of the Royal Society of London. Series B: Biological Sciences* 270, 1887–1892. <https://doi.org/10.1098/rspb.2003.2464>
- Wolfe, C.E.W., Morris, J., 1996. Geologic Map of the Island of Hawaii. Accompaniment to U.S. Department of the Interior and U.S. Geologic Survey map I-2524-A.
- Woodruff, D.R., Meinzer, F.C., 2011. Water stress, shoot growth and storage of non-structural carbohydrates along a tree height gradient in a tall conifer: Growth, water stress and carbohydrate storage. *Plant, Cell & Environment* 34, 1920–1930.
- Whitsell, C.D. 1990. *Acacia koa* grey. *Silvics of North America* Vol. 2, 17-28.
- Wright, S.D., Yong, C.G., Dawson, J.W., Whittaker, D.J., Gardner, R.C., 2000. Riding the ice age El Nino? Pacific biogeography and evolution of *Metrosideros* subg. *Metrosideros*

(Myrtaceae) inferred from nuclear ribosomal DNA. Proceedings of the National Academy of Sciences 97, 4118–4123. <https://doi.org/10.1073/pnas.050351197>

## 3.7 Figures

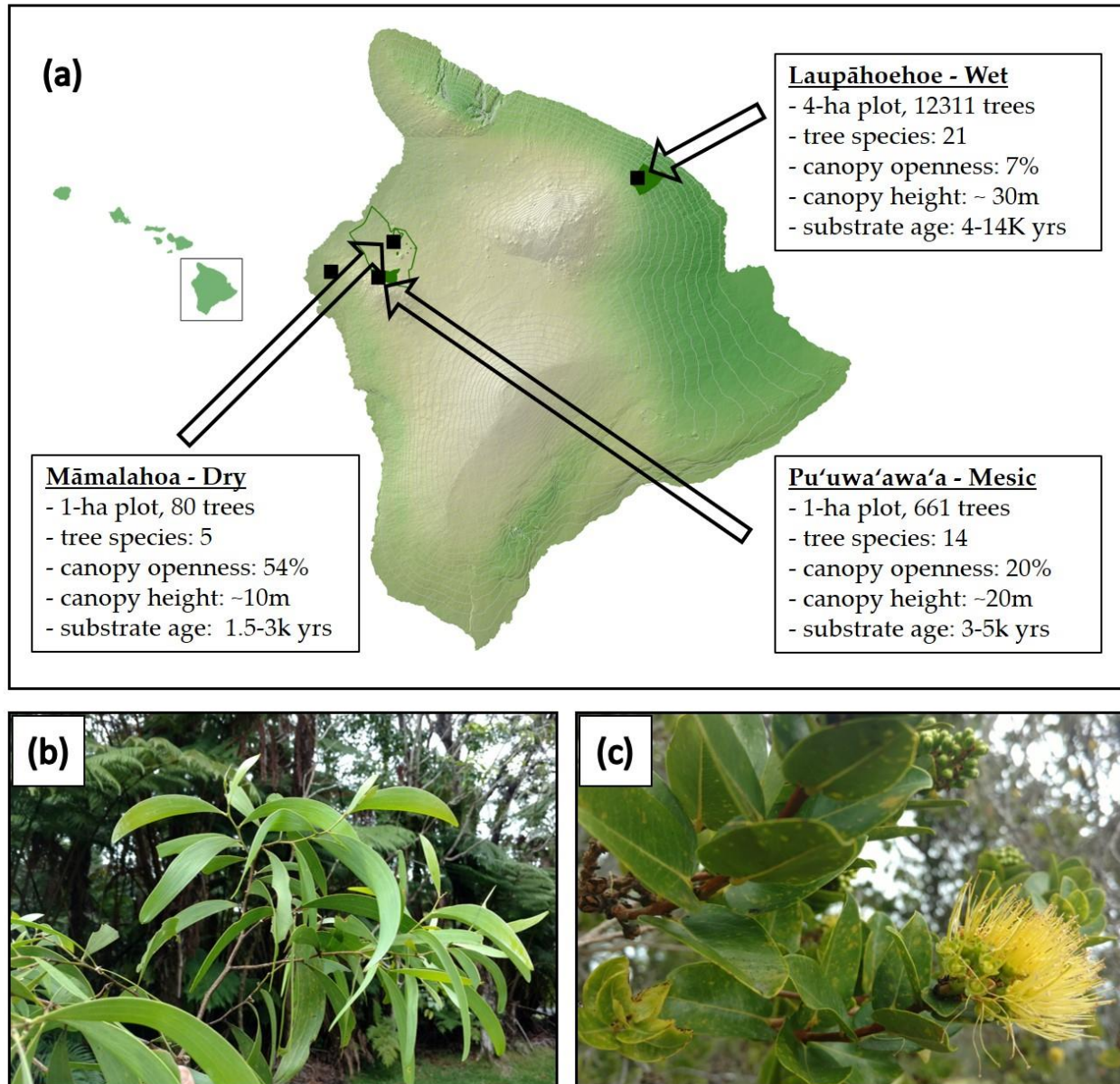


**Figure 3-1: Site locations and study species foliage**

(a) Map of the island of Hawai'i. Black squares on map show the location of the HIPPNET permanent survey plots. (b) Typical display of *A. koa* phyllodes; phyllodes shown ~ 12cm in length. (c) Typical display of *M. polymorpha* leaves; leaves shown ~ 4cm.

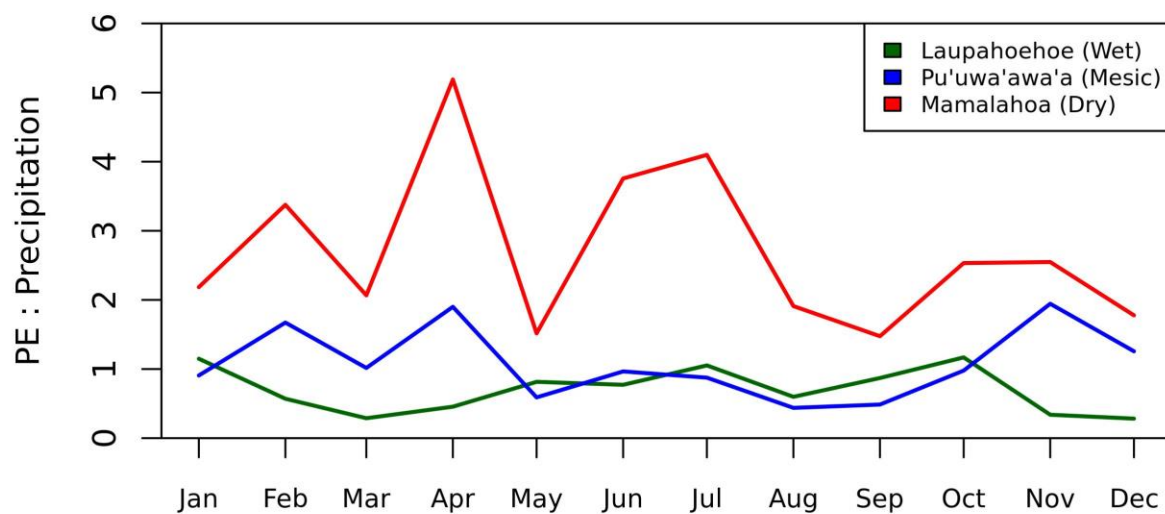


**Figure 3-2: PET : Precipitation ratio**

The ratio of potential evapotranspiration (PET) to precipitation on a monthly basis at each site. PET was calculated using the Priestley-Taylor method. Monthly averages were computed using eight, five and six years of data for the wet, mesic and dry sites, respectively.

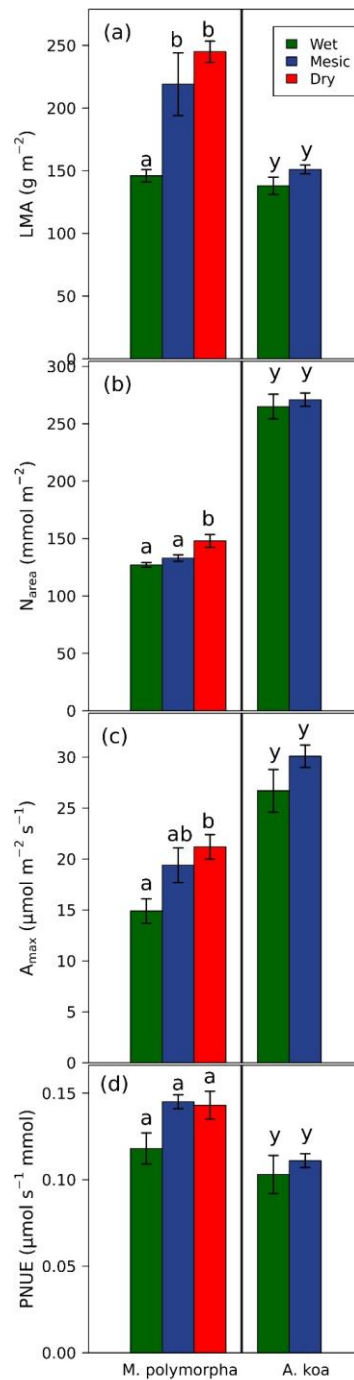


**Figure 3-3: Variation in traits related to photosynthesis**

a. Leaf mass per area (LMA), b. amount of nitrogen per unit leaf area ( $N_{\text{area}}$ ), c. maximum photosynthetic rate ( $A_{\text{max}}$ ) and d. maximum potential photosynthetic nitrogen use efficiency (PNUE) for both species at all study sites. Letters above bars represent groups within species, where bars that share a common letter are not significantly different from each other in the displayed metric. Confidence intervals represent one standard error.

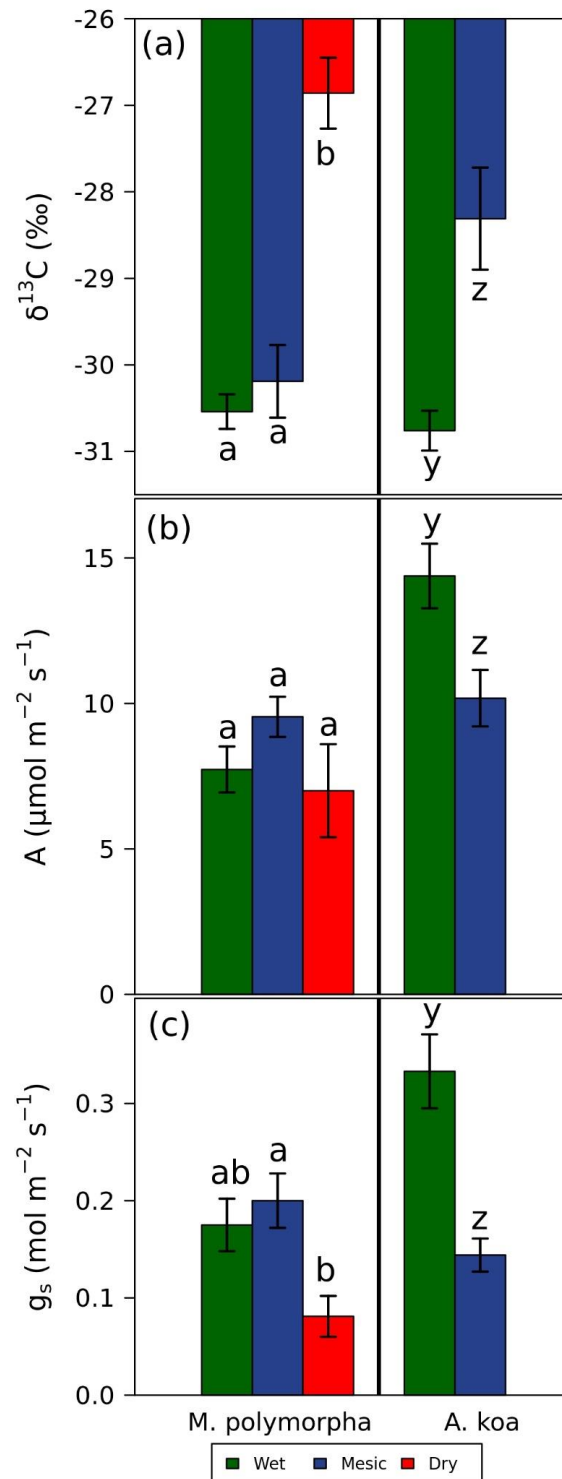


**Figure 3-4: Gas exchange traits**

Fractionation of carbon 13 in foliage ( $\delta^{13}\text{C}$ ), time-integrated assimilation ( $A$ ) and time-integrated (assimilation weighted) stomatal conductance ( $g_s$ ) in both species. Panels b and c calculated from  $\delta^{13}\text{C}$  data (see methods). Letters above bars represent groups within species, where bars that share a common letter are not significantly different from each other in the displayed metric.

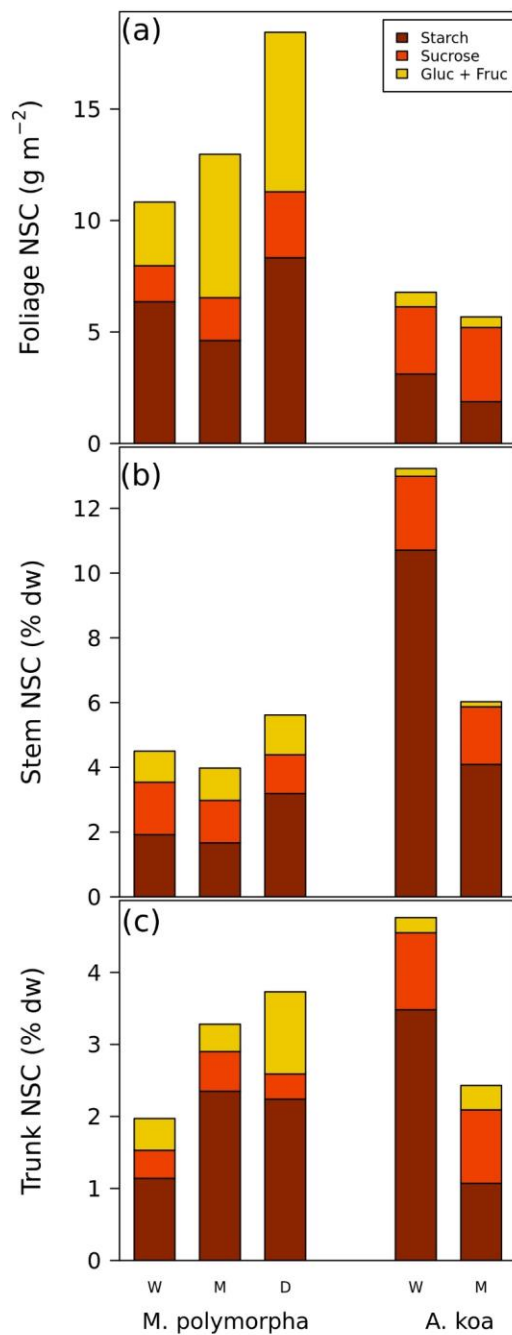


**Figure 3-5: NSC concentrations**

Concentration of total NSC (starch, sucrose, and glucose + fructose) in the foliage, stem, and trunk tissue of *M. polymorpha* and *A. koa* at the wet (W), mesic (M) and dry (D) sites.

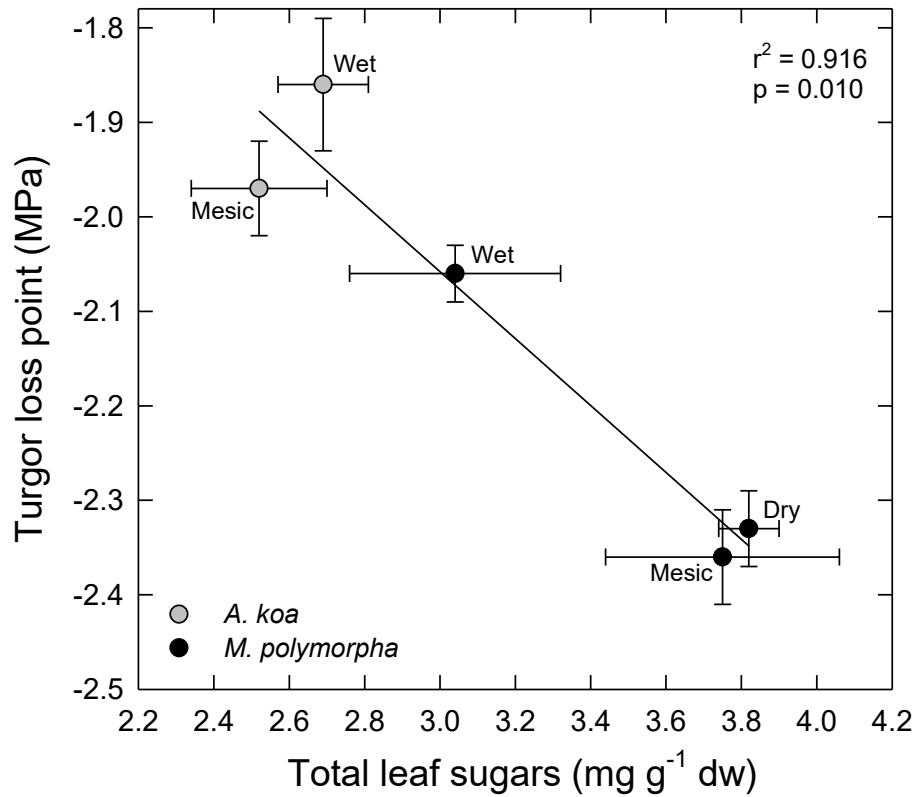


**Figure 3-6: Turgor loss point vs. Total leaf sugars**

Regression between leaf turgor loss point and total leaf sugar concentration, using the mean values at each site and each species. Error bars represent one standard deviation.

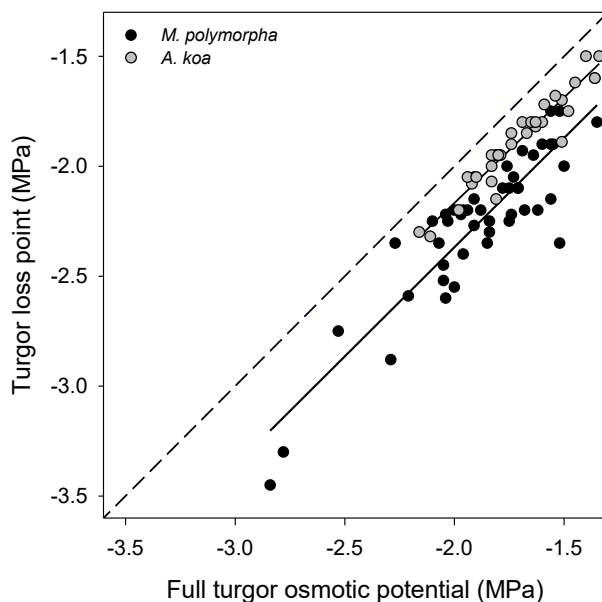


**Figure 3-7: Turgor loss point vs. Full turgor osmotic potential**

Turgor loss point vs. full turgor osmotic potential from all rounds of P-V curve data at all sites. Dashed line represents 1:1 line. Thin solid line represents the linear regression of *A. koa* data, thick solid line is regression for *M. polymorpha* data. Both regressions had  $R^2$  values  $> 0.9$  and  $p$  values  $< 0.001$ . The offset between the two regression lines and the 1:1 line can be viewed as estimates of the range of potential maximum turgor.

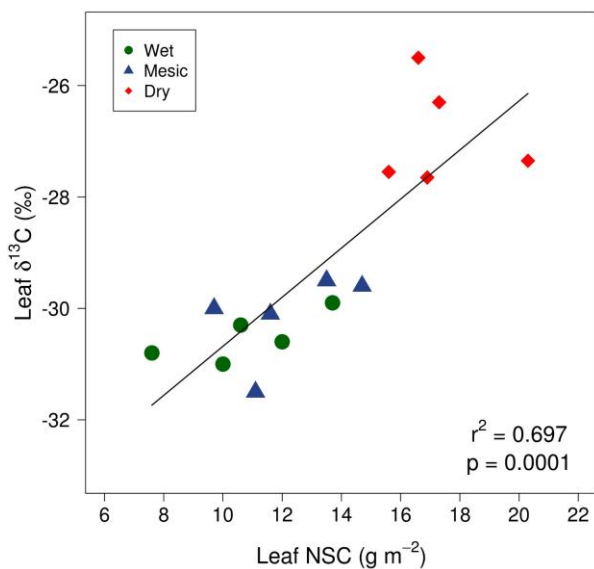


**Figure 3-8: Foliar  $\delta^{13}\text{C}$  vs total foliar NSC concentration for *M. polymorpha* at all three sites.**

### 3.7 Tables

**Table 3-1: Site climate characteristics**

Summary of mean annual rainfall, temperature, and atmospheric vapor pressure deficit (VPD) at each study site. Values in parentheses represent one standard error. VPD was calculated using temperature and relative humidity data collected at ten-minute intervals just above canopy height. Extant, complete years of data at the Laupāhoehoe, Pu'u Wa'awa'a and Māmalahoa climate stations are 8, 5 and 6 respectively.

Site Descriptor	Site Name	Mean Annual			Elevation (m)
		Rainfall (mm)	Temperature (°C)	VPD (kPa)	
Wet	Laupāhoehoe	6773 (742)	15.9 (0.230)	0.248 (0.013)	1145
Mesic	Pu'u Wa'awa'a	886 (177)	14.4 (0.147)	0.282 (0.005)	1659
Dry	Māmalahoa	554 (79)	20.3 (0.176)	0.623 (0.024)	636

**Table 3-2: Leaf water relation traits**

Osmotic potential at full turgor ( $\Psi_{\pi 100}$ ), water potential at turgor loss point ( $\Psi_{TLP}$ ), shoot capacitance (C) and shoot bulk modulus of elasticity (MOE) for each species at each site. Values in parentheses represent one standard error. Letter designations go by column within species and represent groupings within which no pair-wise differences between means were found, as determined using the Tukey's Honest Significant Difference (HSD) test with a p value threshold of  $p < 0.05$ . Letter codes a, b and c used to denote groupings among *M. polymorpha* sites, and letters y and z used for groupings between *A. koa* sites. P values below site values are from one-way analysis of variance (ANOVA) within species across study sites. The Plasticity index represents the range of means across sites divided by the maximum mean, expressed as a percentage.

	$\Psi_{\pi 100}$ (MPa)	$\Psi_{TLP}$ (MPa)	C (g g <sup>-1</sup> MPa <sup>-1</sup> )	MOE (MPa)
<i>M. polymorpha</i>				
Wet	-1.77 (0.03) a	-2.06 (0.03) a	0.090 (0.004) a	24 (4) a
Mesic	-1.96 (0.06) a	-2.36 (0.05) b	0.061 (0.007) b	26 (2) ab
Dry	-1.86 (0.10) a	-2.33 (0.05) b	0.033 (0.002) c	39 (4) b
p value	0.17	0.001	< 0.001	0.025
plasticity index	9.7%	12.7%	63.3%	38.5%
<i>A. koa</i>				
Wet	-1.70 (0.07) y	-1.86 (0.07) y	0.068 (0.009) y	30 (3) y
Mesic	-1.76 (0.03) y	-1.97 (0.05) y	0.069 (0.010) y	26 (4) y
p value	0.45	0.23	0.9	0.45
plasticity index	3.4%	5.6%	1.4%	13.3%

**Table 3-3: Relative basal area increment**

Mean relative basal area increment (RBAI) for each species at all sites. Growth values from all measured trees in HIPNET plots with diameters at breast height between 10cm and 60cm. Values in parentheses represent one standard error.

Site	Relative Basal Area Increment (%/yr)			
	<i>M. polymorpha</i>		<i>A. koa</i>	
	mean (s.e)	n	mean (s.e)	n
Wet	3.3 (.20) a	608	5.2 (0.39) y	197
Mesic	0.73 (.10) b	440	10.2 (1.1) z	67
Dry	1.0 (.01) b	162		

## CHAPTER 4

### BIOCHEMICAL AND STOMATAL EFFECTS ON NET ASSIMILATION IN TWO CO-OCCURRING CONIFER SPECIES EXPOSED TO LONG-TERM WARMING AND HEATWAVE CONDITIONS

Adam Sibley, Forest Ecosystems and Society, Oregon State University

Sanna Sevanto, Atmosphere, Climate and Ecosystem Science Department, Los Alamos Nat'l Lab

Frederick C. Meinzer, Pacific Northwest Research Station, USDA Forest Service

Adam Collins, Atmosphere, Climate and Ecosystem Science Department, Los Alamos Nat'l Lab

Danielle Ulrich, Department of Ecology, Montana State University

Christopher Still, Forest Ecosystems and Society, Oregon State University

## Abstract

Simulations of future climate predict that many parts of the planet will experience higher air temperatures ( $T_{\text{air}}$ ) via a combination of elevated baseline  $T_{\text{air}}$  and more frequent, more severe, and/or longer duration heatwaves (IPCC 2014). The temperature of a tree's foliage ( $T_{\text{leaf}}$ ) exerts strong control over the net rate of carbon dioxide assimilation ( $A_{\text{net}}$ ) in leaves, meaning that future warming has the potential to impact the long-term carbon balance of trees. In this study, we observed  $A_{\text{net}}$  and the component processes that determine  $A_{\text{net}}$  in mature *juniperus monosperma* (juniper) and *pinus edulis* (piñon pine) trees exposed to long-term, moderate warming as well as short-term, heatwave-like warming in the field. Results show that the optimum temperature for photosynthesis shifted more in juniper than piñon in response to moderate, long-term warming, though an apparent decrease in stomatal conductance and stomatal responsiveness to VPD was seen in both species in response to long-term warming. During simulated heatwave conditions, a large reduction of  $A_{\text{net}}$  was observed in juniper compared to long-term heated or control branches. The primary cause of this reduction does not appear to be biochemical limitations, but rather physiological impairment that led to low stomatal conductance values. Low stomatal conductance was observed at all measurement temperatures in heatwave foliage, in spite of measurements being taken on excised shoots with the cut ends submerged in water for several hours before measurement. Values of stomatal conductance in heatwave treated piñon were low, but not distinguishable from control and long-term heated groups and did not result in significant differences between groups in  $A_{\text{net}}$ . The results of this study suggest that heatwaves may negatively impact the carbon balance of trees beyond the time period when the heatwave event occurs, with one possible mechanism being induced embolism in spite of nearly full stomatal closure.

## 4.1 Introduction

Simulations of future climate predict that many parts of the planet will experience higher air temperatures ( $T_{\text{air}}$ ) via a combination of elevated baseline  $T_{\text{air}}$  and more frequent, more severe, and/or longer duration heatwaves (IPCC 2014). The temperature of a tree's foliage ( $T_{\text{leaf}}$ ) exerts strong control over the net rate of carbon dioxide assimilation ( $A_{\text{net}}$ ) in leaves, meaning that future warming has the potential to impact the long-term carbon balance of trees. Acclimation in this context would mean shifting leaf level physiological traits so that a comparable level of  $A_{\text{net}}$  is maintained under warmer temperature regimes. In contrast, lack of acclimation or impairment of physiological processes related to carbon acquisition would result in lower levels of  $A_{\text{net}}$  and may lead over time to diminished growth rates, greater susceptibility to damage by insects or pathogens, or mortality. In the case of extremes like heatwaves, damage to cellular processes may require a lengthy recovery period and leave trees susceptible to greater harm from subsequent droughts (Marias et al 2016). The high vapor pressure deficit (VPD) conditions that foliage experiences during heatwaves also have the potential to induce xylem embolism despite stomatal closure, affecting both regulation of gas exchange and the ability to adequately rehydrate after heat and/or drought events.

At least three major aspects of leaf physiology are involved in determining acclimation or impairment of  $A_{\text{net}}$  at above-normal temperatures: 1) rates of biochemical reactions involved in carbon fixation and Ribulose 1,5-Biphosphate (RuBP) regeneration; 2) rates of mitochondrial respiration; and 3) the response of stomata to higher temperature and/or VPD (Kumarathunge et al. 2019). Both photosynthesis and respiration rely on enzyme-catalyzed reactions that have generally well understood temperature dependencies (Young et al. 2015), though considerable

variation exists between species (Kumarathunge et al. 2019) and across different times of year (Kosugi and Matsuo 2006, Sage and Kubien 2007). The net effect of acclimation or impairment of each of these processes determines whether trees that are exposed to higher  $T_{\text{air}}$  – either in short-term heatwaves or long-term temperature regime shifts - will be able to acclimate and preserve their carbon balance. It is well understood that plants adjust on the biochemical level to shift the optimal temperature for photosynthesis ( $T_{\text{opt}}$ ) as growth temperature changes on seasonal scales (Mooney and West 1964, Sage and Kubien 2007). However, the degree of acclimation of  $A_{\text{net}}$  to higher growth temperatures varies considerably among tree species (Sage and Kubien 2007) and genotypes (Benomar et al. 2019). Furthermore, the extent to which acclimation to temperatures within an annual cycle translates to an ability to acclimate to heatwave conditions is uncertain.

In this study we examined two co-occurring conifer trees, piñon pine (*Pinus edulis Engelm.*) and one-seed juniper (*Juniperus monosperma Engelm. Sarg.*, hereafter simply juniper). High temperature and drought events across the Southwestern United States in the early 2000s led to tree mortality in piñon-juniper woodlands, with much higher mortality rates among piñon pines than juniper (Breshears et al. 2009). Investigations into the mechanisms involved have stressed the importance of depleted resin reserves in droughted trees (Gaylord et al. 2013) which may be explained by prolonged reductions in photosynthetic uptake (Lajtha and Barnes 1991) that leaves droughted trees more susceptible to damage by beetles (Gaylord et al. 2013, Floyd et al. 2009). In the early 2010s, the survival mortality (SUMO) experiment began at Los Alamos National Laboratory, where infrastructure was built to expose piñon pine and juniper trees to drought and / or elevated ambient  $T_{\text{air}}$  conditions so that physiological response to warmer and drier conditions

could be studied explicitly. Observations at the site from 2012 - 2014 did not show a significant reduction in maximum assimilation rates ( $A_{\max}$ ) or stomatal conductance ( $g_s$ ) measured on intact branches on heated trees compared to control trees (Grossiord et al. 2017a); however, by 2016, canopy conductance and branch xylem conductivity were both significantly lower in heated juniper trees, and in both species  $g_s$  was less responsive to VPD in heated trees compared to control trees (Grossiord et al. 2017b). While these results suggested that heating alone (i.e., no imposed drought) may have had long-term effects on stomatal regulation of gas exchange, no explicit accounting was done for potential acclimation of cellular respiration or the biochemistry of photosynthesis to higher air temperature.

In this study, we used branches sampled in 2018 from trees in the long-term heated and control treatment groups to construct photosynthesis temperature response curves. Using these curves, we examined the magnitude of change in the optimum temperature for photosynthesis ( $T_{\text{opt}}$ ), the rate of decline in  $A_{\text{net}}$  past the optimum, and the response of  $g_s$  to increasing VPD for both groups. Within these same two treatment groups we used fluorescence measurements to derive the ratio of variable to maximum fluorescence ( $F_v / F_m$ ) for dark-adapted leaves across a range of  $T_{\text{leaf}}$  values to ascertain when the function of photosystem II became damaged in each group. In 2019, we imposed heatwave-like  $T_{\text{air}}$  conditions on select foliage from long-term heated trees for three weeks to test how the factors which control  $A_{\text{net}}$  responded to heatwave conditions. Using foliage from control trees, long-term heated trees, and the heatwave treated foliage, we measured net assimilation vs. intercellular  $\text{CO}_2$  concentration ( $A\text{-}C_i$ ) curves at 25, 35, and 45 °C to examine differences in the temperature dependencies of the component processes of  $A_{\text{net}}$  – specifically, the maximum rate of carboxylation ( $V_{\text{cmax}}$ ), maximum electron transport rate ( $J_{\text{max}}$ ), and dark

respiration ( $R_d$ ). Values of each metric were compared among treatment groups to test whether either species experienced detrimental effects of high  $T_{air}$ , or conversely acclimated to hotter conditions.

## 4.2 Methods

### 4.2.1 Site Description

This study took place at the Survival/Mortality Experiment site (SUMO) at Los Alamos National Laboratory. This site was designed to test different combinations of warming and drought treatments by intentionally stressing piñon pine and juniper trees in ways that are representative of expected conditions in the year 2100 under “business-as-usual” climate warming scenarios (Figure 1). The site has been described in depth in other publications (Garcia-Forner et al. 2016) and has been used in numerous studies which interrogated the physiological effects of drought and heat stress on mature trees in the field (Garcia-Forner et al. 2016, McDowell et al. 2013, Grossiord et al. 2017). Briefly, the elevation of the site is 2175 m above sea level, mean annual temperature is 9.1°C, and mean annual precipitation is 481 mm, based on 30-year climate normals (period 1981 – 2010, [weathermachine.lanl.gov](http://weathermachine.lanl.gov)). The hottest months of the year are typically July and August with mean daily temperatures of 20.1 and 18.8 °C and mean daily maximums of 27.4 and 25.6 °C. Early summer is characterized by an early summer dry period (rainfall in May and June averages 35 and 38 mm), followed by a monsoon season that typically starts between late June and late July and lasts several months (July and August rainfall averages are 72 and 92 mm). The combined temperature and precipitation regimes of the monsoon season make it the portion of the year that is most favorable to carbon assimilation but also the most likely period of time for high  $T_{air}$  to occur. Sampling in this study was conducted in August to

ensure that monsoon conditions had arrived and stomatal conductance ( $g_s$ ) values for trees in the field were above the dormancy-like levels observed in the dry early summer (Garcia-Forner et al. 2016).

The sampling design used in this study used a subset of the SUMO infrastructure, shown in Figure 1 a - b. For each tree species, five individuals were selected that had not been exposed to either artificial drought or long-term heating treatments (control groups). Five individuals of each species were selected from the long-term heating chambers (heated groups). On each of the trees in the heated groups, a branch was selected to be placed in front of a panel heater to raised leaf temperatures beyond the baseline  $+5^\circ\text{C}$  warming (heatwave groups, Figure 1c). For logistical reasons, panels were only used to expose trees in warming chambers to heatwave conditions, though it would have been advantageous to expose control trees to heatwave temperatures as well. The warming setups are described in greater detail in the following section.

#### ***4.2.2 Long-term and short-term warming***

Whole-tree, long-term warming was accomplished inside open-top plexiglass chambers (Figure 1b) via heating and cooling units with thermostats set to maintain air temperature ( $T_{\text{air}}$ )  $5^\circ\text{C}$  above ambient. These chambers were constructed and turned on approximately five years before our first round of data collection in August of 2018, resulting in a near constant  $+5^\circ\text{C}$  both day and night (see Garcia-Forner et al. 2016). After the first data collection, in fall of 2018 the heating and cooling units were turned off but the chambers remained in place, creating a greenhouse effect that resulted in  $\sim+5^\circ\text{C}$  temperature elevation during the day. During this period chamber air cooled after sunset at a rate such that it matched ambient  $T_{\text{air}}$  after a number of hours. Thus, the foliage samples collected during the second measurement campaign (August

2019) experienced five years where  $T_{\text{air}}$  was  $+5^{\circ}\text{C}$  twenty-four hours a day, and one year where daytime temperatures were  $\sim+5^{\circ}\text{C}$ . For the period of the second sampling (August 5<sup>th</sup> – September 6<sup>th</sup> of 2019), the chamber heating and cooling units were turned back on, and  $+5^{\circ}\text{C}$  was maintained twenty-four hours a day.

Short-term, high temperature (“heatwave”) warming was achieved by positioning individual branches  $\sim 15$  cm from the surface of 200 W electric panel heaters (Fig 1c., Cozy Safe Chicken Coop 200W Heater, Cozy Products, Elmhurst, IL.). The panel heaters were turned on twenty-four hours a day from August 14<sup>th</sup> to September 6<sup>th</sup>, 2019. The panels had internal thermostats with a shutoff value of  $75^{\circ}\text{C}$  and were observed to approach this value at mid-day with full sun exposure. Foliage samples were taken from the heatwave treated foliage on Sept. 4<sup>th</sup> and 5<sup>th</sup>.

#### ***4.2.3 Measuring leaf temperatures***

During the second measurement campaign in August 2019 we quantified leaf temperatures ( $T_{\text{leaf}}$ ) in the field using two methods. In the first method fine wire thermocouples were nested into the foliage on seven heatwave treatment branches (three piñon, four juniper). Measurements were taken every 10 minutes for the duration of the heatwave treatment (section 2.2). Care was taken to position the thermocouples in close contact with foliage, though no adhesive was applied as might be done on broadleaf foliage because of the scale like (juniper) and needle shaped (piñon) foliage of the gymnosperms examined in this study. These measurements are best interpreted as a composite of  $T_{\text{leaf}}$  and boundary layer  $T_{\text{air}}$  temperature. On 8 out of 21 heatwave days, measurements for both species approached or exceeded  $40^{\circ}\text{C}$  at midday, with slightly hotter temperatures in piñon foliage (Figure 2).

The second method of observing  $T_{\text{leaf}}$  involved taking a series of images with a handheld thermal camera (T450sc, FLIR, Wilsonville, OR) in 2019. Images were taken on Aug 24<sup>th</sup>, a clear day during the heatwave treatment period where maximum ambient  $T_{\text{air}}$  reached 31.5°C. Images were taken of control, heated, and heatwave treatment foliage at three different time points: early morning (8:20 – 9:00 am), mid-morning (10:45 – 11:30 am) and mid-day (13:00 – 13:50 pm). At each tree we took one image of sunlit and one image of shaded foliage. Thermal images were imported into imageJ, and a random sampling of 100 pixels which only contained foliage were selected for analysis. Careful attention was paid to selecting pure pixels without edge effects, as pixels mixed with background objects like the sky, heater panels, or chamber scaffolding would not represent a true  $T_{\text{leaf}}$  estimate. Temperatures values extracted from the selected pixels were pooled with foliage belonging to the same treatment + species + time of day + illumination group to produce histograms representing the range of  $T_{\text{leaf}}$  experienced through the course of the morning and early afternoon for this day.

#### ***4.2.4 Temperature response curves***

During our 2018 measurement campaign, we measured the response of carbon assimilation in sample foliage to variations in  $T_{\text{leaf}}$  (T-response curves). This was accomplished using two portable gas exchange systems equipped with expanded temperature control kits (LI-6400-XT, LI-COR, Lincoln NE). With this setup we were able to systematically vary the “block” temperature of each instrument’s cuvette between 10 and 50 °C, which induced a range of air temperature inside the cuvette of 12 to 47.8 °C and measured leaf temperatures between 14.7 and 41.9 °C. Branch samples of sufficient size to run multiple response curves were obtained from each tree in the control ( $n = 5$ ) and long-term heating ( $n = 5$ ) groups during the morning, and the cut ends of the branches were immediately submerged in water and re-cut to prevent embolism.

Samples were kept in a climate-controlled growth chamber with their cut ends in a water-filled florist tube until they were ready for measurement, either on the day of sampling or the following day.

For each measurement, a bundle of foliage was selected to enclose in the instrument cuvette. The needles were fanned out to form a single layer across the aperture of the upper and lower jaws. In some cases, more than one layer of foliage needed to be enclosed to achieve sufficient flux of CO<sub>2</sub> to confirm that net assimilation was positive at 20°C. In these cases, the standard equation for boundary layer conductance in the Licor calculation set returns unrealistic values, and a fixed value of 400 mmol m<sup>-2</sup> s<sup>-1</sup> was used. In all cases, care was taken to make the T<sub>leaf</sub> thermocouple contact foliage to ensure proper measurement of leaf temperature. Photon flux density was set to 2000 μmol m<sup>-2</sup> s<sup>-1</sup> and CO<sub>2</sub> concentration was maintained at 400 ppm. Before the experiment started we determined that 15% relative humidity (RH) was the maximum that could be achieved in a lab setting at a T<sub>block</sub> of 50°C. RH was subsequently fixed to 15% for each measurement temperature, resulting in a range of leaf-to-air VPD values of ~ 1.5 – 6.0 kPa. Measurements began at T<sub>block</sub> = 20°C after gas exchange rates stabilized, followed by measurements at T<sub>block</sub> of 15, 10, 25, 30, 35, 40, 45 and 50 °C. At each measurement temperature, net assimilation (A<sub>net</sub>) was allowed to stabilize before five consecutive measurements were made, which were later averaged to control for minor fluctuations in instrument readings. After each curve was completed, the foliage that was enclosed in the cuvette was excised from the main stem so that leaf area could be quantified. Sample foliage was plucked from the stems, arranged on a scanner, and analyzed using the measure area function in imageJ.

For each T-response curve, we plotted both  $A_{\text{net}}$  and  $A_{\text{net}}/C_i$  normalized to the maximum observed value for each against  $T_{\text{leaf}}$ , and a second order polynomial was fit so that metrics of interest could be extracted (Figure 4).  $A/C_i$  was chosen as a response variable to minimize the effect of changes in  $g_s$  across measurement temperatures and to isolate the effects of biochemical processes on photosynthetic performance. From each fit we extracted the optimum temperature for photosynthesis ( $T_{\text{opt}}$ ), maximum net assimilation rate ( $A_{\text{max}}$ ), stomatal conductance ( $g_s$ ) at 25°C, the slope of a line fit to  $g_s$  vs leaf-to-air vapor pressure deficit ( $\text{VPD}_{\text{lta}}$ ), and the slope of the linear portion of the decline in  $A_{\text{net}}$  or  $A_{\text{net}}/C_i$  at high temperature. For the last metric, the slope was fit to points from the last 5 measurement temperatures and is expressed as a % decline per °C.

#### 4.2.5 A-C<sub>i</sub> curves

During our 2019 measurement campaign, we measured the response of net photosynthesis to varying intercellular CO<sub>2</sub> concentrations (A-C<sub>i</sub> curves) on five samples each from the control, heated and heatwave foliage of each species. Sample collection, preparation, insertion into the cuvette and measurement of leaf area followed the procedures described in section 2.4. For each replicate we conducted separate A-C<sub>i</sub> curves with  $T_{\text{air}}$  set to 25, 35, and 45 °C. For each curve ambient CO<sub>2</sub> ( $C_a$ ) concentration was set to 400 ppm until  $A_{\text{net}}$  stabilized, then was lowered to 300, 200, 100, 50, returned to 400, then raised to 600, 800, 1000, 1300, 1600, and 1900 ppm. In cases where the observed A-C<sub>i</sub> relationship appeared not to reach a plateau on the LI6400 display, extra points were manually logged at 2100 and 2300 ppm. From the initial point of each curve ( $C_a = 400\text{ppm}$ , equilibrium  $A_{\text{net}}$ ) we extracted the following to compare between treatment groups and measurement temperatures: stomatal conductance to water vapor ( $g_s$ ), transpiration rate (E), and  $A_{\text{net}}$ . To fit A-C<sub>i</sub> curves, we used the *fitacis* function from the *plantecophys* package

(version 1.4.4, Duursma 2015) in R (R Core Team 2020). From the fitted curves we extracted or calculated the following: maximum carboxylation rate ( $V_{\text{cmax}}$ ), the ratio of  $V_{\text{cmax}}$  at measurement  $T_{\text{leaf}}$  to  $V_{\text{cmax}}$  at 25°C ( $V_{\text{cmax}} : V_{\text{cmax}25}$ ), maximum electron transport rate ( $J_{\text{max}}$ ), the  $C_i$  value at the transition from  $A_c$  to  $A_j$  limited photosynthesis, leaf respiration ( $R_d$ ), and the ratio of leaf respiration to gross assimilation ( $R_d : A_{\text{gross}}$ ), where  $A_{\text{gross}}$  is equal to  $R_d$  plus  $A_{\text{net}}$ .

#### 4.2.6 $F_v/F_m$ measurements

The ratio of variable fluorescence to maximum fluorescence ( $F_v/F_M$ ) was measured on control and long-term heated foliage that was exposed to temperatures ranging from 25 to 65 °C. The methodology we followed was based on Marias et al. 2017. Briefly, shoots were harvested from each control and long-term heated tree in the study and brought to a darkened lab room with the cut ends in water filled florist tubes. Three needles from the second cohort on each piñon shoot and an equivalent area of juniper foliage were selected, placed in plastic bags and submerged in a water bath at 25°C for fifteen minutes. These steps were repeated for nine bath temperatures, ranging from 25 to 65°C in increments of 5°C. After the bath, foliage was removed from the bags and left in the dark for twenty-four hours before fluorescence measurements.  $F_v/F_M$  was measured using a mini-PAM fluorometer (Heinz Walz GmbH, Effeltrich, Germany).  $F_0$ , or minimum fluorescence, was measured using a red LED source (650 nm, 0.15  $\mu\text{mol photons m}^{-2} \text{s}^{-1}$  PAR) with a pulse width of 3  $\mu\text{s}$  and pulse modulation at 0.6 kHz. Maximum fluorescence ( $F_M$ ) was measured using a saturating pulse from a white actinic light source for 0.8 s (18,000  $\mu\text{mol photons m}^{-2} \text{s}^{-1}$  PAR).  $F_v/F_M$  was then calculated as

$$\frac{F_v}{F_M} = \frac{F_M - F_0}{F_M}$$

## 4.3 Results

### 4.3.1 *T*-response curve results

In response to long-term heating of 5°C,  $T_{opt}$  in juniper shifted 2.9 °C ( $p = 0.03$ ), while in piñon the shift was 2.4 °C and not statistically significant ( $p = 0.15$ , Figure 4, Table 1). When the effect of  $g_s$  was removed by analyzing the response of  $A_{net} / C_i$  to increasing  $T_{leaf}$ , the shift in  $T_{opt}$  in juniper was preserved but became virtually nonexistent in piñon (Figure 4). The rate of decline with increasing  $T_{leaf}$  became significantly steeper in the linear portion of the  $A_{net}$  vs.  $T_{leaf}$  curves for piñon ( $p = 0.04$ ), though not in the  $A_{net}/C_i$  vs.  $T_{leaf}$  curves (Table 1). Differences between juniper treatment groups were not significant in either case. In both species there was an apparent but not statistically significant decline in  $A_{max}$  from control to heated trees (13% and 24% in juniper and piñon, respectively) and  $g_s$  at 25°C (26% and 15%). The slope of the response of  $g_s$  to  $VPD_{lta}$  decreased significantly from control to heated trees: by 68% in piñon and 61% in juniper (Figure 5, table 1).

### 4.3.2 *A-C<sub>i</sub>* and *F<sub>v</sub>/F<sub>m</sub>* results

Results from A-C<sub>i</sub> curve analysis and data taken from A-C<sub>i</sub> datasets showed that a greater reduction of  $A_{net}$  occurred in heatwave-treated juniper foliage compared to control and long-term heated foliage, while heatwave-treated piñon responded similarly to the other treatment groups. At 25°C no significant differences existed between groups in piñon for any of the metrics we calculated (Table 2). Similarly, at 45°C there was no difference in all eight measurable metrics (Table 4). Finally, at 35°C transpiration rate ( $E$ ) and  $A_{net} : E$  were different between groups for pinon pine (Table 3, Figure 6). In contrast, foliar function in juniper was significantly changed by exposure to the heatwave conditions. At the mildest measurement temperature ( $T_{air} = 25°C$ )

the following relationships proved significant:  $A_{\text{net}}$  at ambient  $\text{CO}_2$  was lower,  $g_s$  and  $E$  were lower,  $A_{\text{net}} : E$  was higher, and both  $R_d$  and  $R_d : A_{\text{gross}}$  were higher when comparing heatwave to either control or heated foliage (Table 2). This pattern was preserved at  $T_{\text{air}} = 35^\circ\text{C}$  (Table 3), while at a measurement temperature  $45^\circ\text{C}$  only  $g_{\text{sH}_2\text{O}}$  and  $E$  differed for juniper. Examining the differences between groups revealed that diminished  $A_{\text{net}}$  in heatwave-treated juniper was attributable to higher  $R_d$ , resulting in a higher  $R_d : A_{\text{gross}}$  ratio (Figure 7), as well as to  $g_s$  values roughly  $\frac{1}{4}$  the magnitude of the control and long-term heated groups. The combination of lower  $g_s$ , lower  $E$  but also lower  $A_{\text{net}}$  resulted in a higher instantaneous water use efficiency ( $A_{\text{net}} : E$ ) in heatwave treated foliage (Figure 6, Tables 2 and 3).

In regard to the biochemical reactions of photosynthesis, juniper was relatively insensitive to long-term heating and the heatwave treatment while the rate of carboxylation reactions ( $V_{\text{cmax}}$ ) in piñon were more sensitive to heatwave temperatures than photosystem II function. In juniper foliage, the ratio of  $V_{\text{cmax}} : V_{\text{cmax}25}$  followed the expected relationship with temperature in all groups (Figure 7). The three treatment groups in piñon did not test as significantly different from each other in  $V_{\text{cmax}} : V_{\text{cmax}25}$  using Tukey's HSD at any measurement  $T_{\text{leaf}}$ . However, a noticeable pattern can be seen in Figure 7 where the ratio declines between  $35^\circ\text{C}$  and  $45^\circ\text{C}$  in the control group, which proves to be a significant departure from the expected ratio when tested with a  $t$ -test (Table 5). In the heated and heatwave treated groups the ratio did not deviate significantly from the expected relationship at  $45^\circ\text{C}$ , suggesting acclimation, which allowed higher carboxylation rates to be sustained at high  $T_{\text{leaf}}$ .  $J_{\text{max}}$  estimates in both species did not follow a discernable pattern of either acclimation or impairment. Given the relatively high  $C_i$  values at the transition point from  $A_c$  to  $A_j$  limitation (Tables 2 – 4), the rate-limiting step in both species at

any  $T_{\text{leaf}} > 25$  °C was likely to have been carboxylation at normal ambient  $\text{CO}_2$  concentrations. Of note,  $J_{\text{max}}$  became more difficult to estimate at higher  $T_{\text{air}}$  values, particularly across piñon and independent of treatment groups. At 35°C only three of five curves resulted in a useable  $J_{\text{max}}$  estimate in each treatment group, and at 45°C only one or two of five were usable. This was caused by a noticeable flattening of the curve, indicating  $A_c$  limitation across a much higher range of  $C_i$  values (Figure 8). Results from fluorescence measurements corroborated the notion that electron transport rate, which is associated with photosystem II function, was not likely to become the limiting factor at high  $T_{\text{leaf}}$ , as values of  $F_v/F_m$  did not depart from their maximum value until treatment temperatures above 45°C (Figure 9).

#### 4.4 Discussion

As plants globally are exposed to higher growing season  $T_{\text{air}}$  and more frequent and / or more intense heatwaves in the future, acclimation of the physiological traits governing  $A_{\text{net}}$  will be critically important. Without acclimation of  $A_{\text{net}}$ , carbon acquisition may decrease to the point that diminished growth, reduced ability to repair damage, and reduced defense compound production leads to higher mortality rates. The results of our study indicate greater acclimation to long-term heating in juniper compared to piñon, but juniper also experienced diminished  $A_{\text{net}}$  and more signs of physiological impairment after exposure to heatwave conditions compared to piñon. The tree species examined in our study are adapted to semi-arid and arid climate regions where maximum  $T_{\text{air}}$  at the hot end of their range can surpass 40°C in the summertime. Our results suggest that both species are capable of maintaining or adjusting photosynthetic biochemistry to deal with imposed heatwave conditions, but that both long-term warming and heatwave  $T_{\text{air}}$  may lead to changes in stomatal function that could have a significant impact on the long-term carbon balance of these species.

#### ***4.4.1 Response to long-term, moderate warming***

The observed rise in  $T_{opt}$  in juniper in response to 5°C long-term warming - whether or not the influence of  $g_s$  has been factored out (compare  $A_{net}$  or  $A_{net}/C_i$  curves, Figure 4) and despite an apparent decline in the overall magnitude of  $g_s$  (Table 1) and its responsiveness to VPD (Figure 5) - suggests that either a change in mesophyll conductance ( $g_m$ ) or a change in biochemistry was responsible for the observed acclimation. Owing to our study design, the effects of  $g_m$  and Rubisco activase cannot be disentangled, though acclimation of either may explain the different acclimation responses of juniper and piñon.  $g_m$  has been shown to increase exponentially with increasing  $T_{leaf}$  (Bernacchi et al. 2002), though there is considerable variability in the strength of the exponential relationship among species (Scafaro et al. 2011, Walker et al. 2013) and in some species  $g_m$  appears to be temperature independent over wide ranges of  $T_{leaf}$  (Warren and Dryer 2006). Differences among species are likely explained by a combination of differences in leaf anatomy, morphology, and biochemical properties (Warren 2008), which leads to different levels of acclimation potential (Flexas et al. 2007). In addition to  $g_m$  acclimation, studies have shown that an increase in Rubisco activase concentration can be responsible for observed acclimation to increased temperature in many species (Sage and Kubein 2007, Benomar et al. 2019), though only at moderate temperatures given the rapid rate at which Rubisco activation declines at moderately high to high temperatures (Feller et al 1998, Salvucci et al. 2001, Crafts-Brandner and Law 2000, Haldimann and Feller 2004). Difference in acclimation in either  $g_m$  or Rubisco activase concentration may explain the differences in  $T_{opt}$  acclimation between our species. One possible explanation for greater acclimation in juniper compared to piñon relates to the more anisohydric behavior of juniper compared to piñon (Meinzer et al. 2014); that is, on a diurnal scale, minimum  $g_s$  is observed at higher water potentials in piñon than in juniper. This would

translate to minimum  $g_s$  earlier in the day for piñon, such that photosynthesis would be at a minimum during the hottest part of the day, and acclimation of  $T_{opt}$  would not necessarily confer a benefit in the way that it would to juniper.

Despite the apparently greater acclimation of carboxylation capacity in juniper to long-term, moderate warming, both species experienced an apparent loss in stomatal responsiveness to VPD and lower  $g_s$  at  $T_{air} = 25^\circ\text{C}$  in heated trees (Table 1), in line with the findings of Grossiord et al. (2017b). Over the range of observed  $VPD_{lta}$  in this study, the response of  $g_s$  followed a linear relationship. The negative exponential relationship between VPD and  $g_s$  observed in numerous other studies (Oren et al 1999, Wu et al. 2019), was not observed in our data, as the minimum leaf-to-air VPD was 1.7 kPa in our T-response curves and 2.2 kPa in our A-Ci curve runs.

Though the range of  $VPD_{lta}$  tested in this study was high, environmental conditions at the study site and across much of the range of piñon juniper woodland routinely reach these levels. For example, during the month of August 2019, atmospheric VPD outside of the warming chambers exceeded 2 kPa on 89% of days, and on those days the average time of exceedance was 10:01am (SD 1hr 40min) with a mean daily maximum of 3.3 kPa (SD 0.71). While Grossiord et al. (2017b) suggest that a decrease in xylem conductivity may explain observations of lower canopy conductance in heated trees, changes in stomata on heated foliage may also explain observed differences in our study (Figure 5). In a warming experiment involving two co-occurring subtropical tree species (Wu et al. 2018), one species displayed smaller stomata in the warming treatment group, while the other displayed decreased stomatal density. Given the relatively small elevation of  $T_{air}$  in that study ( $2^\circ\text{C}$ ) compared to our long-term heat treatments ( $5^\circ\text{C}$ ), it is plausible that a change in size or density of stomata could have occurred on leaf cohorts established during the six years of imposed warming.

#### 4.4.2 Response to heatwave

Heatwave conditions induced greater physiological change in juniper than in piñon, resulting in significantly diminished  $A_{\text{net}}$  in heatwave-treated foliage (Figure 7). Of the possible mechanisms which could explain diminished  $A_{\text{net}}$  in the heatwave group are increased respiration, lower stomatal conductance, or impairment of the biochemical reactions involved in photosynthesis. Among these options, our results suggest that impairment of photosynthetic biochemistry was not a primary factor. In juniper, the temperature response of  $V_{\text{cmax}}$  followed the expected relationship in all three treatment groups, with no apparent heatwave-induced impairment (Figure 7). In piñon, control group  $V_{\text{cmax}}$  departed significantly from the expected temperature response (Table 5); however, after exposure to heatwave conditions, acclimation occurred and the temperature response was not significantly different from expected. While we do not have fluorescence measurements for heatwave-treated foliage,  $F_v/F_m$  values from the control and long-term heated groups in both species did not decrease until  $T_{\text{leaf}}$  reached 50°C (Figure 9), suggesting that photosystem II impairment was not a likely cause of reduced  $A_{\text{net}}$ . Of the remaining possibilities, increased respiration may partially explain differences between species, with stomatal restriction of gas exchange being the most likely cause of low  $A_{\text{net}}$  in both species.

A recent review of the effects of heatwaves on mitochondrial respiration (Scafaro et al. 2021) outlined several mechanisms that cause rapid increases in respiration at temperatures above  $T_{\text{opt}}$  for photosynthesis, but below the maximum temperature for R ( $T_{\text{max}}$ ), which is often as high as 50 – 60°C. These include increased maintenance costs, such as increased protein synthesis to replace those which have denatured, increased heat shock protein (HSP) synthesis, or activation of metabolic pathways that cope with reactive oxygen species, which increase at high  $T_{\text{leaf}}$  due to

membrane disruption (Millenaar and Lambers 2003, Millar et al. 2011). After more severe heat damage has occurred, the respiratory flux of CO<sub>2</sub> can increase due to a loss of mitochondrial membrane integrity and subsequent loss of feedback controls (Hüve et al. 2017). In our study, no significant change was seen in R<sub>d</sub> between any treatment groups at any measurement temperature in piñon, nor did the temperature response of respiration as measured by Q<sub>10</sub> test as significantly different across groups (1.4, 1.9, and 1.4 in control, long-term heated, and heatwave groups). In juniper, the ratio of R<sub>d</sub> : A<sub>gross</sub> was significantly higher in the heatwave foliage at measurement temperatures of 25 and 35 °C, but R<sub>d</sub> was only significantly higher than the other groups at 25°C, and Q<sub>10</sub> values were not significantly different (1.95, 1.65, 1.09). Of note is the nearly flat response of R<sub>d</sub> in the heatwave foliage to T<sub>leaf</sub> (Q<sub>10</sub> near one). These data should be interpreted with caution, as R<sub>d</sub> is notoriously difficult to estimate accurately from A-C<sub>i</sub> data (Sharkey 2016), in part because it is estimated by a non-linear solver applied to an equation where the R<sub>d</sub> term is effectively used to move A<sub>c</sub> and A<sub>j</sub> curves up or down to achieve the best fit between measured and modelled data (Duursma 2015). More rigorous estimation of R<sub>d</sub> after heatwave exposure may be needed to confirm the patterns observed in this study. If increased maintenance costs or loss of feedbacks which regulate R explain observed patterns of elevated R<sub>d</sub> in juniper, the results of our study may suggest that the heatwave effects linger for > 24 hrs past the last exposure to high T<sub>air</sub>, even when observed at moderate measurement T<sub>air</sub> (25°C, Table 2). While the patterns in R<sub>d</sub> were somewhat difficult to interpret, observed patterns in g<sub>s</sub> were more consistent and explained a large portion of the observed decrease in A<sub>net</sub> in juniper.

Stomatal conductance values were markedly lower in heatwave-treated foliage in juniper, but not in piñon (Figure 6). Though different foliar anatomy between species makes comparing g<sub>s</sub> on a

per leaf area basis difficult, one interpretation may be that piñon  $g_s$  values were so low in control and long-term heated groups that little reduction in  $g_s$  was possible in the heatwave group. It is notable that even though shoot samples were given adequate time to fully rehydrate,  $g_s$  was greatly diminished in heatwave-treated juniper foliage. Most *Cupressaceae* have been shown to rely more heavily on low  $\Psi_{\text{Leaf}}$  to achieve stomatal closure, as opposed to a strong abscisic acid (ABA) mediated response (Brodribb et al. 2014), suggesting that a lack of rehydration and subsequent raising of  $\Psi_{\text{Leaf}}$  is a more likely explanation of continued low  $g_s$  than a buildup of ABA in foliage. Low stomatal conductance may be explained by xylem embolism in foliage or stems (Creek et al. 2020) or impairment of outside-xylem hydraulic pathways (Scoffoni et al. 2017) induced by high VPD during the heatwave treatments. In this scenario, it is possible that the effects of a heatwave would linger well past the point when temperatures return to normal. While foliar water uptake during monsoon rains or after dew formation may allow trees to refill embolized stem xylem post-heatwave (McCulloh et al. 2011), it is unclear how reliable or effective this mechanism would be for leaf xylem in our study species, and what cellular damage may occur in the meantime. To the extent that old xylem is abandoned and new xylem must be generated to restore hydraulic conductivity, heatwaves may impose significant carbon costs for our study species.

#### 4.5 Conclusion

In this study we evaluated acclimation of carbon assimilation to two kinds of imposed temperature regimes - long term exposure to a uniform, 5°C increase in temperature, and short-term exposure to heatwave-like temperatures exceeding 40°C on multiple days. Our results suggest that juniper is more likely to acclimate to moderate, long-term warming in the future compared to piñon, but that significant reduction in  $A_{\text{net}}$  occurred in juniper after the imposed

heatwave. Given our results and those of prior studies, we hypothesize that physiological impairment which leads to diminished  $g_s$  is likely to limit  $A_{net}$  before impairment of photosynthetic biochemistry occurs. In both study species, stomatal conductance values of foliage exposed to heatwave were very low, even after sampled shoots were given adequate time to rehydrate. When the effects of stomatal restriction were factored out ( $A_{gross}/C_i$ ), photosynthetic performance in heatwave foliage was more similar to the control and heat-treated groups in juniper, while both  $A_{net}$  and  $g_s$  were low across groups in piñon.

While in our study one branch of each tree was exposed to heatwave  $T_{air}$  and VPD, in a real heatwave the entire tree would experience elevated temperatures and desiccating conditions. If the results we observed generally represent heatwave consequences for foliage across large portions of the canopy, the imposed carbon cost of a heatwave may extend far beyond diminished  $A_{net}$  during the event, involving significant requirements to grow new xylem to support foliar water needs. Crown dieback may also be a possibility if damage is too widespread to fully compensate for with the trees extant carbon reserves. Future studies should consider the effect of long-term warming on stomatal characteristics of new leaf cohorts. Future studies should also examine  $\Psi_{leaf}$  and loss of xylem conductivity before, during and after heatwave conditions in conjunction with observations of photosynthetic function and gas exchange in order to assess the impact of heatwaves on tree carbon balance both during and after the heatwave occurs.

#### **4.6 Acknowledgements**

The authors would like to acknowledge the help of Max Ryan and Turin Dickman in collecting field samples and doing lab analysis. This research was supported by the Los Alamos National

Laboratory (LANL) through its Center for Space and Earth Science (CSES). CSES is funded by LANL's Laboratory Directed Research and Development (LDRD) program under project number 20210528CR.

#### 4.7 References

- Benomar, L., Moutaoufik, M.T., Elferjani, R., Isabel, N., DesRochers, A., El Guellab, A., Khelifa, R., Idrissi Hassania, L.A., 2019. Thermal acclimation of photosynthetic activity and RuBisCO content in two hybrid poplar clones. *PLoS ONE* 14, e0206021. <https://doi.org/10.1371/journal.pone.0206021>
- Bernacchi, C.J., Portis, A.R., Nakano, H., von Caemmerer, S., Long, S.P., 2002. Temperature Response of Mesophyll Conductance. Implications for the Determination of Rubisco Enzyme Kinetics and for Limitations to Photosynthesis in Vivo. *Plant Physiology* 130, 1992–1998. <https://doi.org/10.1104/pp.008250>
- Breshears, D.D., Myers, O.B., Meyer, C.W., Barnes, F.J., Zou, C.B., Allen, C.D., McDowell, N.G., Pockman, W.T., 2009. Tree die-off in response to global change-type drought: mortality insights from a decade of plant water potential measurements. *Frontiers in Ecology and the Environment* 7, 185–189. <https://doi.org/10.1890/080016>
- Brodribb, T.J., McAdam, S.A.M., Jordan, G.J., Martins, S.C.V., 2014. Conifer species adapt to low-rainfall climates by following one of two divergent pathways. *Proceedings of the National Academy of Sciences USA* 111, 14489–14493. <https://doi.org/10.1073/pnas.1407930111>
- Crafts-Brandner, S.J., Law, R.D., 2000. Effect of heat stress on the inhibition and recovery of the ribulose-1,5-bisphosphate carboxylase/oxygenase activation state *Planta* 212: 67-74.
- Creek, D., Lamarque, L.J., Torres-Ruiz, J.M., Parise, C., Burrett, R., Tissue, D.T., Delzon, S., 2020. Xylem embolism in leaves does not occur with open stomata: evidence from direct observations using the optical visualization technique. *Journal of Experimental Botany* 71, 1151–1159. <https://doi.org/10.1093/jxb/erz474>
- Duursma, R.A., 2015. Plantecophys - An R Package for Analysing and Modelling Leaf Gas Exchange Data. *PLoS ONE* 10, e0143346. <https://doi.org/10.1371/journal.pone.0143346>
- Feller, U., Crafts-Brandner, S.J., Salvucci, M.E., 1998. Moderately High Temperatures Inhibit Ribulose-1,5-Bisphosphate Carboxylase/Oxygenase (Rubisco) Activase-Mediated Activation of Rubisco1. *Plant Physiology* 116, 539–546. <https://doi.org/10.1104/pp.116.2.539>
- Flexas, J., Ribas-Carbó, M., Diaz-Espejo, A., Galmés, J., Medrano, H., 2008. Mesophyll conductance to CO<sub>2</sub>: current knowledge and future prospects. *Plant Cell Environ* 31, 602–621. <https://doi.org/10.1111/j.1365-3040.2007.01757.x>

- Floyd, M.L., Clifford, M., Cobb, N.S., Hanna, D., Delph, R., Ford, P., Turner, D., 2009. Relationship of stand characteristics to drought-induced mortality in three Southwestern piñon–juniper woodlands. *Ecological Applications* 19, 1223–1230. <https://doi.org/10.1890/08-1265.1>
- Garcia-Forner, N., Adams, H.D., Sevanto, S., Collins, A.D., Dickman, L.T., Hudson, P.J., Zeppel, M.J.B., Jenkins, M.W., Powers, H., Martínez-Vilalta, J., McDowell, N.G., 2016. Responses of two semiarid conifer tree species to reduced precipitation and warming reveal new perspectives for stomatal regulation: Stomatal regulation in piñon and juniper trees. *Plant, Cell & Environment* 39, 38–49. <https://doi.org/10.1111/pce.12588>
- Gaylord, M.L., Kolb, T.E., Pockman, W.T., Plaut, J.A., Yezpez, E.A., Macalady, A.K., Pangle, R.E., McDowell, N.G., 2013. Drought predisposes piñon–juniper woodlands to insect attacks and mortality. *New Phytologist* 198, 567–578. <https://doi.org/10.1111/nph.12174>
- Grossiord, C., Sevanto, S., Adams, H.D., Collins, A.D., Dickman, L.T., McBranch, N., Michaletz, S.T., Stockton, E.A., Vigil, M., McDowell, N.G., 2017a. Precipitation, not air temperature, drives functional responses of trees in semi-arid ecosystems. *Journal of Ecology* 105, 163–175. <https://doi.org/10.1111/1365-2745.12662>
- Grossiord, C., Sevanto, S., Borrego, I., Chan, A.M., Collins, A.D., Dickman, L.T., Hudson, P.J., McBranch, N., Michaletz, S.T., Pockman, W.T., Ryan, M., Vilagrosa, A., McDowell, N.G., 2017b. Tree water dynamics in a drying and warming world: Future tree water dynamics. *Plant, Cell & Environment* 40, 1861–1873. <https://doi.org/10.1111/pce.12991>
- Grossiord, C., Sevanto, S., Dawson, T.E., Adams, H.D., Collins, A.D., Dickman, L.T., Newman, B.D., Stockton, E.A., McDowell, N.G., 2017c. Warming combined with more extreme precipitation regimes modifies the water sources used by trees. *New Phytologist* 213, 584–596. <https://doi.org/10.1111/nph.14192>
- Haldimann, P., Feller, U., 2004. Inhibition of photosynthesis by high temperature in oak (*Quercus pubescens* L.) leaves grown under natural conditions closely correlates with a reversible heat-dependent reduction of the activation state of ribulose-1,5-bisphosphate carboxylase/oxygenase. *Plant Cell & Environment* 27, 1169–1183. <https://doi.org/10.1111/j.1365-3040.2004.01222.x>
- Huve, K., Michele, I., Ivanova, H., Keerberg, O., Parnik, T., Rasulov, B., Niinemets, U., 2012. Temperature responses of dark respiration in relation to leaf sugar concentration. *Physiologia Plantarum*, 144 (4), 320-324.
- IPCC, 2014: Climate Change 2014: Synthesis Report. Contribution of Working Groups I, II and III to the Fifth Assessment Report of the Intergovernmental Panel on Climate Change [Core Writing Team, R.K. Pachauri and L.A. Meyer (eds.)]. IPCC, Geneva, Switzerland, 151 pp.
- Kosugi, Y., Matsuo, N., 2006. Seasonal fluctuations and temperature dependence of leaf gas exchange parameters of co-occurring evergreen and deciduous trees in a temperate broad-leaved forest. *Tree Physiology* 26, 1173–1184. <https://doi.org/10.1093/treephys/26.9.1173>

- Kumarathunge, D.P., Medlyn, B.E., Drake, J.E., Tjoelker, M.G., Aspinwall, M.J., et al. 2019. Acclimation and adaptation components of the temperature dependence of plant photosynthesis at the global scale. *New Phytol* 222, 768–784. <https://doi.org/10.1111/nph.15668>
- Lajtha, K., Barnes, F.J., 1991. Carbon gain and water use in pinyon pine-juniper woodlands of northern New Mexico: field versus phytotron chamber measurements. *Tree Physiology* 9, 59–67. <https://doi.org/10.1093/treephys/9.1-2.59>
- McCulloh, K.A., Johnson, D.M., Meinzer, F.C., Lachenbruch, B., 2011. An annual pattern of native embolism in upper branches of four tall conifer species. *American Journal of Botany* 98, 1007–1015. <https://doi.org/10.3732/ajb.1000503>
- Meinzer, F.C., Woodruff, D.R., Marias, D.E., Mcculloh, K.A., Sevanto, S., 2014. Dynamics of leaf water relations components in co-occurring iso- and anisohydric conifer species: Dynamics of leaf water relations components. *Plant, Cell & Environment* 37, 2577–2586. <https://doi.org/10.1111/pce.12327>
- Millar, A.H., Whelan, J., Soole, K.L., Day, D.A., 2011. Organization and Regulation of Mitochondrial Respiration in Plants. *Annual Review of Plant Biology* 62, 79–104. <https://doi.org/10.1146/annurev-arplant-042110-103857>
- Millenaar, F.F., Lambers, H., 2003. The Alternative Oxidase: in vivo Regulation and Function. *Plant Biology* 5, 2–15. <https://doi.org/10.1055/s-2003-37974>
- McDowell, N.G., Fisher, R.A., Xu, C., Domec, J.C., Hölttä, T., Mackay, D.S., Sperry, J.S., Boutz, A., Dickman, L., Gehres, N., Limousin, J.M., Macalady, A., Martínez-Vilalta, J., Mencuccini, M., Plaut, J.A., Ogée, J., Pangle, R.E., Rasse, D.P., Ryan, M.G., Sevanto, S., Waring, R.H., Williams, A.P., Yeepez, E.A., Pockman, W.T., 2013. Evaluating theories of drought-induced vegetation mortality using a multimodel-experiment framework. *New Phytologist* 200, 304–321. <https://doi.org/10.1111/nph.12465>
- Marias, D.E., Meinzer, F.C., Still, C., 2017. Leaf age and methodology impact assessments of thermotolerance of *Coffea arabica*. *Trees* 31, 1091–1099. <https://doi.org/10.1007/s00468-016-1476-4>
- Marias, D.E., Meinzer, F.C., Still, C., 2017. Impacts of leaf age and heat stress duration on photosynthetic gas exchange and foliar nonstructural carbohydrates in *Coffea arabica*. *Ecology and Evolution* 7, 1297–1310. <https://doi.org/10.1002/ece3.2681>
- Medlyn, B.E., Dreyer, E., Ellsworth, D., Forstreuter, M., Harley, P.C., Kirschbaum, M.U.F., Le Roux, X., Montpied, P., Strassmeyer, J., Walcroft, A., Wang, K., Loustau, D., 2002. Temperature response of parameters of a biochemically based model of photosynthesis. II. A review of experimental data: Temperature response of photosynthetic parameters - review. *Plant, Cell & Environment* 25, 1167–1179. <https://doi.org/10.1046/j.1365-3040.2002.00891.x>

- Mooney, H.A., West, M., 1964. Photosynthetic Acclimation of Plants of Diverse Origin. *American Journal of Botany* 51, 825-827
- Oren, R., Sperry, J.S., Katul, G.G., Pataki, D.E., Ewers, B.E., Phillips, N., Schäfer, K.V.R., 1999. Survey and synthesis of intra- and interspecific variation in stomatal sensitivity to vapour pressure deficit: Intra- and interspecific variation in stomatal sensitivity to vapour pressure deficit. *Plant, Cell & Environment* 22, 1515–1526. <https://doi.org/10.1046/j.1365-3040.1999.00513.x>
- R Core Team (2020). R: A language and environment for statistical computing. R Foundation for Statistical Computing, Vienna, Austria. URL <https://www.R-project.org/>
- Sage, R.F., Kubien, D.S., 2007. The temperature response of C<sub>3</sub> and C<sub>4</sub> photosynthesis. *Plant, Cell & Environment* 30, 1086–1106. <https://doi.org/10.1111/j.1365-3040.2007.01682.x>
- Salvucci, M.E., Osteryoung, K.W., Crafts-Brandner, S.J., Vierling, E., 2001. Exceptional Sensitivity of Rubisco Activase to Thermal Denaturation in Vitro and in Vivo. *Plant Physiol.* 127, 1053–1064. <https://doi.org/10.1104/pp.010357>
- Scafaro, A.P., Fan, Y., Posch, B.C., Garcia, A., Coast, O., Atkin, O.K., 2021. Responses of leaf respiration to heatwaves. *Plant, Cell & Environment* 202 1; 1-12. <https://doi.org/10.1111/pce.14018>
- Scafaro, A.P., Von Caemmerer, S., Evans, J.R., Atwell, B.J., 2011. Temperature response of mesophyll conductance in cultivated and wild *Oryza* species with contrasting mesophyll cell wall thickness. *Plant, Cell & Environment* 34, 1999–2008. <https://doi.org/10.1111/j.1365-3040.2011.02398.x>
- Scoffoni, C., Albuquerque, C., Brodersen, C.R., Townes, S.V., John, G.P., Bartlett, M.K., Buckley, T.N., McElrone, A.J., Sack, L., 2017. Outside-Xylem vulnerability, not xylem embolism, controls leaf hydraulic decline during dehydration. *Plant Physiology* 173, 1197–1210. <https://doi.org/10.1104/pp.16.01643>
- Sharkey, T.D., 2016. What gas exchange data can tell us about photosynthesis: Gas exchange data and photosynthesis. *Plant, Cell & Environment* 39, 1161–1163. <https://doi.org/10.1111/pce.12641>
- Walker, B., Ariza, L.S., Kaines, S., Badger, M.R., Cousins, A.B., 2013. Temperature response of in vivo Rubisco kinetics and mesophyll conductance in *Arabidopsis thaliana* : comparisons to *Nicotiana tabacum*: In vivo Rubisco kinetics and mesophyll conductance. *Plant Cell Environ* 36, 2108–2119. <https://doi.org/10.1111/pce.12166>
- Warren, C.R., 2008. Stand aside stomata, another actor deserves centre stage: the forgotten role of the internal conductance to CO<sub>2</sub> transfer. *Journal of Experimental Botany* 59, 1475–1487. <https://doi.org/10.1093/jxb/erm245>

- Warren, C., Dreyer, E. 2006. Temperature response of photosynthesis and internal conductance to CO<sub>2</sub>: results from two independent approaches. *Journal of Experimental Botany* 57, 3057–3067. <https://doi.org/10.1093/jxb/erl067>
- Wu, G., Liu, H., Hua, L., Luo, Q., Lin, Y., He, P., Feng, S., Liu, J., Ye, Q., 2018. Differential Responses of Stomata and Photosynthesis to Elevated Temperature in Two Co-occurring Subtropical Forest Tree Species. *Frontiers in Plant Science*. 9, 467. <https://doi.org/10.3389/fpls.2018.00467>
- Wu, J., Serbin, S.P., Ely, K.S., Wolfe, B.T., Dickman, L.T., Grossiord, C., Michaletz, S.T., Collins, A.D., Detto, M., McDowell, N.G., Wright, S.J., Rogers, A., 2019. The response of stomatal conductance to seasonal drought in tropical forests. *Global Change Biology* 26, 823–839. <https://doi.org/10.1111/gcb.14820>
- Young, J.N., Goldman, J.A.L., Kranz, S.A., Tortell, P.D., Morel, F.M.M., 2015. Slow carboxylation of Rubisco constrains the rate of carbon fixation during Antarctic phytoplankton blooms. *New Phytol* 205, 172–181. <https://doi.org/10.1111/nph.13021>

## 4.8 Figures

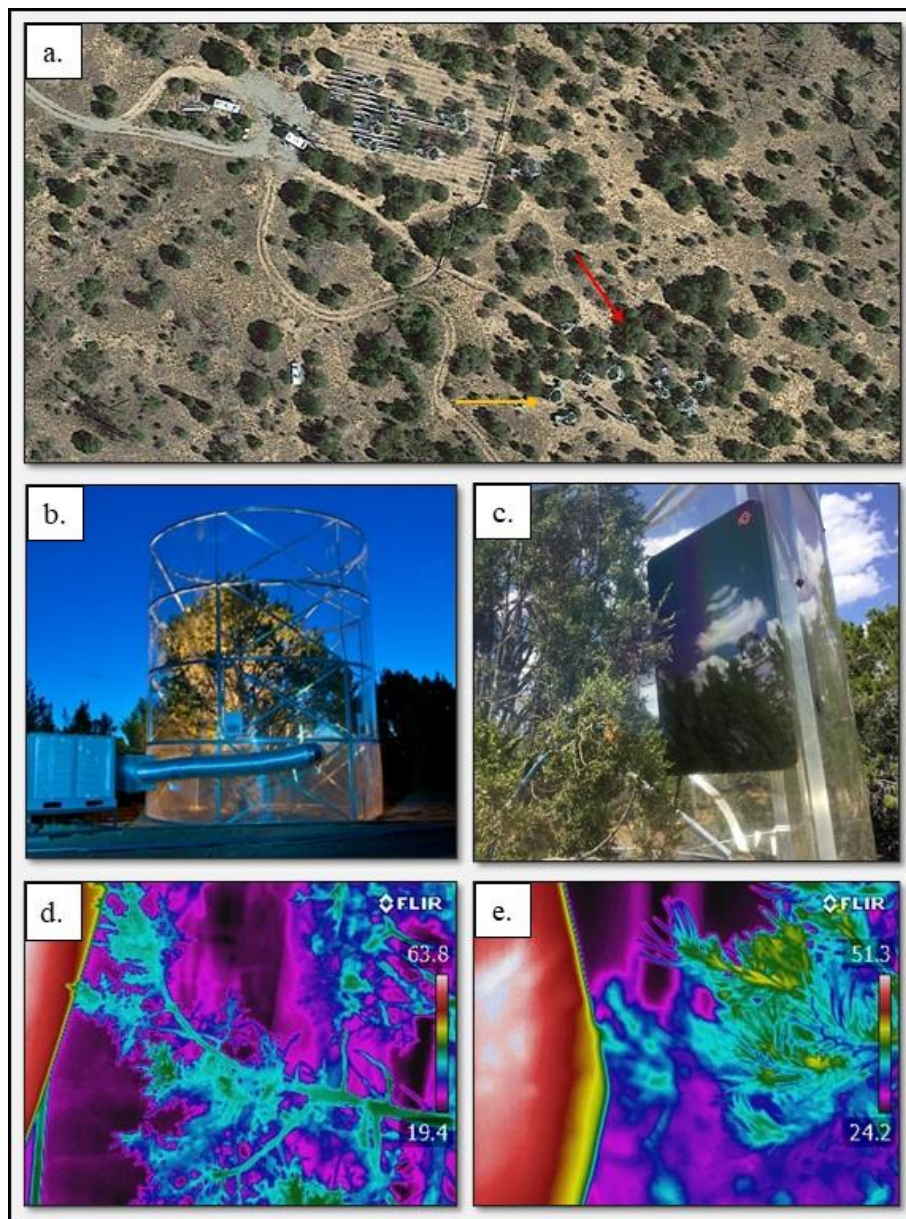


**Figure 4-1 Study site and warming infrastructure.**

(a) Layout of study site. Warming chambers indicated with yellow arrow, control tree group with red arrow. (b) Plexiglass warming chamber around mature piñon pine tree, with heating and cooling unit attached. (c) Juniper foliage positioned in front of 200W panel heater. (d) and (e), thermal images of juniper and piñon pine foliage respectively, positioned in front of panel heaters (red area on the side of both images).

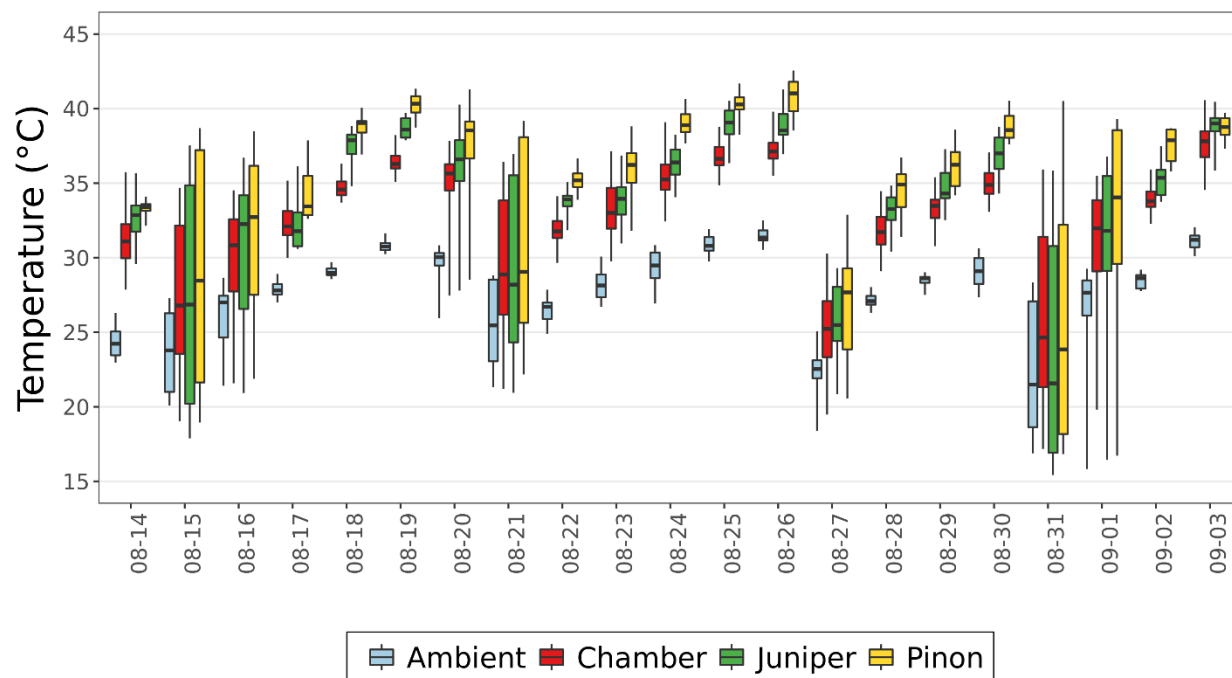


**Figure 4-2. Air and leaf temperatures throughout heatwave period**

Boxplots represent temperature values measured between 11:00am and 14:00pm on each day of the heatwave experiment. Ambient air temperature measured by a free-standing weather station. Chamber air temperatures represent an average across all chambers used in this study. Leaf temperatures shown here were measured using fine-wire thermocouples nestled in heatwave treatment branches and represent an average across all measurements ( $n = 4$  for juniper,  $n = 3$  for piñon).

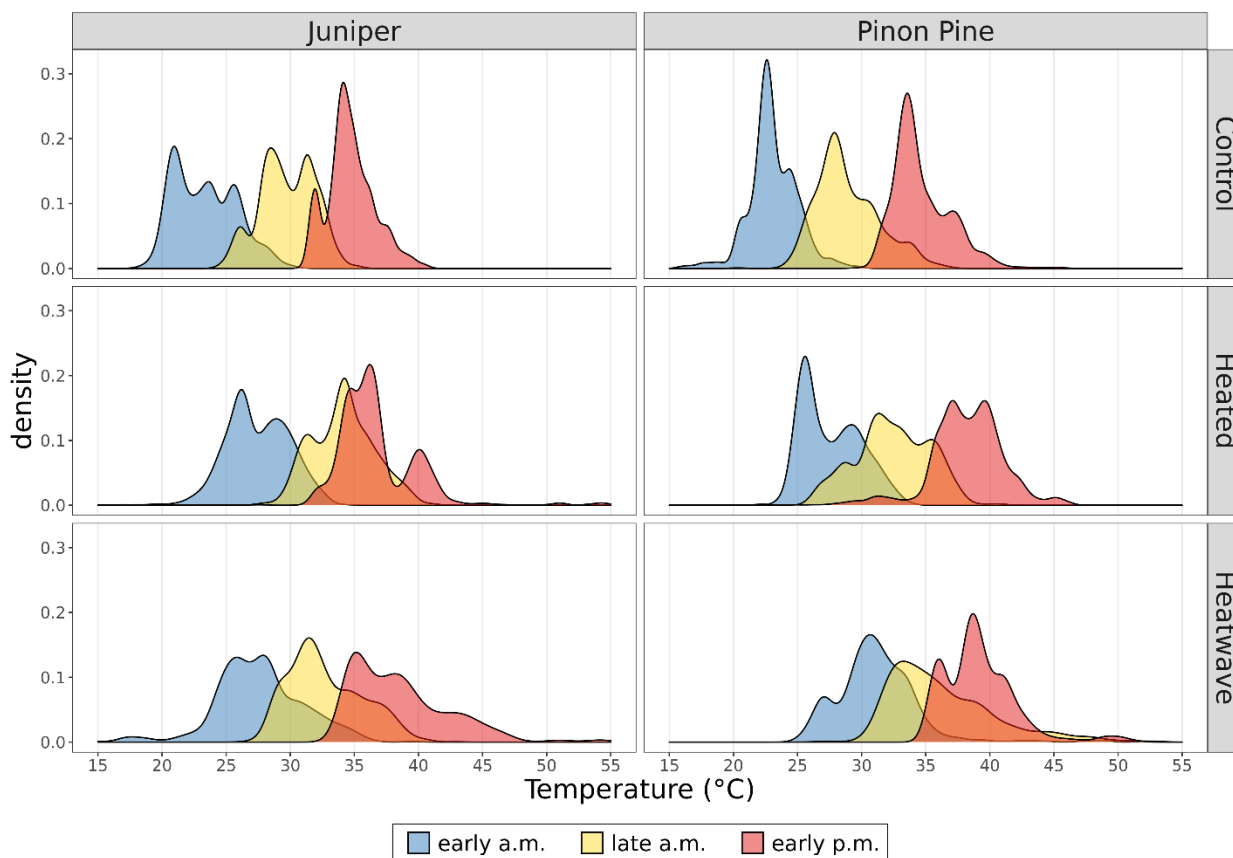


**Figure 4-3 Diurnal variation in foliage temperature**

Temperature distributions of sunlit juniper and piñon foliage in the control, heated, and heatwave treatment groups. Temperatures measured using handheld thermal camera. Each distribution represents 500 pixels (100 pixels sampled from each of 5 images) taken in the early morning (8:20 – 9:00), late morning (10:45 – 11:30) and early afternoon (13:00 – 13:50) on August 24<sup>th</sup>, 2019.

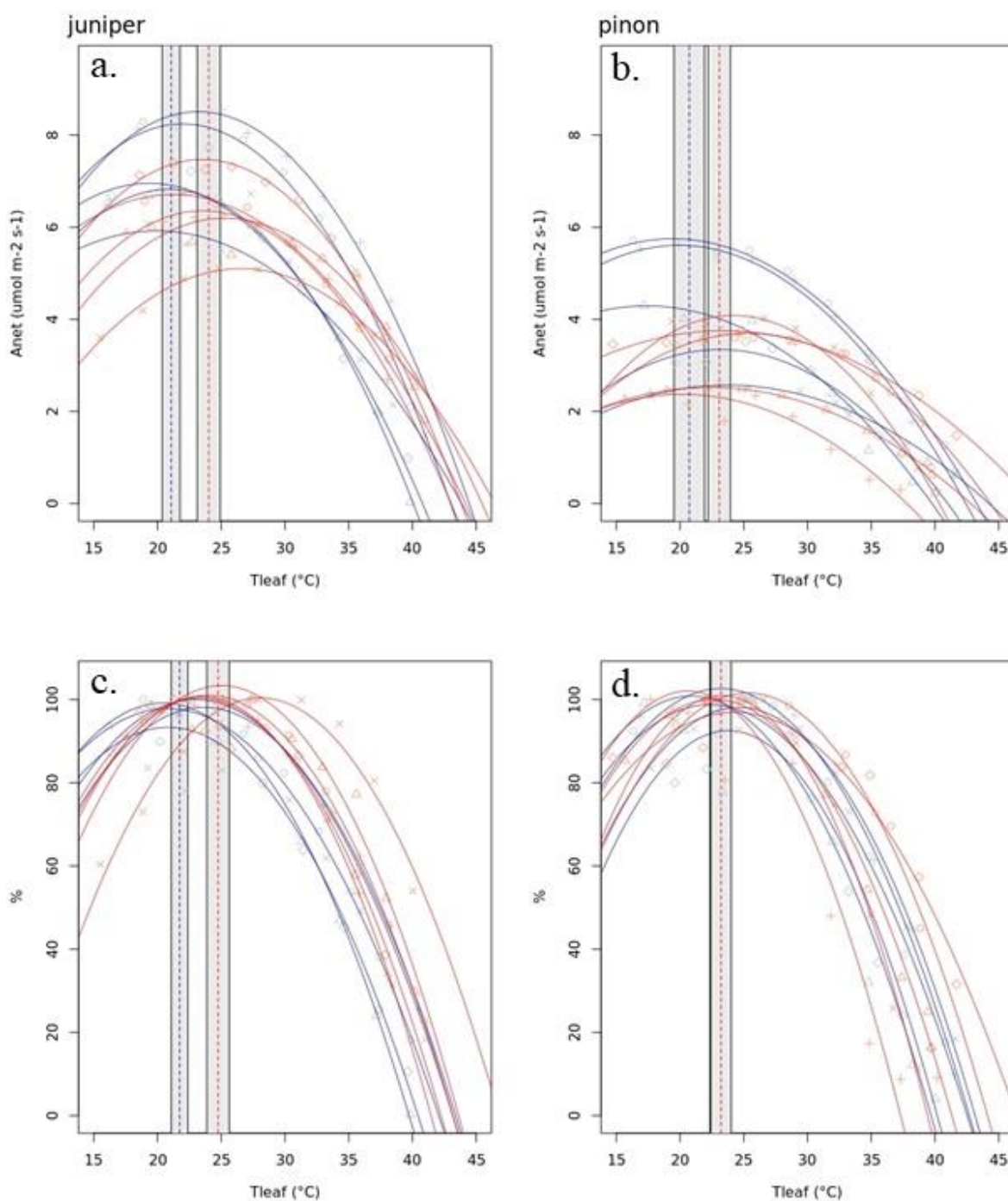


**Figure 4-4 Temperature response curves.**

Temperature response curves for juniper (panels a, c) and piñon pine (panels b, d). All panels show the individual response curves for the control and heated trees (blue and red lines and symbols, respectively). Dashed vertical lines show the mean optimal temperature for each group and the gray shading represents one standard error. Panels a and b show net assimilation rates. Panels c and d show  $A_{net}$  divided by  $C_i$ , normalized to the maximum value of each curve.

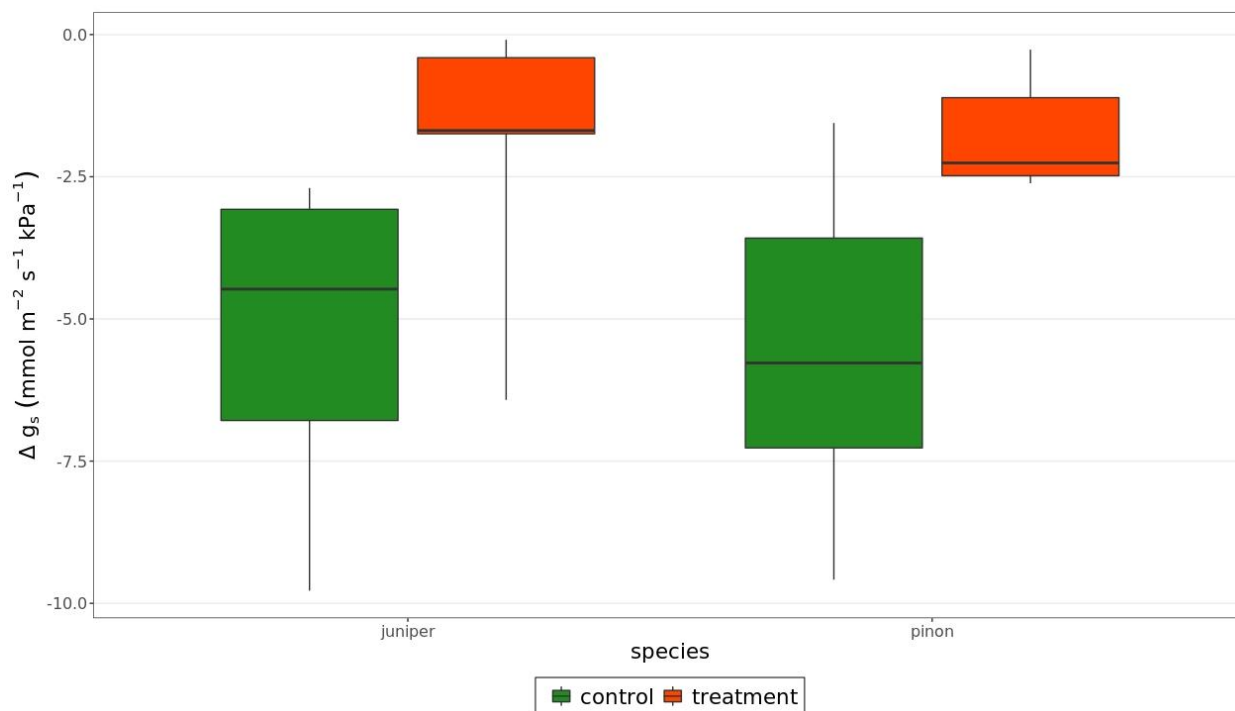


**Figure 4-5 Response of stomatal conductance to VPD.**

Response of stomatal conductance ( $g_s$ ) to increasing vapor pressure deficit (VPD) in the control and heated groups of each species. Values on the y-axis represent the slope of a linear regression fitted to  $g_s$  and VPD measurements taken from each temperature response curve. Variation in VPD was caused by varying  $T_{\text{blk}}$  between 10 and 50 °C, while keeping RH constant at 15%.

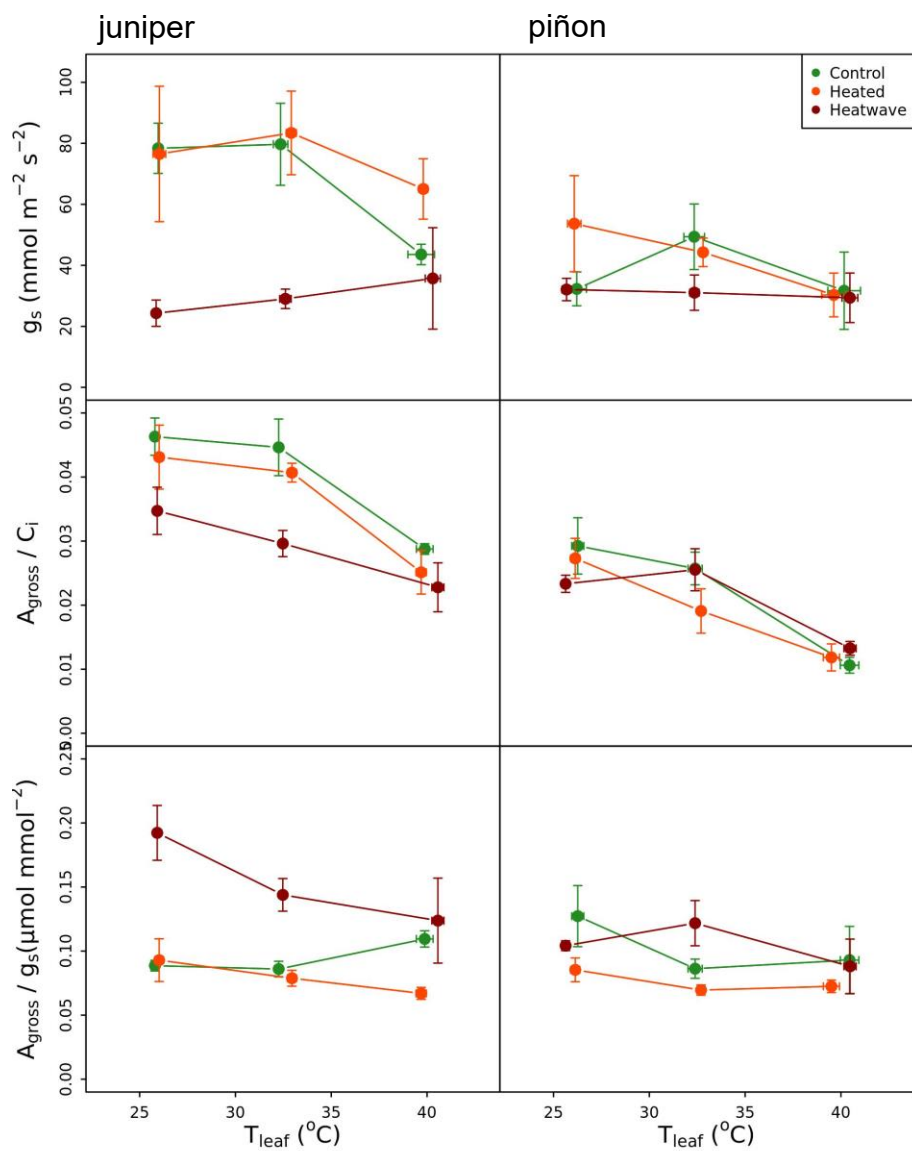


**Figure 4-6 Stomatal regulation of gas exchange**

Stomatal conductance to  $CO_2$ ,  $A_{gross}$  divided by  $C_i$ , and water use efficiency ( $A_{gross}$  divided by stomatal conductance to water vapor) as a function of leaf temperature in control, heated, and heatwave foliage.  $g_{sCO_2}$ ,  $g_{sH_2O}$  and  $A_{gross}$  taken from first point of A- $C_i$  curves, where  $A_{net}$  reached equilibrium and  $C_a = 400$  ppm. Juniper measurements represented in left column; piñon measurements in right column.

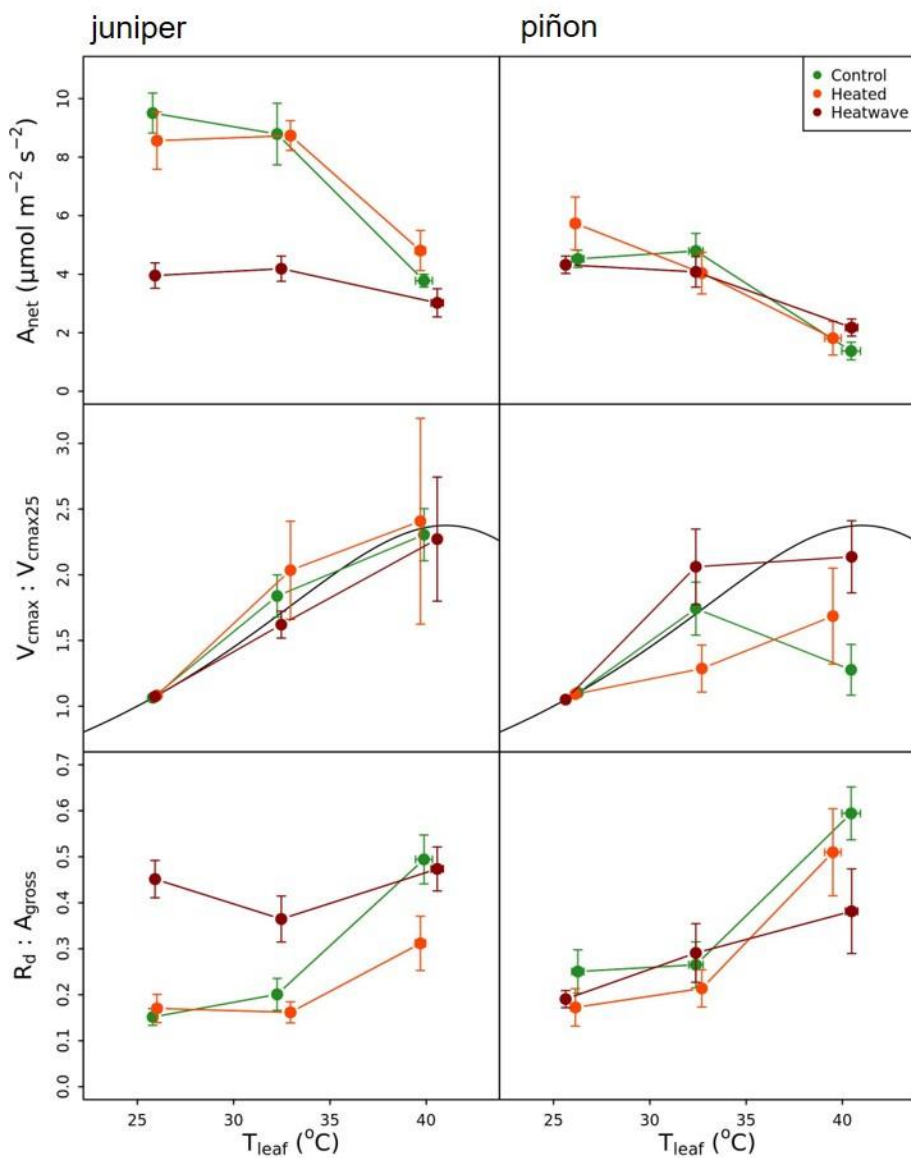


**Figure 4-7:  $A_{\text{net}}$ ,  $V_{\text{cmax}}$  ratio, and  $R_d : A_{\text{gross}}$  ratio from A-C<sub>i</sub> data.**

$A_{\text{net}}$  (panels a and b), the ratio of  $V_{\text{cmax}}$  measured at a given  $T_{\text{leaf}}$  to  $V_{\text{cmax}}$  measured at 25 $^{\circ}\text{C}$  (c and d), and the ratio of  $R_d$  to  $A_{\text{gross}}$  (e and f) in juniper (left column) and piñon (right column). Error bars represent one standard error. Curve shown in black in panels c and d is the mean temperature response function based on Kumarathunge et al. (2019).

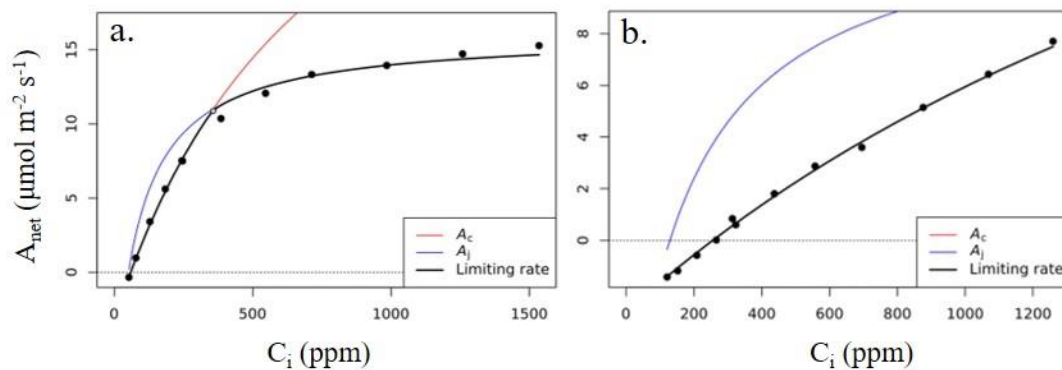


**Figure 4-8 Example A- $C_i$  curves at 25 and 45 °C measurement temperature.**  
A- $C_i$  curves from the same piñon tree and sample foliage run at  $T_{\text{air}}$  25°C (panel a) and 45°C (panel b).

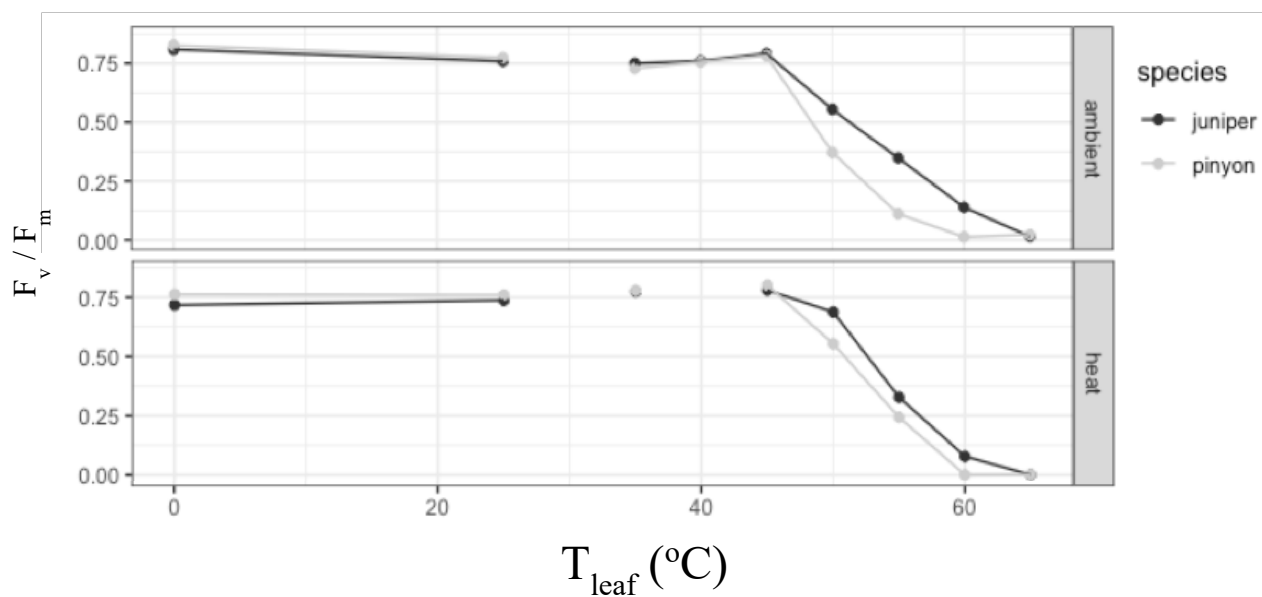


**Figure 4-9  $F_v/F_m$  ratios**  
 $F_v/F_m$  ratio as a function of water bath treatment temperature ( $T_{\text{leaf}}$ ) in control ("ambient") and long-term heat treated ("heat") trees.

## 4.9 Tables

**Table 4-1 T-response curve metrics**

Mean of each metric extracted from the polynomial curves fit to the T-response data from each tree in the control and heated groups in the study. Where appropriate, the means from the  $A_{net}$  and the  $A_{net}/C_i$  curves are both included. Metrics where a significant difference exists ( $p < 0.05$  level) between means within species are indicated in bold.

Metric	Units	Curve Type	Juniper		Piñon	
			Control	Heated	Control	Heated
$A_{max}$	$\mu\text{mol m}^{-2} \text{s}^{-1}$	$A_{net}$	7.28 (0.480)	6.36 (0.385)	4.31 (0.621)	3.28 (0.349)
$g_s$ at $T_{air} = 25^\circ\text{C}$	$\text{mmol m}^{-2} \text{s}^{-1}$	$A_{net}$	53.8 (5.67)	39.7 (4.28)	22.9 (4.02)	19.4 (3.21)
$g_s$ response to VPD	$\text{mmol m}^{-2} \text{s}^{-1} \text{kpa}^{-1}$	$A_{net}$	-5.38 (1.32)	-2.08 (1.14)	<b>-5.60 (1.33)</b>	<b>-1.80 (0.480)</b>
$T_{opt}$	$^\circ\text{C}$	$A_{net}$	<b>21.1 (0.697)</b>	<b>24.0 (0.904)</b>	20.7 (1.19)	23.1 (0.879)
		$A_{net} / C_i$	<b>21.7 (0.649)</b>	<b>24.8 (0.876)</b>	23.0 (0.636)	23.21 (0.795)
Slope of decline	% per $^\circ\text{C}$	$A_{net}$	6.45 (0.450)	5.88 (0.249)	<b>6.07 (0.197)</b>	<b>7.22 (0.393)</b>
		$A_{net} / C_i$	6.68 (0.267)	7.08 (0.210)	6.83 (0.334)	7.61 (0.404)

**Table 4-2 A-C<sub>i</sub> curve metrics at 25°C measurement temperature**

Metrics which describe the physiological condition of control, heated, and heatwave treated juniper and piñon trees at a measurement  $T_{air}$  of 25°C. Values of net assimilation ( $A_{net}$ ), gross assimilation ( $A_{gross}$ ), stomatal conductance ( $g_s \text{H}_2\text{O}$ ) and transpiration ( $E$ ) are taken from the first measurement of each A-C<sub>i</sub> curve, where  $C_a = 400$  ppm and foliage have established an equilibrium in  $A_{net}$ ,  $V_{cmax}$ ,  $J_{max}$ ,  $C_i$  at the transition from  $A_c$  to  $A_j$  limitation, and  $R_d$  are derived from curves fit to the A-C<sub>i</sub> data. Compact letter display indicates whether differences between treatment groups within species are significant, as determined using a Tukey HSD test and a threshold of  $p < 0.05$ .

			juniper			piñon		
25°C	metric	units	control	heated	heatwave	control	heated	heatwave
Carbon Assimilation	$A_{net\ 400}$	$\mu\text{mol m}^{-2} \text{ s}^{-1}$	9.51 (0.68) a	8.56 (0.98) a	<b>3.95 (0.43) b</b>	4.52 (0.29) a	5.74 (0.9) a	4.32 (0.3) a
	$V_{cmax}$	$\mu\text{mol m}^{-2} \text{ s}^{-1}$	57.6 (2.8) a	55 (7.2) a	46.9 (3.7) a	38 (5.4) a	34.7 (3.9) a	28.4 (1.9) a
	$V_{cmax} : V_{cmax\ 25}$	ratio	1.06 (0.01) a	1.08 (0.019) a	1.07 (0.011) a	1.1 (0.027) a	1.09 (0.02) a	1.05 (0.014) a
	$J_{max}$	$\mu\text{mol m}^{-2} \text{ s}^{-1}$	102 (9.8) a	112 (17) a	87.6 (4.2) a	69.8 (7.6) a	74.4 (5) a	62 (3.3) a
	$C_i$ transition	ppm	398 (49) a	546 (77) a	510 (110) a	505 (76) a	769 (190) a	676 (57) a
Water	$g_s\ H_2O$	$\text{mmol m}^{-2} \text{ s}^{-1}$	127 (9.6) a	125 (26) a	<b>39.1 (4.9) b</b>	52 (6.4) a	86.9 (18) a	51.6 (4.2) a
	E	$\text{mmol m}^{-2} \text{ s}^{-1}$	3.72 (0.26) a	3.38 (0.53) a	<b>1.18 (0.14) b</b>	1.62 (0.19) a	2.25 (0.37) a	1.34 (0.1) a
	$A_{net} : E$	ratio	2.56 (0.093) a	2.62 (0.21) a	<b>3.4 (0.17) b</b>	2.9 (0.27) a	2.57 (0.13) a	3.26 (0.19) a
Respiration	$R_d$	$\mu\text{mol m}^{-2} \text{ s}^{-1}$	1.65 (0.11) a	1.81 (0.38) a	<b>3.31 (0.47) b</b>	1.57 (0.39) a	1.08 (0.18) a	1.01 (0.1) a
	$R_d : A_{gross}$	ratio	0.152 (0.018) a	0.17 (0.031) a	<b>0.451 (0.041) b</b>	0.251 (0.047) a	0.173 (0.041) a	0.191 (0.019) a

**Table 4-3 A-C<sub>i</sub> curve metrics at 35°C measurement temperature**

Metrics extracted from A-C<sub>i</sub> curve data as described in table 2, but at a measurement T<sub>air</sub> of 35°C.

			juniper			piñon		
35°C	metric	units	control	heated	heatwave	control	heated	heatwave
Carbon Assimilation	$A_{net\ 400}$	$\mu\text{mol m}^{-2} \text{ s}^{-1}$	8.79 (1.1) a	8.74 (0.51) a	<b>4.19 (0.43) b</b>	4.79 (0.6) a	4.04 (0.71) a	4.08 (0.52) a
	$V_{cmax}$	$\mu\text{mol m}^{-2} \text{ s}^{-1}$	<b>99.4 (9.4) b</b>	<b>92.2 (2.9) ab</b>	<b>69.9 (4.7) a</b>	57.4 (5.6) a	41.7 (9.1) a	54.7 (6.5) a
	$V_{cmax} : V_{cmax\ 25}$	ratio	1.84 (0.16) a	2.03 (0.42) a	1.62 (0.1) a	1.74 (0.2) a	1.29 (0.18) a	2.06 (0.29) a
	$J_{max}$	$\mu\text{mol m}^{-2} \text{ s}^{-1}$	152 (13) a	155 (6.2) a	109 (3.7) b	103 (14) a	79 (16) a	102 (23) a
	$C_i$ transition	ppm	533 (37) a	676 (57) a	649 (110) a	842 (110) a	843 (90) a	917 (93) a
Water	$g_s\ H_2O$	$\text{mmol m}^{-2} \text{ s}^{-1}$	130 (16) a	136 (16) a	<b>46.7 (3.6) b</b>	79.8 (12) a	71.4 (5.4) a	50 (6.6) a
	E	$\text{mmol m}^{-2} \text{ s}^{-1}$	5.19 (0.5) a	5.73 (0.58) a	<b>1.91 (0.11) b</b>	<b>3.13 (0.42) b</b>	<b>2.72 (0.26) ab</b>	<b>1.9 (0.19) a</b>
	$A_{net} : E$	ratio	1.68 (0.046) a	1.55 (0.12) a	<b>2.18 (0.16) b</b>	<b>1.61 (0.19) ab</b>	<b>1.45 (0.13) a</b>	<b>2.15 (0.18) b</b>
Respiration	$R_d$	$\mu\text{mol m}^{-2} \text{ s}^{-1}$	2.11 (0.29) a	1.67 (0.22) a	2.37 (0.32) a	1.75 (0.41) a	0.985 (0.13) a	1.69 (0.46) a
	$R_d : A_{gross}$	ratio	0.201 (0.035) a	0.162 (0.023) a	<b>0.365 (0.05) b</b>	0.265 (0.05) a	0.214 (0.041) a	0.291 (0.064) a

**Table 4-4 A-C<sub>i</sub> curve metrics at 45°C measurement temperature**Metrics extracted from A-C<sub>i</sub> curve data as described in table 2, but at a measurement T<sub>air</sub> of 45°C.

			juniper			piñon		
45°C	metric	units	control	heated	heatwave	control	heated	heatwave
Carbon Assimilation	A <sub>net 400</sub>	μmol m <sup>-2</sup> s <sup>-1</sup>	3.78 (0.22) a	4.81 (0.68) a	3.02 (0.48) a	1.38 (0.3) a	1.81 (0.64) a	2.18 (0.29) a
	V <sub>cmax</sub>	μmol m <sup>-2</sup> s <sup>-1</sup>	124 (9.3) a	103 (12) a	105 (25) a	42.3 (5.3) a	50.2 (7.9) a	57.3 (6.9) a
	V <sub>cmax</sub> : V <sub>cmax 25</sub>	ratio	2.3 (0.2) a	2.41 (0.78) a	2.27 (0.53) a	1.28 (0.19) a	1.69 (0.47) a	2.14 (0.31) a
	J <sub>max</sub>	μmol m <sup>-2</sup> s <sup>-1</sup>	124 (9) a	115 (11) a	109 (12) a	--	--	--
	C <sub>i</sub> transition	ppm	564 (59) a	806 (110) a	702 (180) a	--	--	--
Water	g <sub>s</sub> H <sub>2</sub> O	mmol m <sup>-2</sup> s <sup>-1</sup>	70.3 (3.8) ab	105 (11) a	57.7 (19) b	51.1 (14) a	48.8 (8.2) a	47.3 (9.3) a
	E	mmol m <sup>-2</sup> s <sup>-1</sup>	4.77 (0.31) ab	6.15 (0.84) a	3.31 (0.9) b	2.75 (0.7) a	2.87 (0.43) a	2.67 (0.46) a
	A <sub>net</sub> : E	ratio	0.804 (0.062) a	0.812 (0.11) a	1.01 (0.19) a	0.581 (0.091) a	0.606 (0.15) a	0.892 (0.19) a
Respiration	R <sub>d</sub>	μmol m <sup>-2</sup> s <sup>-1</sup>	3.86 (0.63) a	2.17 (0.39) a	2.63 (0.23) a	1.88 (0.23) a	1.98 (0.42) a	1.4 (0.41) a
	R <sub>d</sub> : A <sub>gross</sub>	ratio	0.494 (0.053) a	0.312 (0.059) a	0.474 (0.048) a	0.594 (0.058) a	0.51 (0.11) a	0.381 (0.092) a

**Table 4-5. Results of V<sub>cmax</sub> ratio t-test**Results of t-tests to assess whether measured values of the V<sub>cmax</sub> : V<sub>cmax25</sub> ratio deviate significantly from the expected relationship. Displayed values are p-values.

		juniper			piñon		
		control	heated	heatwave	control	heated	heatwave
Measurement T <sub>air</sub>	35°C	0.493	0.561	0.428	0.852	0.0659	0.278
	45°C	0.8437	0.942	0.866	<b>0.005</b>	0.2592	0.508

## CHAPTER 5

### 5.1 General conclusions

This dissertation highlights the importance of studying microclimate phenomena and tree responses to environmental stressors on mature trees in the natural settings where they occur. Though changes in climate are likely to impact the structure and function of every forested biome, the nature and magnitude of change in local climate will not be uniform geographically (IPCC 2014), nor will change within a forest affect all species equally (Phillips et al. 2010, Johnson et al. 2018, Kumarathunge et al. 2019). In order to predict how forecasted changes will impact specific forest ecosystems, through the work presented here I have endeavored to elucidate how macroscale climate patterns propagate down to the microclimate scale that plant leaves experience (chapter 2). I have also compared the response of co-occurring tree species in two distinct ecoregions to differences in water availability (chapter 3) and imposed changes in ambient air temperature (chapter 4). Briefly, I will outline the key findings of each study and suggest directions for future research.

In chapter 2, our findings highlight the importance of *in situ* measurements for determining the frequency, vertical location, and duration of dew formation in a tall stature forest canopy. Delivery of dew to the canopy may be an important water subsidy which ameliorates drought stress during the dry season in the future in the Pacific Northwest, where changes in the length and severity of the dry season are expected (Mote and Salathe 2010). By comparing measurements at different heights, we determined that the vast majority of summertime dewfall occurs in the upper 20 - 30% of the canopy, where foliar water stress is perennially the greatest (Domec et al. 2008). The frequency of dew formation among the four dry seasons in our study averaged 28.5% of nights

and occurred throughout the season – that is, without need for antecedent rainfall to add humidity to the atmosphere. Our comparison of dew prediction using in-tree meteorological instruments vs. instruments in a nearby clearing highlight the importance of knowing within-canopy microclimate conditions, as a small difference in estimation of dewpoint depression led to large classification errors. The dew spray experiment we conducted at the end of the fourth summer of observation demonstrated that uptake of foliar water occurred. Uptake may have been more substantial if the study tree had experienced a greater moisture deficit during the 2020 dry season and pre-dawn shoot water potentials ( $\Psi_{\text{Leaf}}$ ) were lower at the time of spraying. Future work focused on the impact of dew wetting in the forest type studied here should look to quantify both dew formation frequency and plant water stress across a topographic gradient, where microclimate conditions (Rupp et al. 2020) as well as plant available soil water vary substantially.

In chapter 3, our findings show the effectiveness of comparing species across their native range in locations with different water availability as a way of assessing potential plastic adjustment to traits which confer drought resistance. The key findings of this study were that ‘ōhi‘a displayed significantly more plasticity in leaf level traits, including turgor loss point ( $\Psi_{\text{TLP}}$ ), capacitance (C) and modulus of elasticity (MOE). Though stomatal restriction of gas exchange increased at the dry end of it’s range, ‘ōhi‘a displayed compensatory changes in maximum carbon assimilation rate ( $A_{\text{max}}$ ) via increased nitrogen concentration per leaf area ( $N_{\text{area}}$ ), while diminished  $g_s$  in koa was not compensated for, resulting in lower time-averaged carbon assimilation (A). Finally, analysis of foliar nonstructural carbohydrate (NSC) concentrations suggested that NSCs played a role in determining  $\Psi_{\text{TLP}}$  in ‘ōhi‘a, while no such relationship was found in koa. Taken together, these results show that ‘ōhi‘a will be able to rely on drought tolerating strategies during future drought,

while koa will need to rely on drought avoidant strategies. Future work on drought vulnerability in koa and 'ōhi'a dominated forests could advance the current understanding by examining individuals closer to the dry extreme of each species range, which are expected to become drier in the future (Fortini et al. 2017).

In chapter 4, our findings demonstrate the effects of both moderate, long-term warming and short-term, heatwave-like warming on the photosynthetic performance of juniper and piñon trees. While the preponderance of evidence suggests that combined heat and drought lead to higher mortality rates in piñon (Breshears et al. 2009, Gaylord et al. 2013, Floyd et al. 2009, Lajtha and Barnes 1991), past studies did not explicitly consider the effects of high heat on the factors that determine net carbon assimilation ( $A_{\text{net}}$ ). While greater acclimation to a moderate increase in temperature was seen in juniper, surprisingly, the negative effects of heatwave conditions were more pronounced in juniper, with relatively smaller differences between piñon control trees and heatwave trees. Though the mechanisms underlying the significant reduction in  $A_{\text{net}}$  post-heatwave in juniper require further work to understand, two potential explanations present themselves. First, increased respiration rates as cells attempt to replace denatured proteins or produce heatshock proteins may bring down  $A_{\text{net}}$  (Scafaro et al. 2021). Second, reduced stomatal conductance post heatwave, in spite of shoot rehydration, suggests that xylem embolism may have prevented cut shoots from rehydrating to the point that opening of stomata – and allowing gas exchange – was not possible (Brodribb et al. 2014). In this second scenario, the effect of high air temperature was likely via a concomitant rise in vapor pressure deficit that induced  $\Psi_{\text{Leaf}}$  low enough to embolize leaf and/or stem xylem. While the exact mechanisms for reduced  $A_{\text{net}}$  require further work to clarify, it is clear that the imposed heatwave had a substantial effect on net carbon uptake. Future

work should investigate more closely how exposure to heatwaves affects respiration rates in piñon and juniper, and measurements of  $\Psi_{\text{Leaf}}$  and percent loss of xylem conductivity as heatwave conditions progress should be made in order to elucidate how high leaf-to-air VPD may impair stomatal function. Future studies should also include a post-heatwave period of observation, which would allow researchers to quantify how long the detrimental effects of heatwave last.

Predicting how changes in climate will unfold in a future with rising atmospheric greenhouse gas concentrations - and then predicting the cascade of effects that will ripple through the biosphere - represents a monumental task that requires an all-hands-on-deck effort from scientists of all disciplines. This dissertation represents work done on the fine scale of leaf-level response to changing environmental conditions in forested ecosystems, and contains methods which can serve to clarify how individual tree species will respond to future increases in environmental stress.

## 5.2 References

- Breshears, D.D., Myers, O.B., Meyer, C.W., Barnes, F.J., Zou, C.B., Allen, C.D., McDowell, N.G., Pockman, W.T., 2009. Tree die-off in response to global change-type drought: mortality insights from a decade of plant water potential measurements. *Frontiers in Ecology and the Environment* 7, 185–189. <https://doi.org/10.1890/080016>
- Brodribb, T.J., McAdam, S.A.M., Jordan, G.J., Martins, S.C.V., 2014. Conifer species adapt to low-rainfall climates by following one of two divergent pathways. *Proceedings of the National Academy of Sciences USA* 111, 14489–14493. <https://doi.org/10.1073/pnas.1407930111>
- Domec, J.-C., Lachenbruch, B., Meinzer, F.C., Woodruff, D.R., Warren, J.M., McCulloh, K.A., 2008. Maximum height in a conifer is associated with conflicting requirements for xylem design. *Proceedings of the National Academy of Sciences* 105, 12069–12074. <https://doi.org/10.1073/pnas.0710418105>
- Floyd, M.L., Clifford, M., Cobb, N.S., Hanna, D., Delph, R., Ford, P., Turner, D., 2009. Relationship of stand characteristics to drought-induced mortality in three Southwestern piñon–juniper woodlands. *Ecological Applications* 19, 1223–1230. <https://doi.org/10.1890/08-1265.1>

- Fortini, L.B, Jacobi, J.D., Price, J.P. 2017. Chapter 3. Projecting end-of-century shifts in the pattern of plant available water across Hawai'i to assess implications to vegetation shifts. U.S. Geological Survey Professional Paper 1834.
- IPCC, 2014: Climate Change 2014: Synthesis Report. Contribution of Working Groups I, II and III to the Fifth Assessment Report of the Intergovernmental Panel on Climate Change [Core Writing Team, R.K. Pachauri and L.A. Meyer (eds.)]. IPCC, Geneva, Switzerland, 151 pp.
- Johnson, D.J., Needham, J., Xu, C., Massoud, E.C., Davies, S.J., et al. 2018. Climate sensitive size-dependent survival in tropical trees. *Nature Ecology and Evolution* 2, 1436–1442. <https://doi.org/10.1038/s41559-018-0626-z>
- Kumarathunge, D.P., Medlyn, B.E., Drake, J.E., Tjoelker, M.G., Aspinwall, M.J., et al. 2019. Acclimation and adaptation components of the temperature dependence of plant photosynthesis at the global scale. *New Phytol* 222, 768–784. <https://doi.org/10.1111/nph.15668>
- Lajtha, K., Barnes, F.J., 1991. Carbon gain and water use in pinyon pine-juniper woodlands of northern New Mexico: field versus phytotron chamber measurements. *Tree Physiology* 9, 59–67. <https://doi.org/10.1093/treephys/9.1-2.59>
- Mote, P.W., Salathé, E.P., 2010. Future climate in the Pacific Northwest. *Climatic Change* 102, 29–50. <https://doi.org/10.1007/s10584-010-9848-z>
- Phillips, O.L., van der Heijden, G., Lewis, S.L., López-González, G., Aragão, L.E.O.C., et. al. 2010. Drought-mortality relationships for tropical forests. *New Phytologist* 187, 631–646. <https://doi.org/10.1111/j.1469-8137.2010.03359.x>
- Rupp, D.E., Shafer, S.L., Daly, C., Jones, J.A., Frey, S.J.K., 2020. Temperature Gradients and Inversions in a Forested Cascade Range Basin: Synoptic- to Local-Scale Controls. *J. Geophys. Res. Atmos.* 125. <https://doi.org/10.1029/2020JD032686>
- Scafaro, A.P., Fan, Y., Posch, B.C., Garcia, A., Coast, O., Atkin, O.K., 2021. Responses of leaf respiration to heatwaves. *Plant, Cell & Environment* 202 1; 1-12. <https://doi.org/10.1111/pce.14018>